ABSTRACT

Title: **VARIATIONAL DATA ASSIMILATION OF SOIL MOISTURE INFORMATION**

Pablo J. Grunmann, Doctor of Philosophy, 2005

Directed By: **Professor Eugenia Kalnay, Department of Meteorology**

Doctor Kenneth Mitchell, National Centers for Environmental Prediction

This research examines the feasibility of using observations of land surface temperatures (in principle available from satellite observations) to initialize soil moisture (which is not available on a continental scale). This problem is important because it is known that wrong soil moisture initial conditions can negatively affect the skill of numerical weather prediction models.

Since this problem requires the availability of a good soil model, considerable effort was devoted to the improvement of several aspects of the NCEP Noah land

surface model and its numerical properties (reliability, efficiency, updates and differentiability). When tested against the experimental station data at Champaign, IL collected by Dr. Tilden Meyers of NOAA/ARL, where the surface fluxes, precipitation, and surface temperature were available, the Noah model forced with observed downward radiative surface fluxes and near-surface meteorology, including precipitation, was able to reproduce the observations quite well.

A method for data assimilation was developed and tested, in a manner similar to 4-dimensional variational assimilation (4D-Var) in the sense of applying the temporal behavior of the observed variable but with a single spatial dimension (land surface models are typically "column models", as they do not usually compute horizontal derivatives). The results show that it is indeed possible to assimilate land surface temperature and use it to correct soil moisture initial conditions, which may manifest significant errors if, for example, the precipitation forcing the model is significantly biased. This is true, however, only if the surface forcings besides precipitation are essentially correct. When surface forcing come from the North American Land Data Assimilation System (NLDAS) as they would be available for operational use over the US, the results are not satisfactory. This is because the assimilation changes the soil moisture to correct for problems in the simulated land surface temperature that are at least partially due to other sources of errors, such as the surface radiative fluxes. We suggest that in order to succeed in the soil moisture initialization, more (and more accurate) observations are needed in order to constrain the dependence of the observation part of the cost function solely on soil moisture.

VARIATIONAL DATA ASSIMILATION OF SOIL MOISTURE
INFORMATION

By

Pablo J. Grunmann

Dissertation submitted to the Faculty of the Graduate School of the
University of Maryland, College Park, in partial fulfillment
of the requirements for the degree of
Doctor of Philosophy
2005

Advisory Committee:
Prof. Eugenia Kalnay, Chair
Dr. Kenneth Mitchell
Prof. Dalin Zhang
Prof. Ferdinand Baer
Prof. James Carton
Prof. Ruth DeFries

Acknowledgements

Table of Contents

iv

List of Tables

List of Figures

Chapter 1

Introduction

Land-surface and soil hydrology models used as a lower boundary condition by coupling with general circulation, climate or weather forecast models have been recognized, over the past few decades, as vital to the quality of the results. Consequently, progressively more sophisticated land surface models have been developed and incorporated for such uses.

In general, computational time constraints and the difficulty in establishing initial conditions in the soil has been a barrier for the use of the most sophisticated land surface models in operational settings. Fortunately, the recent advances in computational power allowed the incorporation of more complex and accurate land-surface models. Still, the problem of estimating initial conditions for soil variables, given that observations of these variables are not generally available, remains an important challenge.

Early studies on the role of soil water (Namias, 1958) within the climate system brought attention to the need of considering surface fluxes and runoff, as affected by the variability of soil moisture. This justified the development of soil models - such as the so-called "bucket model" (Manabe, 1969) - to take into account the evolution of soil moisture and interaction with evaporation and runoff. In 1978, Deardorff showed the importance of the contribution of vegetation to the latent heat flux (evapotranspiration).

At the present time, land-surface models coupled with atmospheric models are expected to reproduce the evolution of land-surface-atmosphere fluxes and soil variables with reasonable accuracy given proper initial conditions and forcing.

Water storage in the soil affects directly evapotranspiration, soil heat storage, thermal conductivity, and the partitioning of energy between latent and sensible fluxes. As a result, it influences the moisture and temperature in the planetary boundary layer and, consequently, the evolution and amount of cloudiness and precipitation (Pan and Mahrt, 1987, Garratt, 1993).

Given recent advances in the state-of-the-art of numerical weather prediction models, the quality of the simulation of the land-surface processes is having a larger impact on the models, due to the increased requirement of accurate lower boundary conditions to interact with the atmospheric models (Chen, F. et al., 1997). For this reason, the quality of the simulation of the soil moisture field is of great importance in order to obtain a proper simulation of land-surface physics and, consequently, positively affect the quality of the weather forecasts (Viterbo and Illari, 1994; Koster and Suarez, 2003).

One problem that has not yet been overcome is how to adjust the soil moisture initial fields (Betts et al., 1996). This problem has serious consequences because, given that soil moisture is a slowly evolving variable, an error in the initial condition will affect the quality of the simulation for a long period of time, even if the correct precipitation is observed and specified (as seen in the experiments described in sections 5.4 and 6.1).

Soil moisture content values are not observed regularly over large areas, making the use of direct soil moisture observations in the data assimilation system impossible. Instead it becomes necessary to use indirect observations of soil moisture, something made possible by its relationship to other observed fields.

Another possible approach is the initialization of soil moisture from climatology as opposed to deriving or inferring it with the use of current observations. The past common approach in most operational numerical weather prediction (NWP) models has been to initialize soil moisture for the forecast cycle with values obtained either from a climatological database or by letting the soil moisture content, as a prognostic variable, to be cycled on itself in continuous adjustment with the rest of the model (Viterbo and Beljaars, 1995). The use of climatological values has the disadvantage of not reflecting real conditions associated to recent past evolution and, therefore, an inherent inability to adapt to anomalous conditions such as wet or dry spells. On the other hand, cycling the soil moisture content as a prognostic variable forced by model precipitation and surface fluxes without corrections derived from observations, may lead to drifting which is seen as a departure from realistic soil

15

moisture over time. This can be produced by inaccuracies in the forcing provided by the companion models, usually radiation and precipitation, both affected by the quality of the prediction of cloudiness within the atmospheric model. As a result, on a time scale of weeks to months, the prediction errors can grow through complex feedback loops, causing excessive accumulation or depletion of soil water stored, leading to systematic under- or overestimation of the actual land-surface evaporation (Viterbo, 1996). At NCEP, the global model in operation, using a version of Noah land surface model for the treatment of land surface and soil variables, applies nudging towards climatology in the Global Data Assimilation System (GDAS) cycle on a 60-day time scale as a means to curtail the effects of drifting (e.g., Kistler et al, 2001). In the ETA model, the soil moisture was being initialized with analysis from the global model; but now, it is cycled continuously on itself (Mitchell, 1998, etc, personal communication).

In this context, it seems desirable to develop data assimilation approaches that could provide the necessary initial soil moisture values derived from non-soil moisture observations, while being consistent with the weather forecast model and sensitive to recent past evolution.

The strong influence of the soil moisture on surface fluxes that, in turn, affect low-level atmospheric parameters, suggests that it is possible to infer a correction to the soil moisture content values based on information from prediction errors on sensitive variables at the lower levels of the atmospheric model (Mahfouf, 1991, Bouttier, et al., 1993).

Another approach could be to infer the corrections to soil moisture from the surface fluxes themselves (van den Hurk et al., 1997; Jones et al., 1998), thus avoiding some of the disadvantages of using error information from near surface parameters, namely, miscalculations caused by components of these errors that have no relationship with soil moisture, such as effects from horizontal advection and situations in which surface fluxes effects are small compared to other effects. However, this method requires having information about the surface fluxes, which, until recently, was not routinely available. As new surface observations became

available with the recent implementation of GEWEX GOES satellite surface products retrieval (Gutman G, 1994; Pinker et al., 1996; Tarpley et al., 1996), there is a new perspective on the range of observations relevant to soil moisture data assimilation and their feasibility of implementation on future operational use.

1.1 Specific goals of this dissertation

The main goal of this thesis is to attempt to develop an approach that could provide the necessary soil moisture values derived from available non-soil observations while being consistent with the model physics and sensitive to recent past evolution. For this purpose, the following steps are defined for this work:

I. Show that the land surface model is realistic at updating the state variables and reproducing accurately the land-atmosphere fluxes when correct forcing and reasonable initial conditions are given. This includes making the necessary adjustments and improvements to the model as well as testing and validating the land-surface model at target sites where surface atmospheric fluxes and soil data are available. The new version of the NCEP model should be able to produce a reasonably unbiased response when verified by observations. Additionally, this upgraded model should also be made to be differentiable as much as necessary to produce the tangent linear of this code. Having this version ready, it will produce a control run (from nearly ideal initial conditions and forcing). A second run with errors and biases in initial conditions or forcing should show a cumulative degraded response due to, e.g., precipitation bias, in contrast to that of the control run response.

II. Develop a data assimilation scheme based on variational techniques. These techniques need to find the minimum of a cost function, procedure that may require computing the gradient of such cost function with respect to the control variables (e.g. initial time soil moisture correction). This gradient would be better calculated by using a differential of the FORTRAN source code (such as the linear tangent or the adjoint model). Consequently,

observations (other than soil moisture) can be used to adjust the trajectory of key state variables to improve the response of the model.

III. Test and assess possible improvements in the predictive ability of the model due to data assimilation by comparing the results with similar experiments but without data assimilation.

Chapter 2
Theoretical overview

In this chapter we discuss the formulation of the data assimilation problem for finding optimal initial conditions for the model's initial soil moisture and optimal parameters.

2.1   General approach

The ability to simulate dynamical-physical processes in nature through the use of a computer model requires a reasonable reproduction in time of the behavior of the variables representing those processes. This depends on the quality of representation of the mechanisms involved and matching the states of the model variables with those of the processes being simulated. In principle, if it were possible to find a perfect match at the initial time between the processes states and the model's (initial condition), the increasing disagreement over time between the two would be attributed mostly to the model's limitation in including and performing accurately all the required elements and their dynamics as involved in those processes.

In reality, neither condition is completely satisfied but it is desirable to approximate them in a cost-effective way. In this work, we are mostly concerned with finding initial conditions given that the model is satisfactorily capable at reproducing the desired processes from there.

What is meant by a trajectory is the set of time series of the state and output variables calculated by the model (forecast). If the time-span is long enough, a subset composed of just a few critical variables is sufficient to represent the model's trajectory, this is explained by the model's physical constraint between variables (through the model equations). Given this, it is possible to rely on one or very few observed variables (but over a time period) and still expect the model to change its entire trajectory consistently towards matching more closely the behavior of this or these variables.

2.1.1 The problem of model performance versus parameters and initial conditions

Let's call the whole set of model's state variables plus time-dependent outputs as the set of "model predictions" (model calculations). This is everything the model produces by calculating forward in time given a set of initial conditions plus parameters (given or pre-determined).
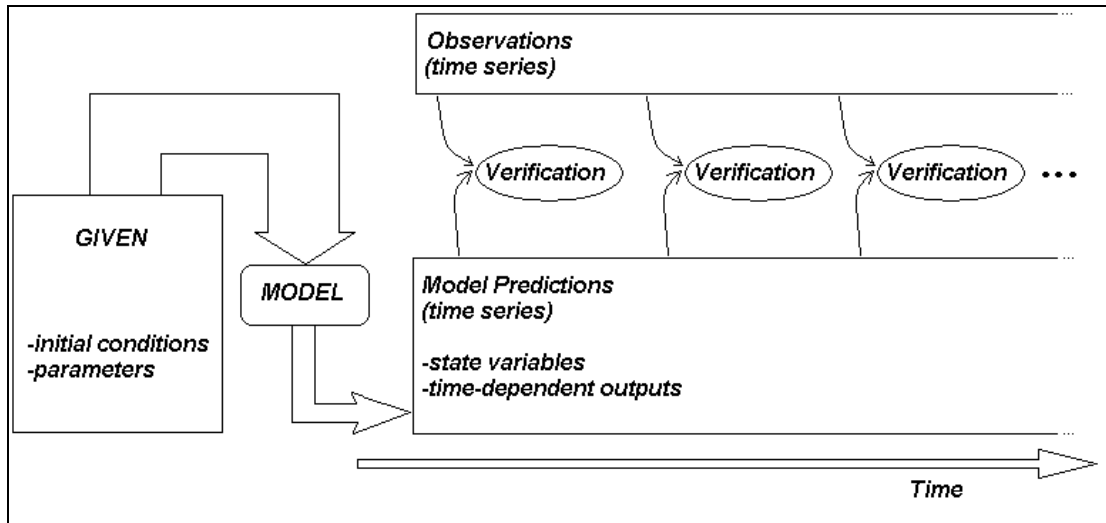
Figure 2-1 Schematic of the setting for changes to the model's parameters or initial conditions based on its adherence to observations.

The problem of improving model performance by making changes to the set of "given" values (model initial conditions and/or modelparameters) relies on being able to compute model error, i.e., a measure of the discrepancy between the whole set of "model predictions" and observations (Figure 2-1).

If enough observations were available as to verify each and every element of the set of "model predictions", it would be possible to construct a model error function that takes as input the multi-dimensional vector with the whole set of the "given" and produces a scalar number. This should also take into account an appropriate normalization for the contribution to the error by each and every one element of the "model predictions" over a period of time (verification window) to the total error.

20

Even in this scenario it is quite likely to find more than one set of the "given" producing minima in the error function as a result of compensation or contradicting effects within elements of the "given" set. In some cases, increasing the time-span of the verification window would reduce the number of dissimilar sets that produce a minimum in the error function (for example, two different sets of the "given" may seem equally satisfactory over a certain month but one of them seems better when the verification window extends over many months or the entire year). If many different sets of possible "given" are still found after all attempts, a simplification of the model may be considered, which could mean just to set some elements of the "given" as constant (no longer part of the error function domain) but they have to be identified and chosen. This deals into the limitations of models mandated by our limitations in verification.

In real life, having enough observations as to verify each and every element of the set of "model predictions" may certainly not be possible. Instead, only a subset of "model predictions" can be verified. This increases the likelihood of having different sets of "given" that appear to minimize the model error function.

2.2   Variational assimilation

The basic variational assimilation problem, for the purpose of correcting the initial conditions to be used by the model, consists of: first, computing a function (cost function) that measures the distance between the observed variables and their corresponding model-produced variables, (this distance between model and observations relates to the model error with respect to those observations) and, second, find the minimum of that function with respect to modifications done to the initial conditions (control variables). Running the model from those "optimal" initial conditions should lead to a trajectory much closer to that of the equivalent observations.

The search for those "optimal" initial conditions can be put as a version of the basic variational problem:

$$\min_{f(t)} I \quad \text{where} \quad I = \int_a^b f(t)dt \qquad (2.1)$$

In our case, *f(t)* would represent the magnitude of the terms in the cost function formula at a certain time *"t"* of the integration, the integral (sum) *"I"* would be the cost function, it includes the behavior of the model within the interval *t=a* and *t=b*. In the case of looking for optimal initial conditions, the changes imposed at time *"to"* affect the behavior of *f(t)* within *[a,b]*.

2.2.1 Cost Function

Given a dynamical physical system described by a model (***M***). The model operates using a set of <u>parameters</u> ***"P"*** [1] (vector of fixed, pre-established values), initial conditions in its <u>state</u> variables ***"S(t_o)"*** [2] (vector ***S*** at time=t_o) and a time-dependent set of external <u>forcing</u> fields, ***"F(t_i)"*** [1] (vector of externally determined, time dependent boundary conditions) producing the time change of state variables ***"S(t_i)"*** [2] and a set of additional output variables, ***"U(t_i)"*** [3], for i=1,2,… time-steps. The difference between ***"S(t_i)"*** and ***"U(t_i)"*** is that ***"S(t_o)"*** is used by the model as initial condition in other words, ***"S(t_i)"*** is required in the computation of ***"S(t_{i+1})"***, while no initial values of ***"U"*** are required to run the model.

With this notation, the model ***M(P, S***(t_o)***, F***(t_i)***)*** generates the time series ***(S***(t_i)***,U***(t_i)***)*** for i=1,2,…,F (t_F is the final time of integration).

Consider a set of observations in space and time, ***O*** (data), and the model simulation of these observations.

We may need to operate on the model output (***S***(t_i)***, U***(t_i)) at each time-step, to transform it into the observational space, so that ***H(S***(t_i)***, U***(t_i)) = ***Z***(t_i) can be compared to ***O***(t_i) (the observational vector).

---

[1] Not changed by the model.
[2] Changed (updated) by the model
[3] Generated by the model

If there is interest in changing the response (behavior) of the model so that its predictions better approximate the systematic characteristics of the observations ("tuning the model"), the control variables to choose would most likely come from the parameters' set (from the **P** vector). A different situation is the need to correct the model trajectory based on comparison with observations. Since the model trajectory is given by the time series of its state variables, in order to correct it we may want to change the initial conditions (from **S**(t_o) vector). Therefore the control variable, **X**, is a subset of the vector (**P, S**(t_o)). In both cases, we want to obtain optimized values that minimize the misfit between observations and corresponding model values. This misfit can be quantified through a function of the form:

$$J(\mathbf{Xo}) = \left(\frac{1}{2}\right) < \mathbf{Z} - \mathbf{O}, \mathbf{Z} - \mathbf{O} > \qquad (2.2)$$

where

$< \cdot, \cdot >$ represents an appropriate inner product, and

$J(\mathbf{Xo})$ represents the cost function to be minimized.

The *control variable*, *Xo*, is an N-dimensional vector, where N is the number of parameters and/or initial conditions to be optimized (size of the problem).

If we express the problem in terms of what we intend to allow to be modified by the optimization process while letting the model use other variables without modification, we can write **M** as a function of the control variable **Xo** and time alone, hence,

$$M = M(X(t_o), t_F) \qquad (2.3)$$

Also, in practical applications, incomplete observations or conditions when sensitivity of the observable variables to the control variable is low, lead to the need to use background fields, X_b, defined from current forecasts before the assimilation process and/or climatological/standard fields that one desires to adopt in case of

absence or unreliability of observations. The use of a background field may also help to find a unique solution.

It is customary to derive a cost function that includes both a background field and observations by finding the solution X that maximizes the joint probability given X_b and O, assumed to be Gaussian random variables with error covariances B and R respectively. This is equivalent (e.g., Kalnay, pp 169-170) to minimizing the following cost function

$$J(\mathbf{Xo}) = \left(\mathbf{Xo} - \mathbf{X_b}\right)^{\mathbf{T}}\mathbf{B}^{-\mathbf{1}}\left(\mathbf{Xo} - \mathbf{X_b}\right) +$$

$$+ \frac{1}{2} \sum_{i\,=\,1}^{k} \left\{\left[\mathbf{M(Xo, t_i)} - \mathbf{O}\right]^{\mathbf{T}}\mathbf{R}^{-\mathbf{1}}\left[\mathbf{M(Xo, t_i)} - \mathbf{O}\right]\right\} \tag{2.4}$$

where

R   is the observational error covariance matrix,

B   is the background error covariance matrix, and

k   is the number of time-steps in the data assimilation window.

Matrices $\mathbf{R}$ and $\mathbf{B}$ are necessary when the model predicted states (background) and observations contain several variables and their reliability varies with time. They also provide scaling of units between variables and with respect to the control variable. The scalar versions of $\mathbf{R}$ and $\mathbf{B}$ have typical magnitudes in the range of the variance of each variable, which means that variables in the cost function are (in first approximation) scaled inversely proportionally to their variance.

Additionally, the cost function **(2.4)** indicates that when the observational errors are much larger than the background errors, the cost function will be more sensitive to the background values and vice-versa.

2.2.2 Cost Function Analysis

The possibility of finding the initial values for soil moisture content (solution to the optimization problem (LeDimet and Talagrand, 1986)) depends entirely on the characteristics of the cost function (convexity, smoothness, behavior of the first

derivative, presence of a minimum inside the physically acceptable region). A cost function without a well defined, physically consistent minimum may indicate lack of sensitivity of the control variables to the observed ones, or insufficiency of observation data necessary to determine a cost function that is sufficiently dependent on the control variables.

The cost function to be examined here will measure the misfit of the model calculated land skin temperature (or LST, Land Surface Temperature, model variable "T1"), to its observational counterpart. To plot a cost function depending on N conditions (control variables), it is necessary to run an N-levels nested loop computation of the function. Each loop computes the function at the points along the range of variation of each condition, so that if one desires to have the N-dimensional grid with the values of the cost function given for all possible combination of conditions (with a resolution of M points taken along each condition) then M^N computations of the cost function would be needed. In this case, where there are only four conditions (the initial soil moisture at each one of the four soil layers of the model), obtaining a grid with 100 values along each soil moisture range would require 100^4 computations of the cost function.

If the conditions of the cost function are the soil moisture at each of the four soil layers of the model, one must be aware of the possibility of one layer erroneously compensating for the error of another, creating spurious secondary minima (Mahfouf, 1991). The solution to this problem relies on being able to discard unrealistic solutions by imposing certain reasonable physical constraints and/or improving/enhancing the amount of information dealt within the cost function (longer time of integration, additional observed variables, improvements in the model). Regarding the physically based constraints, besides the maximum and minimum soil moisture acceptable for each layer, strong differences in soil moisture content between layers have a limited life due to diffusion, making it an unlikely solution. We may anticipate however, that intense drying of the surface layer (also via a dense root layer, through transpiration) due to summertime sunshine conditions may happen during daytime, leading to temporarily strong gradients (with corresponding profile-smoothing refill from adjacent layers during the night).

25

The following guidelines may also be used to plot the cost function:

If the cost function is a scalar function of four variables (4 layer soil moisture), we would need 5 dimensions to plot it, one axis for each variable and one additional to show the function value over each 4-dimensional point $(\theta_1, \theta_2, \theta_3, \theta_4)$[4]. In this case, function cross sections can be examined (plotted) as dependent on only 1 (or 2) of the control variable components at a time, maintaining the other 3 (or 2) remaining ones constant and using the above mentioned guidelines as explained next. Let us consider the case of specifying two of the components (fixed) consistently to each other, but far from optimality: it is expected that the minimum seen on the cost function cross section, dependent on the other two (free) variables, will be shifted in a compensatory direction (opposite to the error introduced in the specified ones with respect to optimality). As an illustration of this effect, Mahfouf (1991), examining a cost function measuring errors on screen level relative humidity and temperature, dependent on the soil moisture for a two-layer model integrated for two days, found a secondary, spurious minimum in which a very moist surface layer, evaporating at a potential rate, was able to compensate for a dry root zone. Given these facts, one should be cautious with solutions showing abrupt differences between layers, unless the observed conditions and events justify the profile.

The limitations given by available observed variables in realistic case scenarios indicate that contingent strategies are necessary in the formulation of the cost function in order to give it the necessary features needed for robust minimization. That means, specifically the presence of a well defined, unambiguous minimum. This issue has to do with the dimensionality of the observed space versus that of the control variable. That means, the higher the dimension or detail (amount of information) in the control variable, the greater will be the required strength or detail of the observed variable(s). In our specific case, there is only one observed variable, the LST (land surface temperature) over time, which has to be compared to the

---

[4] θ_i is the volumetric soil moisture content in soil layer "i".

corresponding variable predicted by the model given an initial soil moisture condition. Preliminary experiments have shown that allowing the cost function to depend on each of the layer depths of the model initial soil moisture state as separate variables does not yield well defined minima (low sensitivity) in addition to leading often to multiple minima. Furthermore, we found that the only possible advantage of making the cost function depend separately on each and all levels of the soil moisture profile, which would be the ability to alter the vertical soil moisture gradients, has no significant impact to the model trajectory. This makes this choice unattractive in a cost-benefit sense.

The alternative that we developed and tested was to devise a cost function dependent only on a correction factor to the total column soil moisture content. The corrections to the soil moisture state obtained by this method are a fixed amount of volumetric soil moisture content added or subtracted to all layers. This way, the total soil moisture content is optimized letting the model itself to adjust the vertical profile when necessary (this adjustment is typically very small and quick because the new profile is similar to the one the model physics was already carrying only shifted towards greater dryness or wetness).

The general form of our cost function that we settled upon is therefore:

$$
\mathbf{J}(x) = \frac{1}{2} \sum_{t=begin}^{end} \left\{ \left(\left[T1_{lsm}(x) \right]_t - \left[T1_{obs} \right]_t \right)^2 + BK_{scale} * x^2 \right\} \tag{2.5}
$$

Here the series $[T1_{lsm}(x)]_t$ is the LST (land surface temperature, model variable "T1") produced by the model over the data assimilation window (time interval) when the soil moisture state variable is changed by **"x"** at a time-step prior to the one that begins the data assimilation window, thus, changing the initial condition from:

$$\textbf{Soil moisture}\left(\textit{time} \ = \ t_o \right) = \begin{bmatrix} \left(\textit{soil moisture in layer 1}\right) \\ \left(\textit{soil moisture in layer 2}\right) \\ \left(\textit{soil moisture in layer 3}\right) \\ \left(\textit{soil moisture in layer 4}\right) \end{bmatrix} \qquad (2.6)$$

to:

$$\textbf{Soil moisture}\left(\textit{time} = t_o \right) = \begin{bmatrix} \left(\textit{soil moisture in layer 1}\right) + x \\ \left(\textit{soil moisture in layer 2}\right) + x \\ \left(\textit{soil moisture in layer 3}\right) + x \\ \left(\textit{soil moisture in layer 4}\right) + x \end{bmatrix} \qquad (2.7)$$

Therefore, our cost function depends on only a single scalar "x" which produces a well defined unambiguous impact on the LST produced by the model. A positive value for x increases the total soil moisture content while a negative one decreases it.

The constant "BK_{scale}", in the term "$BK_{scale}*x^2$" in the cost function formula, is used to scale the magnitude of the background term, which depends on the square of the change made to the soil moisture. This term is calibrated to cause the contribution of the background term to the cost function to be in between the magnitudes of the "model minus observations squared" (first) term for periods of high and low sensitivity of the observed variable to changes in the initial condition. The role of the background term is illustrated in Figure 2-2 and Figure 2-3, in which the axes' scales are kept equal for both the high and low sensitivity conditions cases. In the high sensitivity case (Figure 2-2), the background term has negligible effect on the cost function, while in the low sensitivity case (Figure 2-3), it dominates the function causing its minimum to be located near zero (no change due to data assimilation).
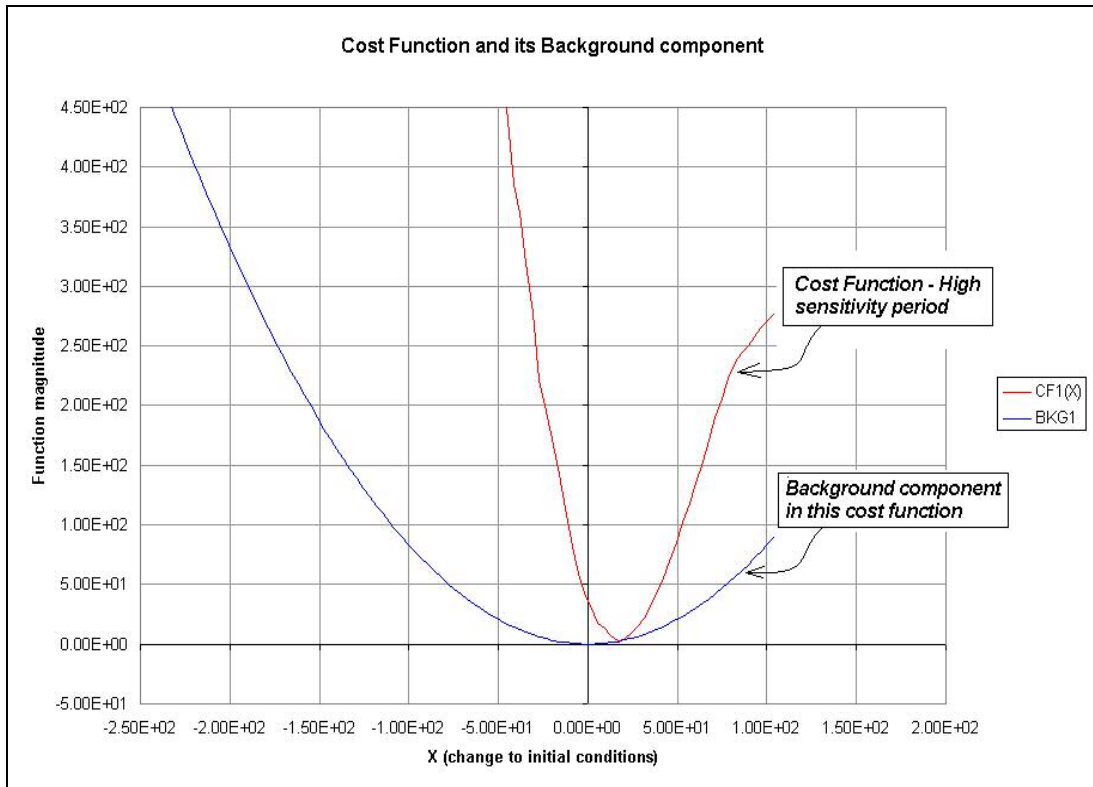
Figure 2-2 Example of the cost function (all terms) and its background component computed during a high sensitivity period over the entire range of the control variable, which represents the possible change to the initial conditions.
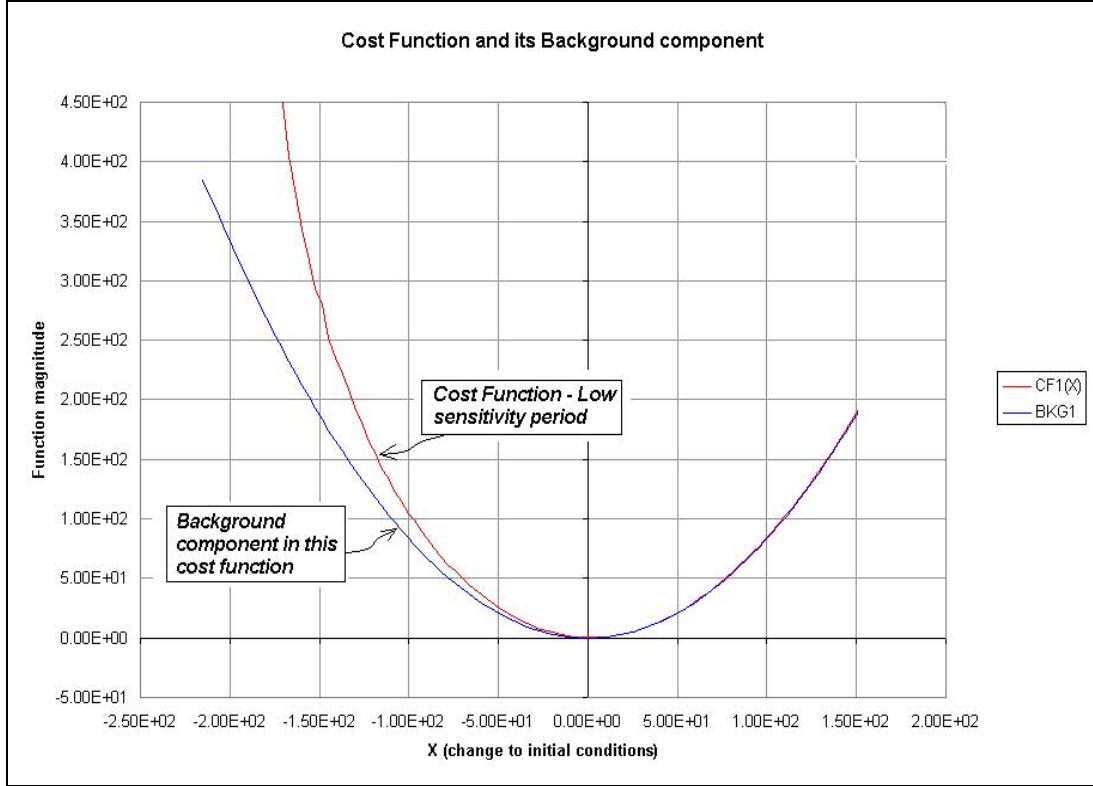
Figure 2-3 Same as Figure 2-2 but for a low sensitivity period.

2.2.3 Gradient and Minimum of the Cost Function

In order to minimize *J* with respect to changes in *x*, minimization algorithms require the gradient of *J(x)* with respect to *x* (Shanno, 1978; Gill et al., 1981; Lewis and Derber, 1985; Nash and Sofer, 1996), denoted as G_x *(x)* (Lewis and Derber, 1985; Navon et al., 1992; Giering and Kaminski, 1996, Kalnay, 2003, pp 181-184 and 264-265). First, collecting all time steps in the data assimilation window into vectors:

$$\mathbf{J}(x) = \frac{1}{2}\left[T1_{lsm}\left(t = begin,end\right) - T1_{obs}\left(t = begin,end\right)\right]^{2} + \frac{1}{2}(end - begin) * \mathbf{BK}_{scale} * x^{2}$$

(2.8)

From an infinitesimal perturbation to the cost function with respect to *x*, one obtains

$$\frac{\partial \mathbf{J}(x)}{\partial \mathbf{x}} = \mathbf{A}_{T1}(x)\left[\mathbf{T1}_{lsm}\left(t = begin,end\right) - \mathbf{T1}_{obs}\left(t = begin,end\right)\right] + \\ + (end - begin) * BKscale * x$$

(2.9)

where

30

$\dfrac{\partial \mathbf{J}(x)}{\partial x}$ is the gradient of the cost function with respect to x, and

$$\mathbf{A}_{T1}(x) = \left\{ \frac{\partial}{\partial x} \left[\mathbf{T1}_{\mathbf{lsm}} \left(\mathbf{t} = begin, end \right) \right] \right\}^{\mathbf{T}}$$ is the conjugate transpose of the tangent

linear model, $L_{T1}(x)$. This conjugate transpose is called the adjoint model.

Now, writing $\mathbf{G_x}(x)$ instead of $\dfrac{\partial \mathbf{J}(x)}{\partial x}$ to more compactly designate the gradient of

the cost function and using $\mathbf{T1}_{lsm}(x)$ as the notation for the model-output of the LST

time series (from $t = begin$ to $t = end$) after the addition of "x" to the initial conditions,

the gradient of our cost function is:

$$\mathbf{G_x}(x) = \mathbf{A_{T1}}(x) \left[\mathbf{T1}_{lsm}(x) - \mathbf{O} \right] + \mathbf{B}^{-1}(x - x_b) \tag{2.10}$$

       In our case, to obtain the value of the correction to the soil moisture, it is

necessary to take this correction to the initial condition of soil moisture as the control

variable x_o. Then, the cost function $J(x_o)$ is set to calculate the squared differences

between model predictions and observations when the model is run from initial

conditions $\boldsymbol{\theta_o} = \boldsymbol{\theta_{bef}} + x_{o*}[1,1,1,1]^{\mathbf{T}}$. By changing x_o the cost function changes value

provided that the variables in the model matching the observed ones are sensitive to

changes in x_o). The purpose is to determine the optimum x_o that minimizes J. In

practice, this requires the numerical minimization of J with respect to the elements of

vector x_o. The minimization algorithms are more effective when the gradient of the

cost function, $\vec{G} = \dfrac{\partial J}{\partial x_o}$, is provided.

2.2.4   Tangent Linear Model and Adjoint

       In order to ensure the validity of the above formula for the gradient, $\mathbf{T1}_{lsm}(x)$

must satisfy certain conditions. For example, discontinuities or severe non-linear

behavior of the model could complicate the computation or effectiveness of the

gradient, therefore it is necessary to test the model, verify its response to a range of

inputs and find suitable options to eliminate or improve problematic behavior

(Vukicevic and Errico, 1993; Zou et al. 1993; D. Zupanski, 1993).

To verify the continuity, the tests consist of imposing an ordered range of initial conditions followed by comparison of the sequence from these initial values against the corresponding results (sensitivity to initial conditions).

Further modifications are necessary when automatic differentiation tools are used, because in programmed codes it is common to encounter certain features that are not directly differentiable or understandable by an automatic differentiation tool, creating the need to prepare the model in a manner that it becomes an automatically differentiable model. These modifications included, in our case, replacement of table look-up functions with their respective formulas, and replacement of problematic logical statements by differentiable functional counterparts. If the modifications are correct (i.e., compatible with the original model), one should expect to obtain an almost identical model with an acceptable performance compared to the original. This is verified by checking the behavior of the modified version against the original, for accuracy and performance.

The development of tangent linear (L_{T1}) and adjoint (A_{T1}) versions of the model was done with the help of one of the above mentioned automatic differentiation tools, in this case, the Tangent linear and Adjoint Model Compiler - TAMC (Giering, R., 1997). These tools are able to substantially reduce the time for coding and error debugging, depending on the original code to be differentiated and on the experience of the user. Unfortunately, at the present stage of development, they still require considerable attention and verification (e.g., Shu-Chih Yang, personal comm., 2004), and specific tests need to be applied to determine whether the tangent linear and adjoint versions are correct (tangent linear and adjoint model validation, Kalnay, 2003, pp 264; Jaervinen, 1993). Even when these tests are satisfied, the results can be incorrect in very subtle but catastrophic ways (e.g., Shu-Chih Yang, personal comm., 2004)

Once a valid version of the adjoint *(A)* is obtained, and a suitable cost function *(J)* defined, its gradient *(G_x)* can be computed with greater precision and less computational cost using the adjoint than with any finite differences method that finds the minimum by using the full model. This is because of the condition error effect

(see Appendix A) that does not permit a very small difference interval in the finite differences approximation for the gradient (Gill et al., 1981; Nash and Sofer, 1996; Appendix A), and because of the fact that the finite differences gradients require, at least N (the dimension of the control variable) computations of the function.

The optimization software uses the gradient obtained by the adjoint approach to perform the minimization of the cost function measuring the misfit between observations and model predictions of land-surface state variables or surface fluxes (cost function) with respect to our control variables. For our data assimilation scheme, the control variable is the change imposed to the initial soil moisture.

In order to test and quantify the effects of the method, it should be first applied within a control region where observations are complete and comprehensive, including soil moisture content. The planned tests consist of running the NCEP land-surface model in a one-dimension column mode at selected sites with observed atmospheric surface-station forcing.

The effects of the method will be assessed by comparing the results from assimilation runs (observed LST modifying the soil moisture through the variational assimilation method) and control runs (without data assimilation). In these experiments two situations could be presented: (a) erroneous initial conditions of soil moisture and (b) correct initial conditions, but soil moisture errors emerge subsequently through degraded surface forcing (e.g. precipitation and surface solar incoming radiation), as it could happen in a coupled land-atmosphere model.

2.2.5 Deriving the data assimilation tools for the Noah LSM

In summary, the calculations needed for data assimilation are:
1) A <u>cost function</u> J based on the observable variable(s) and dependent on our control variable, x;
2) The <u>gradient</u> of this cost function with respect to the control variable;
3) An optimization scheme to <u>minimize</u> J (may require the gradient of J) and;

4) Including the above three calculations via calls to appropriate subroutines in the driver program of Noah LSM in order to return the changes made to the control variable (consequently, changing the model soil moisture state to reflect the data assimilation results).

In our case, the tangent linear of J results in $\dfrac{\partial J}{\partial x}$ which, given the fact that x is one-dimensional (formulas (2.5) to (2.7)), can be calculated explicitly with the tangent linear model rather than through the use of the adjoint model. Since J uses the model in its computation, the gradient of J uses the tangent linear version of the model. The validation of the tangent linear was done by verifying that the series of $\dfrac{J(x_o + \Delta x) - J(x_o)}{\Delta x}$ for decreasing magnitudes of Δx converges to the tangent linear computation of $\dfrac{\partial J}{\partial x}$ at $x=x_o$.

Chapter 3

Description of the Noah Land Surface Model (Noah LSM)

The land-surface model used in this dissertation is the "Noah LSM" (Ek et al., 2003) of NCEP. The Noah LSM evolved from the land component of the Oregon State University (OSU) 1-Dimensional Planetary Boundary Layer (PBL) model (Ek and Mahrt, 1991). It began with the coupling of the Penman potential evaporation approach of Mahrt and Ek (1984) to the multilayer soil model of Mahrt and Pan (1984) and Pan and Mahrt (1987), with addition of a canopy evaporation-transpiration formulation (Jacquemin and Noilhan, 1990; Jarviz, 1976). Further refinements and modifications of the Noah LSM were accomplished by EMC/NCEP and OH/NOAA, including the addition of the surface runoff component from the simple water balance (SWB) model of Schaake et al. (1996) and the snow and frozen ground parameterization of Koren et al. (1999-A). Descriptions of the model during its evolution at NCEP in the 1990's and early 2000's are given in Chen et al. (1996), Koren et al. (1999-A) and Ek et al. (2003).

As it evolved at EMC/NCEP, the Noah LSM was tested and validated by the research community in both uncoupled mode, using observed surface forcing, and in a coupled mode within the NCEP mesoscale Eta model. The uncoupled validations include simulations ranging in length from several months to several years at both single sites in column mode (Luo et al., 2003-A) or across regional (Mitchell et al., 2004) and global domains (Dirmeyer et al., 2002). The coupled validations in the Eta model include Berbery et al. (2003), Betts et al. (1997), Marshall (1998), and Ek et al. (2003).

Some of the previous assessments of the Noah LSM are intercomparisons with other land surface models, indicating that the Noah LSM performs well, falling consistently within the best performing models. Among the most recent, Berbery et al. (1998) compared monthly mean surface fluxes over the entire U. S. domain, from four different models, including the coupled Eta/Noah model. For a list and

description of the coupled and uncoupled validation works on the EMC/NCEP land surface model, see Mitchell et al. (2004) and Ek et al. (2003).

In the present work, we have also conducted major model validation experiments using this model in an uncoupled column mode. Our validation work is discussed in sections 5.1 and 5.4.2.

3.1   Water component

The prognostic equation for the volumetric soil moisture content (θ) follows the Darcy equation for soil hydraulics:

$$\frac{\partial \theta}{\partial t} = \frac{\partial}{\partial z}\left(D(\theta)\frac{\partial \theta}{\partial z} \right) + \frac{\partial K(\theta)}{\partial z} + F_\theta \qquad (3.1)$$

where

$D(\theta)$ is the soil water diffusivity (governs the diffusive flow that vertically distributes soil moisture among adjacent regions of the soil column),

$K(\theta)$ is the hydraulic conductivity (governs the downward vertical drainage) and

F_θ is the soil water sources and sinks (evaporation from the soil surface, transpiration via intake from plant roots and infiltration of precipitation).

Both K and D are functions of the soil moisture content (θ)

3.1.1   Surface Water Budget

Integrating (3.1) over each soil layer and expanding F_θ we have:

$$dz_1\frac{\partial \theta_1}{\partial t} = -\left[D(\theta)\frac{\partial \theta}{\partial z} \right]_{z_1} - K(\theta)_{z_1} + I - E_{dir} - E_{t_1} \qquad (3.2a)$$

(first soil layer)

$$dz_i \frac{\partial \theta_i}{\partial t} = \left[D(\theta) \frac{\partial \theta}{\partial z} \right]_{z_{i-1}} - \left[D(\theta) \frac{\partial \theta}{\partial z} \right]_{z_i} + K(\theta)_{z_{i-1}} - K(\theta)_{z_i} - E_{t_i} \qquad (3.2b)$$

(soil layers i=2,3)

$$dz_4 \frac{\partial \theta_4}{\partial t} = \left[D(\theta) \frac{\partial \theta}{\partial z} \right]_{z_3} + K(\theta)_{z_3} - K(\theta)_{z_4} \qquad (3.2c)$$

(bottom soil layer)

here, subscripts "i" refer to the soil layer numbers (1:surface...4:bottom),

dz_i is the ith soil layer thickness,

I is the surface infiltration $= P_d\text{-}R_1$,

P_d is the precipitation not intercepted by the canopy,

R_1 is the surface runoff,

E_{dir} is the direct evaporation from the top soil layer, and

E_t is the canopy transpiration taken by the canopy roots in the soil layer (the root zone covers up to four layers).

In the absence of snow cover, the total evaporation, E, is the sum of the direct evaporation from the top shallow soil layer, E_{dir}, evaporation of precipitation intercepted by the plant canopy, E_c, and transpiration via the roots, E_t, i.e., $E = E_{dir} + E_t + E_c$. The direct evaporation from the ground surface is:

$$E_{dir} = (1 - \sigma_f) \text{MIN} \left\{ \left(-\left[D(\theta) \frac{\partial \theta}{\partial z} \right]_{z_1} - K(\theta)_{z_1} \right), E_p \right\}, \qquad (3.3)$$

where,

Ep   is the potential evaporation calculated by a Penman-based energy balance approach including a stability-dependent aerodynamic resistance (Mahrt and Ek, 1984), and

σ_f is the fraction of green vegetation cover.

3.1.2 Canopy Evaporation:

The wet canopy evaporation is determined by

$$E_c = \sigma_f E_p \left(\frac{W_c}{S} \right)^n \tag{3.4}$$

where,

Wc is the intercepted canopy water content,

S is the maximum allowed capacity, chosen here to be 0.5 mm,

and $n=0.5$ as formulated in Noilhan and Planton (1989) and Jacquemin and Noilhan (1990).

The intercepted canopy water budget is governed by

$$\frac{\partial W_c}{\partial t} = \sigma_f P - D - E_c \tag{3.5}$$

where P is the input total precipitation. If W_c exceeds S, the excess precipitation (drip D) reaches the ground. Note that what reaches the ground during precipitation is $P_d = (1 - \sigma_f)P + D$.

The canopy evapotranspiration is determined by

$$E_t = \sigma_f E_p B_c \left[1 - \left(\frac{W_c}{S} \right)^n \right] \tag{3.6}$$

where B_c is a function of canopy resistance and is formulated as:

$$B_c = \frac{1 + \dfrac{\Delta}{R_r}}{1 + R_c C_h + \dfrac{\Delta}{R_r}} \tag{3.7}$$

where,

38

C_h is the surface exchange coefficient for heat and moisture,

Δ depends on the slope of the saturation specific humidity curve, and

R_r is a function of surface air temperature, surface pressure, and C_h.

Details on C_h, R_r and Δ are provided by Ek and Mahrt (1991). The canopy resistance R_c is calculated here following the formulation of Jacquemin and Noilhan (1990):

$$R_C = \frac{RS_{MIN}}{LAI * RC_S * RC_T * RC_Q * RC_{SOIL}} \qquad (3.8a)$$

where,

RS_{MIN} is the minimum allowed stomatal resistance,

LAI   is the leaf area index,

RC_S is the contribution due to incoming solar radiation,

RC_T is the contribution due to air temperature at first model level above ground,

RC_Q is the contribution due to vapor pressure deficit at first model level,

RC_{SOIL} is the soil moisture dependent contribution to plant transpiration stress factor.

RC_{SOIL} is calculated as the layer thickness-weighted average of the function $Gx(\theta)$ over all layers that contain plant roots, given by

$$RC_{SOIL} = \sum_{k=1}^{N_{root}} Gx(\theta_k)\left(\frac{dz_k}{z_{root}}\right) \qquad (3.8b)$$

In which $Gx(\theta_k)$ is given by

$$Gx(\theta_k) = \frac{\theta_k - \theta_{WLT}}{\theta_{REF} - \theta_{WLT}} \quad \text{subject to: } 0 \leq Gx \leq 1 \qquad (3.8c)$$

where,

θ_k volumetric soil moisture at soil layer k,

θ_{WLT} wilting point,

θ_{REF} reference soil moisture for plant transpiration stress onset,

N_{root} number of soil layers containing roots,

dz_k thickness of the kth soil layer, and

z_{root} depth of the bottom of the deepest soil layer containing plant roots.

Figure 3-1 illustrates the dependence of Gx with the soil moisture content, θ. Gx is maximum (equal to 1) when θ is equal or greater than θ_{REF} contributing to increase B_c and, consequently, the evapotranspiration, E_t in (3.6).
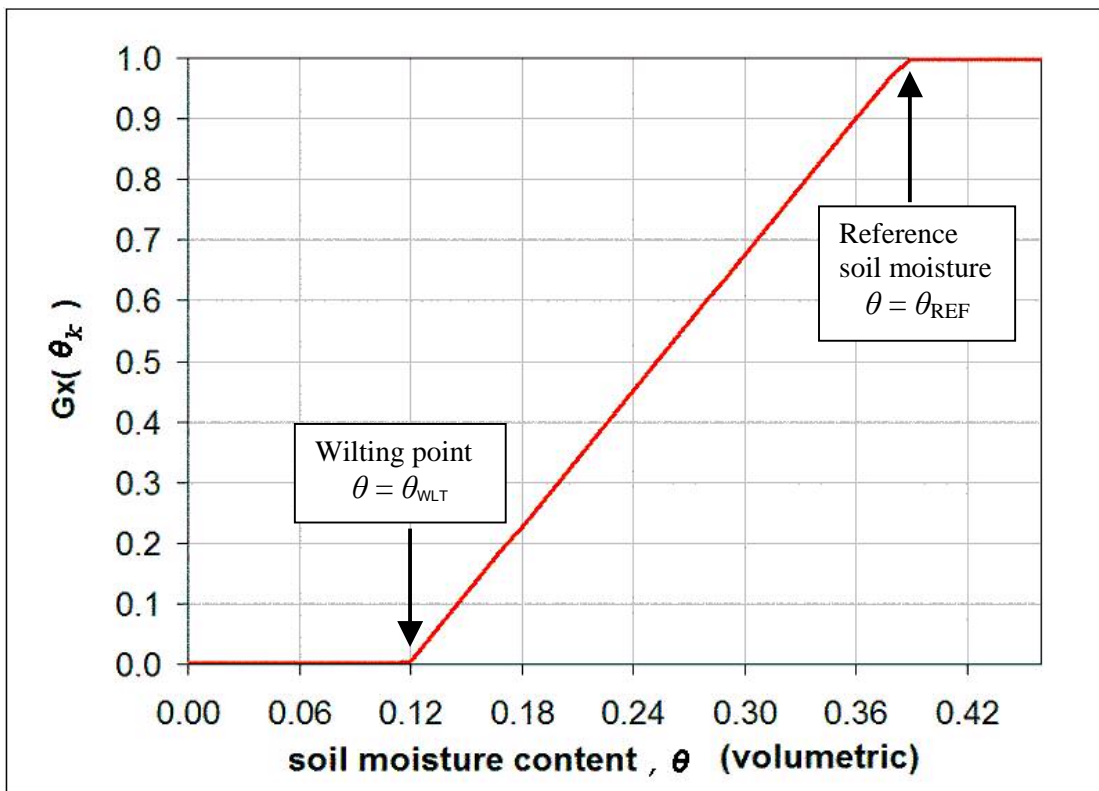
Figure 3-1 Soil moisture stress factor in the plant transpiration, E_t (example).

40

3.2 Energy component

The energy component of the Noah LSM (covering sensible, latent and soil heat fluxes) calculates the energy fluxes at the topmost soil-surface and internal soil heat flow in the soil column.

3.2.1 Relationship between Soil Moisture Content and Land Surface Temperature

The land surface temperature (T_S) is obtained in the model as the solution of the surface energy balance equation. It includes the upward terrestrial radiation (from the soil surface and plant canopy as a single aggregated entity) from the Stefan-Boltzmann equation $L\uparrow = \varepsilon\sigma(T_S)^4$, where, $L\uparrow$ is the upward terrestrial radiation (in W/m^2), σ is the Stefan-Boltzmann constant (in W m^{-2} K^{-4}), ε is the surface emissivity and T_S is the model land surface temperature (LST, in Kelvin units).

The surface energy balance (see schematic in Figure 3-2) that is solved for T_S is given by

$$(1-\alpha)S\downarrow + L\downarrow - \varepsilon\sigma(T_S)^4 = G + H + L_e \tag{3.9}$$

where

α is the surface albedo,

$S\downarrow$ is the downward solar radiation (W/m^2),

$L\downarrow$ is the downward long-wave radiation (W/m^2),

ε is the surface emissivity coefficient is assumed to be 1.0 in Noah LSM in snow-free conditions,

G is the soil heat flux (W/m^2),

H is the sensible heat flux (W/m^2), and

L_e is the latent heat flux (W/m^2).

The sensible heat flux, in turn, also bears a relationship with the land surface temperature:

$$H = \rho_o c_p C_h (T_S - T_{air}) \qquad (3.10)$$

where

ρ_o is the air density (Kg/m^3),

c_p is the specific heat for air ($JKg^{-1}K^{-1}$),

C_h is the turbulent surface exchange coefficient, dependent on the wind speed at the first level above ground (m/s), and

T_{air} is the air temperature at the first level above ground (K).
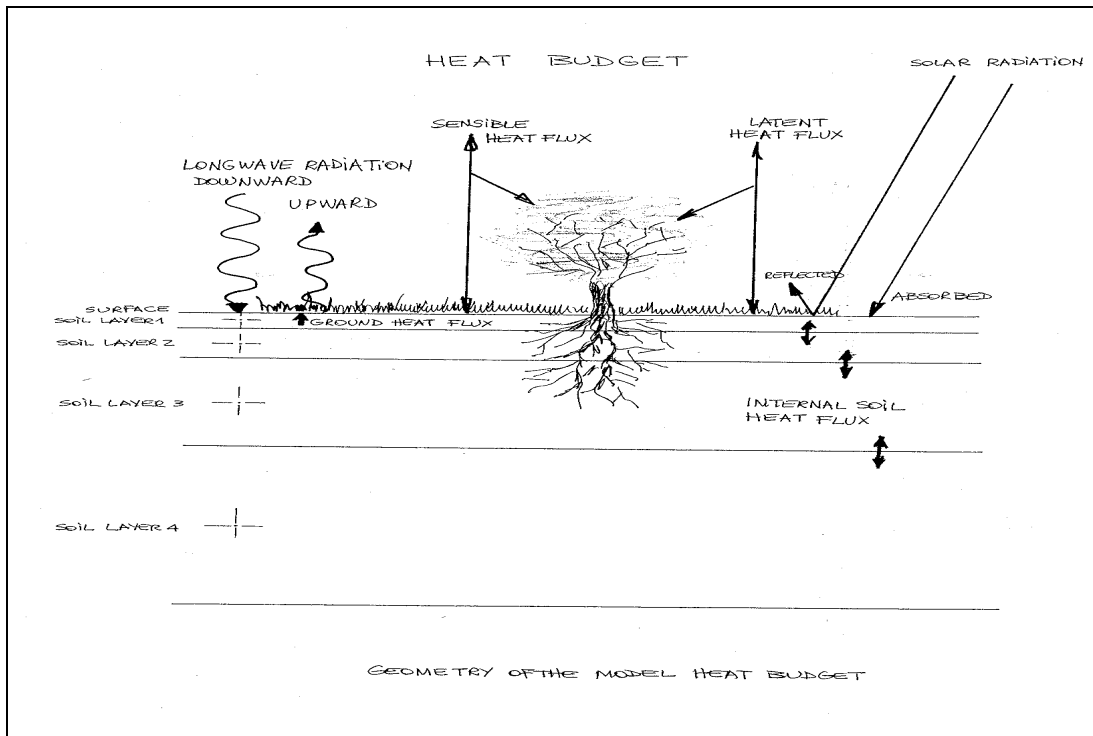
Figure 3-2 Illustration of the NCEP LSM heat budget at the surface (adapted from Ek and Mahrt (1991)).

The dependence of the land surface temperature on the soil moisture content is due to 1) the latent heat flux in the energy balance equation (3.9), and 2) the soil thermal capacity, $C(\theta)$, and soil thermal conductivity, $K_t(\theta)$ (both introduced later in

section 3.2.2), which impact the ground heat flux G in equation (3.9). The soil moisture content influences the latent heat flux through availability of water for evaporation, through the plant stomatal resistance stress factor (see equations (3.6) to (3.8) and Figure 3-1). During the warm season (i.e., without the snowpack sublimation term) the latent heat flux is equal to $L_v E$. Here L_v (J/Kg) is the latent heat of gas-liquid phase change for water and E (m/s) is the total evaporation rate, the sum of the direct evaporation, the transpiration and the canopy evaporation (see Figure 3-3 for a schematic illustration of the moisture budget):

$$E = E_{dir} + E_c + E_t \tag{3.11}$$

The direct evaporation has dependence on the soil moisture content in the upper layer and the rate by which the soil can diffuse water from below; the transpiration is affected by the soil moisture content in the root zone (layers 1-3 in present configuration) due to its stress effect on the canopy resistance.
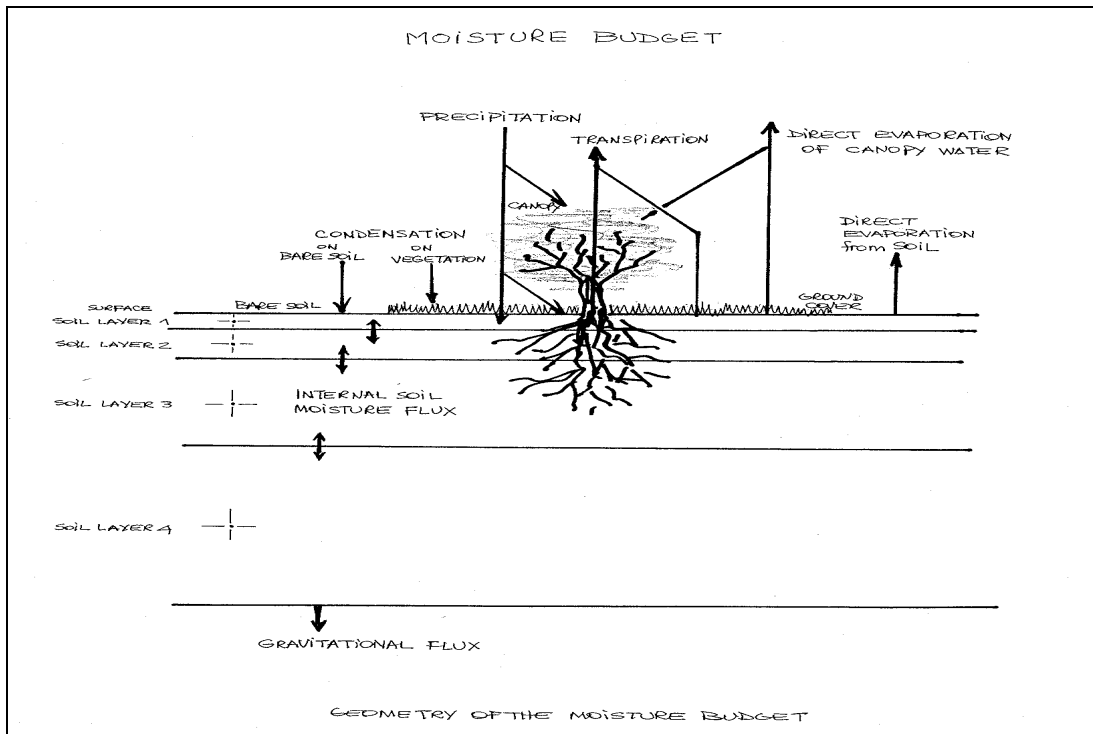
Figure 3-3 Illustration of the NCEP LSM moisture budget (adapted from Ek and Mahrt (1991)).

43

3.2.2 Surface Energy Balance

The land surface temperature is determined following Mahrt and Ek (1984) by solving an explicit linearized version of surface energy balance equation (representing the combined ground/vegetation surface) in equation (3.9). Accompanying this, the soil heat flow is controlled by the usual diffusion equation for soil temperature (T):

$$C(\theta)\frac{\partial T}{\partial t} = \frac{\partial}{\partial z}\left(K_t(\theta)\frac{\partial T}{\partial z}\right) \tag{3.12}$$

where the volumetric heat capacity C and the thermal conductivity K_t are formulated as functions of volumetric soil water content θ (fraction of unit soil volume occupied by water). The prediction of T is performed using the Crank-Nicholson scheme on the layer-integrated form of (3.12) for each soil layer.

3.2.3 Soil heat flow

The layer-integrated form of (3.12) for the i-th soil layer is:

$$\Delta z_i C_i(\theta)\frac{\partial T_i}{\partial t} = \left(K_t(\theta)\frac{\partial T}{\partial z}\right)_{z_{i+1}} - \left(K_t(\theta)\frac{\partial T}{\partial z}\right)_{z_i} \tag{3.13a}$$

The ground heat flux, G is part of this equation applied to the first soil layer:

$$G = \left[K_t(\theta)\right]_{Z_1}\left(\frac{T_S - [T]_{z_1}}{0.5*\Delta z_1}\right) \tag{3.13b}$$

3.3 Order of Computations

Here we briefly describe the model code and computations in order to help understand the variational data assimilation approach in the following chapters.

Main subroutine SFLX state variables (initialization is read from a control file, conditions should reflect state before the first time-step):

(Note: NSOIL=1 to 4 denotes each soil layer of the model.)

1. CMC........................Canopy Moisture Content (m).

2. T1 ....Ground/canopy/snowpack effective land surface temperature (K).

3. STC(NSOIL)............Soil temperature (K).

4. SH2O(NSOIL) ....Unfrozen soil moisture content (volumetric fraction).

5. SICE(NSOIL) ....Frozen soil moisture content (volumetric fraction) = smc - sh2o. SMC(NSOIL)=total soil moisture content . (volumetric fraction).

6. SNOWH..................Actual snow depth (m).

7. SNEQV ....Liquid water-equivalent snow depth (m). note: snow density equals SNEQV divided by SNOWH.

8. ALBEDO ....Surface albedo including snow effect (unitless fraction).

9. CH..........................Surface exchange coefficient for heat and moisture. (m s^{-1}); note: CH is technically a conductance since. it has been multiplied by wind speed.

From the above given settings, inputs and initial conditions, the model computes and updates the following sequence each time-step:

1. snow depth

2. snow density (accounting for new snowfall)

3. snow cover fraction

4. surface albedo (including snow cover effects)

5. soil thermal diffusivity

6. snow roughness length (currently a null/no effect process)

7. surface exchange coefficient for heat/moisture

8. potential evaporation

9. canopy resistance

10. land surface temperature updated via surface energy balance

11. direct evaporation from top soil layer

12. transpiration from vegetation canopy

13. time-rate-of-change of soil moisture

14. hydraulic conductivity and diffusivity

15. forward time-step integration of soil moisture rate-of-change (uses a tri-diagonal matrix solver)

16. soil thermal diffusivity

17. time-rate-of-change of soil temperature

18. soil thermal diffusivity (dependent on soil moist.)

19. determine soil layer interface temperature

20. heat sink/source from soil ice phase change

21. soil thermal diffusivity

22. calculate subzero unfrozen soil water (equilibrium between frozen and liquid water inside the soil for temperatures below 0^oC)

23. forward time step integration of soil temperature rate-of-change (uses a tri-diagonal matrix solver).

Chapter 4
Data Sources Utilized

The two separate data sources used for this work came from data observed at a ground-based flux station in Illinois and data extracted from the North American Land Data Assimilation System (NLDAS) (Mitchell et al., 2004) interpolated in space and time to the flux station.

4.1 Reference site flux station (Tilden Meyers site)

Dr. Tilden Meyers (Atmospheric Turbulence and Diffusion Division - ATDD / NOAA) made available atmospheric, land surface-flux, and soil data collected at a flux station at Bondville, IL. This data is used to provide the model with near ideal atmospheric forcing and validation.

The site is within 5 km of a NOAA SURFRAD site, which provides measurements of direct and diffuse shortwave radiation and the incoming and outgoing longwave components.

Site: Champaign, Illinois (near Bondville).

Latitude: 40 deg 00.366 min N

Longitude: 88 deg 22.373 min W

Elevation: approx 300 m

The variables used for forcing are (given as half-hour averages in this data set) wind speed, air temperature (3 m), relative humidity (3 m), surface pressure, incoming shortwave radiation, incoming longwave radiation and precipitation (half hour accumulation). The site also provides other half hourly data, some of which are used for validation. They are: soil or ground heat flux, land surface temperature (skin temperature), sensible heat flux and latent heat flux.

4.1.1 Filling in gaps of missing data in land surface forcing

The missing data found in the files recorded at the Bondville, IL flux station can appear in the form of long and/or short gaps with alternative data or not. Short gaps (less than four time-steps) are filled with a linear interpolation of the bracketing original data. When alternative data can be found and especially if the gaps are longer, the procedure uses the alternative data converted to represent the magnitude of the original data while using the alternative data variability, as described next:

We have two time series: $s(t)$ and $r(t)$ the first is the data to be used but contains gaps, the second one is the alternative data time series. Let's say series $s(t)$ has a gap bracketed by $t=t_1$ and $t=t_2$. The difference between series $s(t)$ and $r(t)$ at times of observations $t=t_1$ and $t=t_2$ are:

$$d_1 = s(t_1)\text{-}r(t_1) \qquad \text{and} \qquad d_2 = s(t_2)\text{-}r(t_2)$$

then, the correction $d(t)$ made to $r(t)$ for t between t_1 and t_2 will be:

$$d(t) \;=\; d_1 \;+\; \frac{d_2 - d_1}{t_2 - t_1}\,(t - t_1) \qquad\qquad \text{for } t \in \left[t_1, t_2\right] \qquad (4.1)$$

and the corrected $r(t)$ to fill the gap will be $g(t)$:

$$g(t) \;=\; r(t) \;+\; d(t) \qquad\qquad \text{for } t \in \left[t_1, t_2\right] \qquad (4.2)$$

Then the series $g(t)$ is inserted to fill the gap in $s(t)$. It matches $s(t)$ exactly at the last point before the gap ($t=t_1$) and the first point after the gap ($t=t_2$). Figure 4-1 illustrates the case of gaps in downward long wave radiation (series "LW_in" in figure), the alternative data is derived from the thermal emission of the air, i.e. it is proportional to air temperature in Kelvin raised to the fourth power (series LWDN from Ta, in figure). The segments labeled "LW_in fill" in figure represent the result of the transformation given in (4.2).
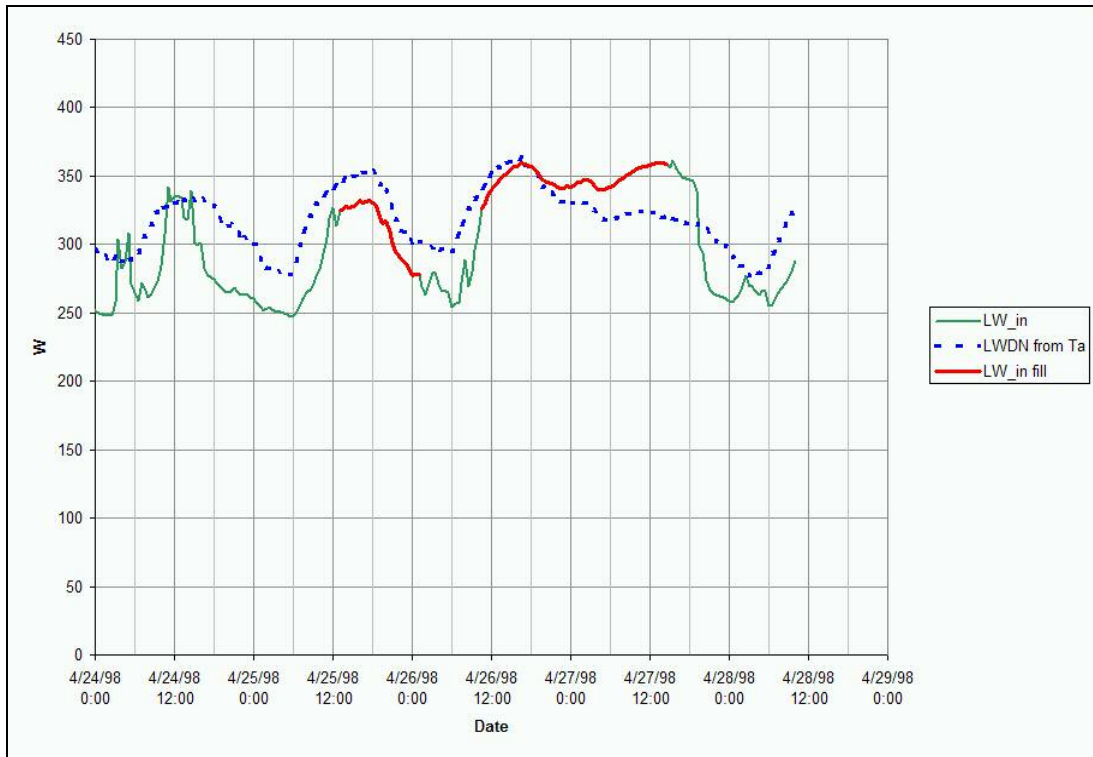
Figure 4-1 Example of filling the gaps in the necessary forcing with the use of appropriately converted alternative data.

4.2 NLDAS forcing

To have a more realistic scenario of the forcing available on a continental scale, we used the North American Land Data Assimilation System (NLDAS) data sets (see Mitchell, K. E., et al. ,2004; Cosgrove, B. A., et al. (2003) and Luo, L., et al. (2003-B) for the NLDAS project, its data and respective validation) interpolated in space and time to match the frequency and location of the surface data collected at Bondville, IL (mentioned above). This helps to provide some idea of the expected distortions in the derivation of real-time surface forcing across a large continental domain and their effect on the model's performance in conditions one step closer to the situation of operational weather forecasting, where forcing is provided by the coupled atmospheric model.

Additionally, some of the required forcing data had to be converted through subroutines that were designed so that all the demands (required input and state variables) for the call to the land surface package could be satisfied.

49

4.3   GOES land surface temperature

The GOES LST fields are included in the NLDAS data set (Mitchell et al. 2004). They are produced by the GCIP (Geostationary Satellite Products for GEWEX Continental-Scale Project) partnership of NESDIS and UMD in GOES land surface products. The retrievals are obtained from GOES-East (GOES-8) and provide fields of hourly LST at 0.5-degree spatial resolution in cloud-free conditions during daytime. The LST retrieval provides a single aggregate LST for each 0.5-degree target scene. The LST fields are bilinearly interpolated to the $\frac{1}{8}$ th-degree NLDAS grid. The GOES LST is retrieved only at 0.5-degree targets deemed 100% cloud-free. Cloud detection is based on that of earlier GOES insolation-retrieval studies such as Tarpley [1979], as refined in later studies such as Pinker et al. (2003). Despite the 100% cloud-free criteria, clouds may still be present in the scene owing to (1) optically thin cirrus, (2) subresolution or ''subpixel'' cloud (fair weather cumulus), and (3) difficulty of cloud detection over snow cover. GOES LST is retrieved by the so-called ''split-window'' technique of Wu et al. (1999), in which LST is obtained from a linear regression of the GOES brightness temperatures in the 11 mm and 12 mm bands. The regression coefficients were derived assuming a surface emissivity of $\varepsilon = 1$. This assumption is valid over land surfaces of non-sparse vegetation or snow-pack, but less valid over rather bare soils (wherein $\varepsilon = 0.91$–0.97). Uncertainty from emissivity issues is avoided in this study by staying over non-sparse vegetation and by our application of $\varepsilon = 1$ in (1) the Noah model and (2) the GOES retrievals. Examples of validation of the GOES LST retrievals against LST measurements at surface flux stations is given in Mitchell et al., (2004).

Chapter 5

Evaluation and Improvement of the Noah Land Surface Model Performance

As described in Chapters 1 and 3, this work applies the Noah Land Surface Model and part of the work in this thesis consisted of the contributions that brought the model to the version used in the experiments.

The following changes were made in preparation for this research, in order to have this new version of the Noah model source code running and validated with the new data. Some of these changes were necessary in order to make the source code suitable for automatic adjoint application. The new code, with the snow and frozen soil parameterizations, (Koren et al., 1999-A) needed to receive the updates I had already prepared for the previous version (Chen F. et al., 1996). The task of including in the new version the upgrades done to the previous one had to be performed carefully to avoid conflicts with this new version. In addition, the replaced or modified subroutines were tested against the new ones to ensure similar or better behavior and performance.

One of the major advantages of the first implemented updates was the elimination of 1600 lines of tables used by a look-up function. The solution obtained was the replacement of this function by a new one containing the appropriate formulas at an equal or greater precision without an increase in computational time.

Other modifications include the preparation of a more documented and appropriate control-file, the modification and rearrangement of array declarations and the argument section of subroutines to make the program acceptable by our local machines' Fortran compiler.

To run the package off-line, it is necessary to have a driver program to read the control file, lower atmosphere surface forcing, precipitation forcing, radiation forcing, calculate variables not directly available, convert units if necessary, and make the call to the land surface package subroutine in a time loop.

5.1 Improved physics

Victor Koren (1999-A) showed that frozen soil has an effect on the precipitation-runoff partitioning during flood events, on the soil hydrology and on soil thermal properties and fluxes. He devised the subroutines to include a physically based representation of cold season processes in the Noah Land Surface Model. The extensions include the effects of frozen ground, patchy snow cover, and temporal-spatial variability in snow properties. In the research for this dissertation, the validation experiments indicated that the model's ground heat flux was greater than the observed (Figure 5-1) while the sensible heat flux was smaller than the observed (Figure 5-2).
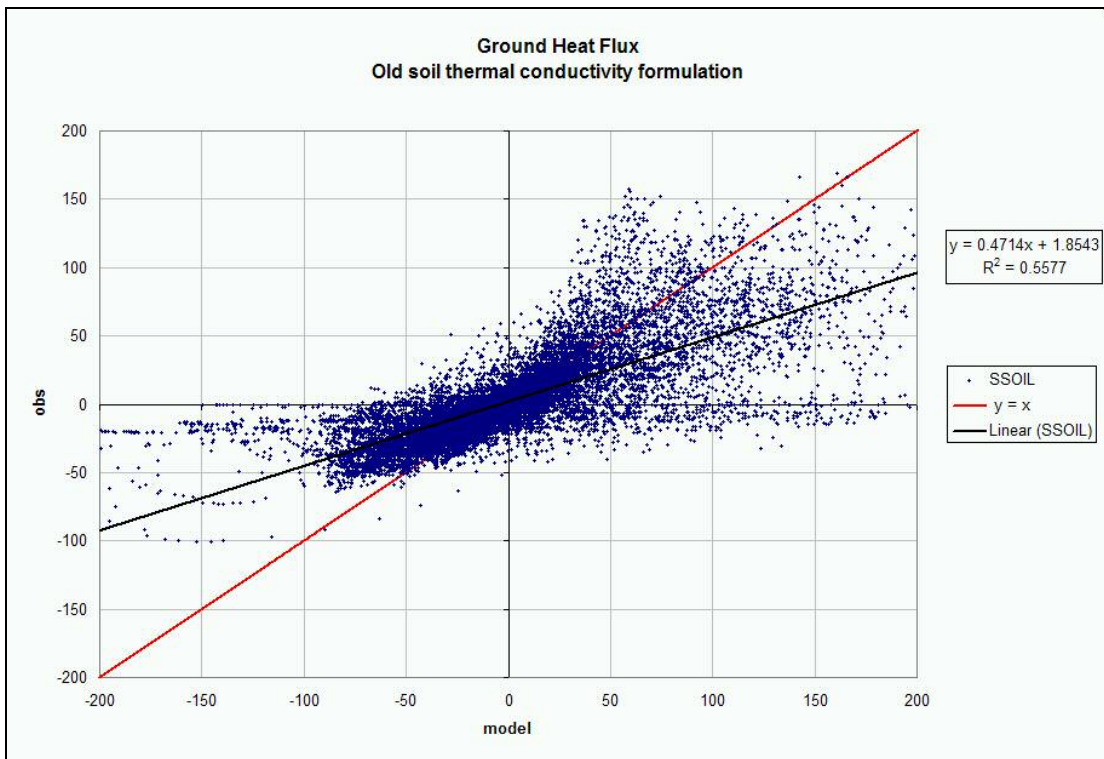
Figure 5-1 Ground heat flux (W/m^2) for the model versus observations using the old soil thermal conductivity formulation.
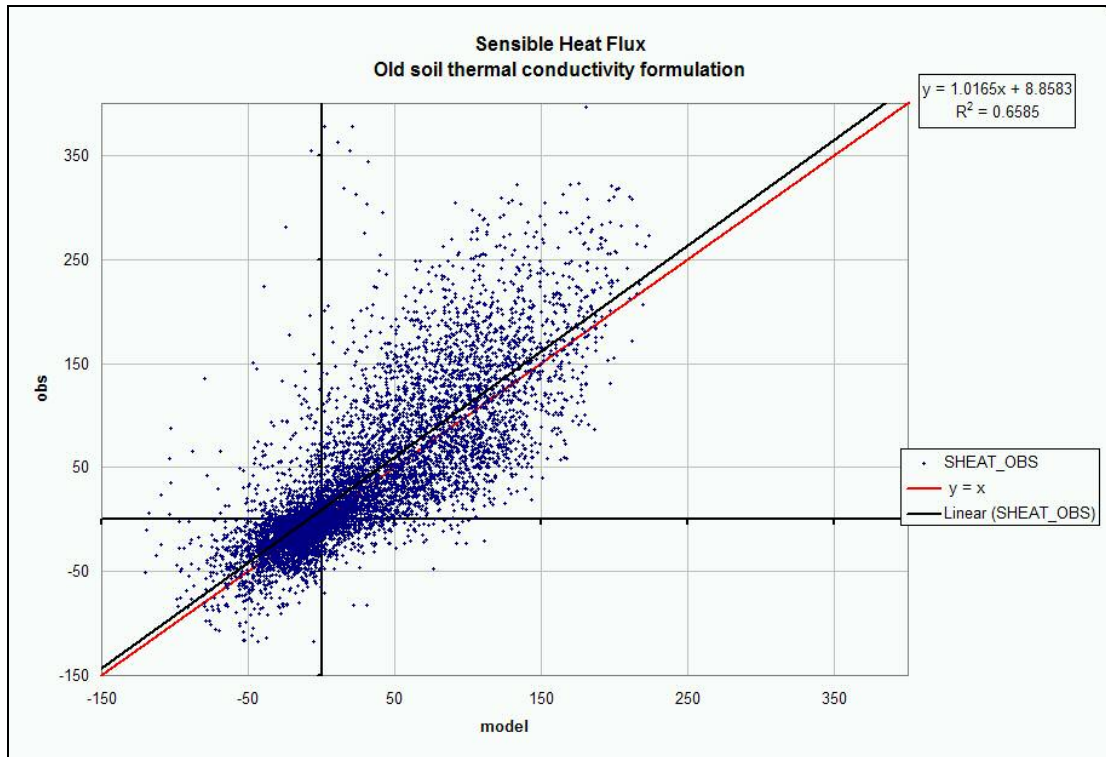
Figure 5-2 Sensible heat flux (W/m^2) for the model versus observations using the old soil thermal conductivity formulation.

The above results, in combination with similar published results obtained in the PILPS-2c (Liang, X.et. al., 1998) test and the coupled Eta model study of Marshall (1998), revealed the existence of problems in the ground heat flux because of the function applied to calculate soil thermal conductivity. Thus, a new function for the soil thermal conductivity (Peters-Lidard, et al., 1998) was adopted. A new subroutine was coded for the soil thermal conductivity, and it was tested against the old one (Figure 5-3). The original function in the old subroutine would produce a change from minimum to maximum values of conductivity within a small interval of the soil moisture range, while the new function gives a gradual variation of conductivity for the whole range. For the months covered by the experiments, soil moisture was moderate to high. As a result, the old subroutine would compute an excessively high conductivity, leading to an increased ground heat flux and a compensation impact on sensible and latent heat flux. The Peters-Lidard approach for soil thermal conductivity is supported by field measurements (Peters-Lidard et al., 1998). As shown in Fig. 5-3, the old formulation tends to underestimate thermal

conductivity for dry soils while overestimating it for moist soils due to its "step-like" features. The new formula produces a more gradual change of soil thermal conductivity as a function of soil moisture content.
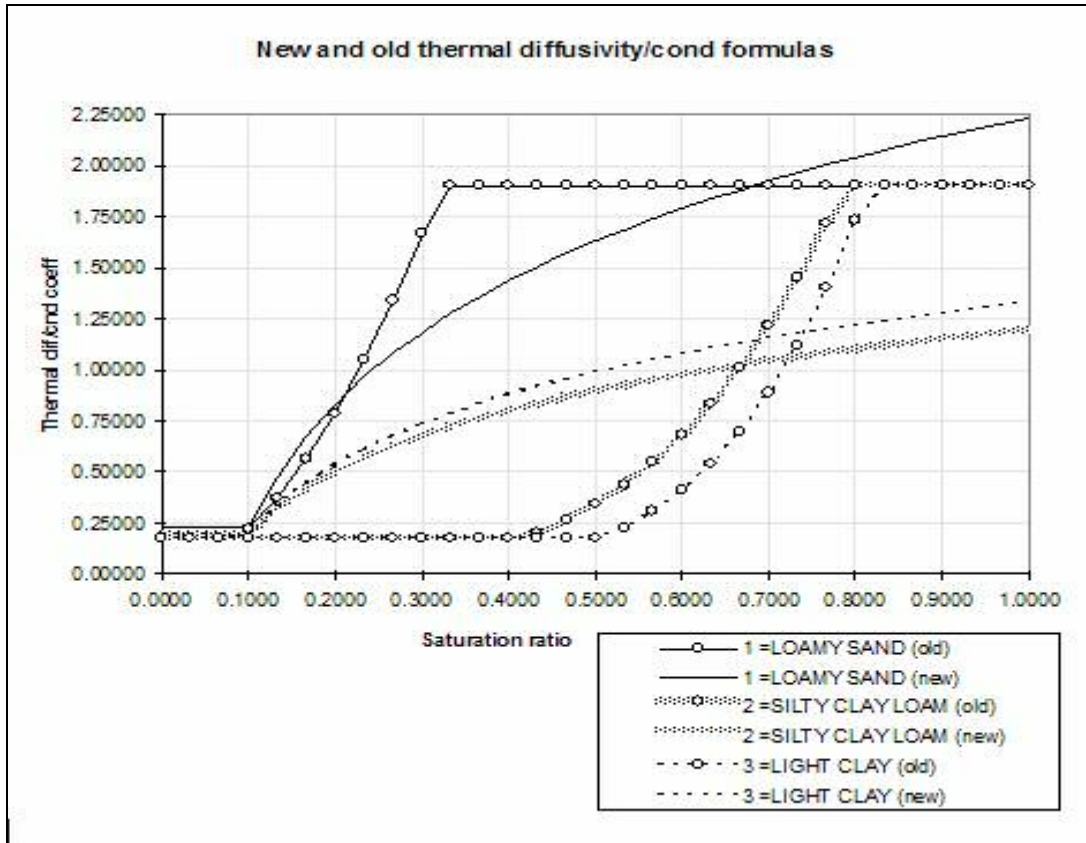
Figure 5-3 Soil thermal conductivity as calculated by the new subroutine compared to the old one (marked with circles) for three main types of soils (marked with specific line-types).

As new data were coming from the Bondville site, we enlarged our data set enough to perform a spin up initialization using a one-year cycle, plus a control experiment using the following year data. All of this was run with the latest improvements incorporated in the model.

5.1.1 Soil drainage

During the runs conducted to test the model it was found necessary to verify the behavior of the calculated hydraulic conductivity and diffusivity as it depends strongly on soil type and soil moisture (Figure 5-4 and Figure 5-5). Drainage experiments were performed with the model in which, starting from a near maximum

soil moisture condition, the model is executed for long periods of time (more than one year) without the effects of precipitation, evaporation or soil water diffusion, thus isolating the effect of gravitational drainage. A problem was found leading to an unrealistic drainage from the first layer (Figure 5-6), which was corrected (Figure 5-7). In Figure 5-6 the effects of gravitational drainage have been isolated, showing the unrealistic drainage due to the original problem in the code. The first soil layer would quickly lose its moisture content, which would pass through layers 2 and 3 until collected by layer 4. Figure 5-7, where the effects of gravitational drainage have been again isolated by turning off precipitation, evaporation and diffusion, shows that after the problem was corrected, the new results have the expected behavior.
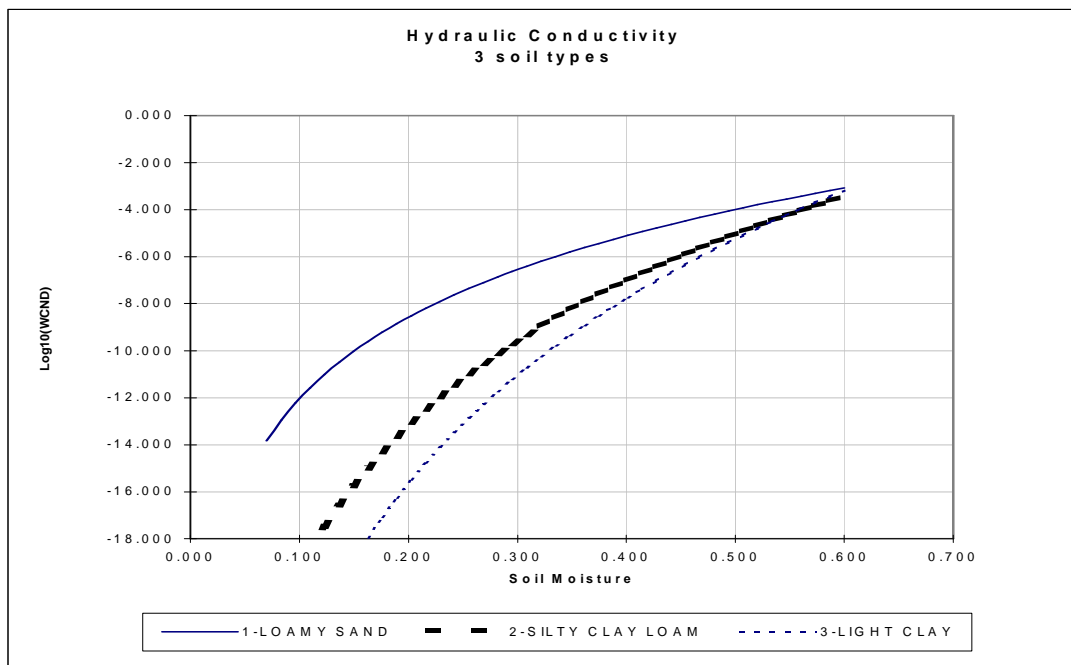
Figure 5-4 Hydraulic conductivity K(θ) (logarithmic scale), for 3 soil types, as a function of soil moisture content (volumetric).
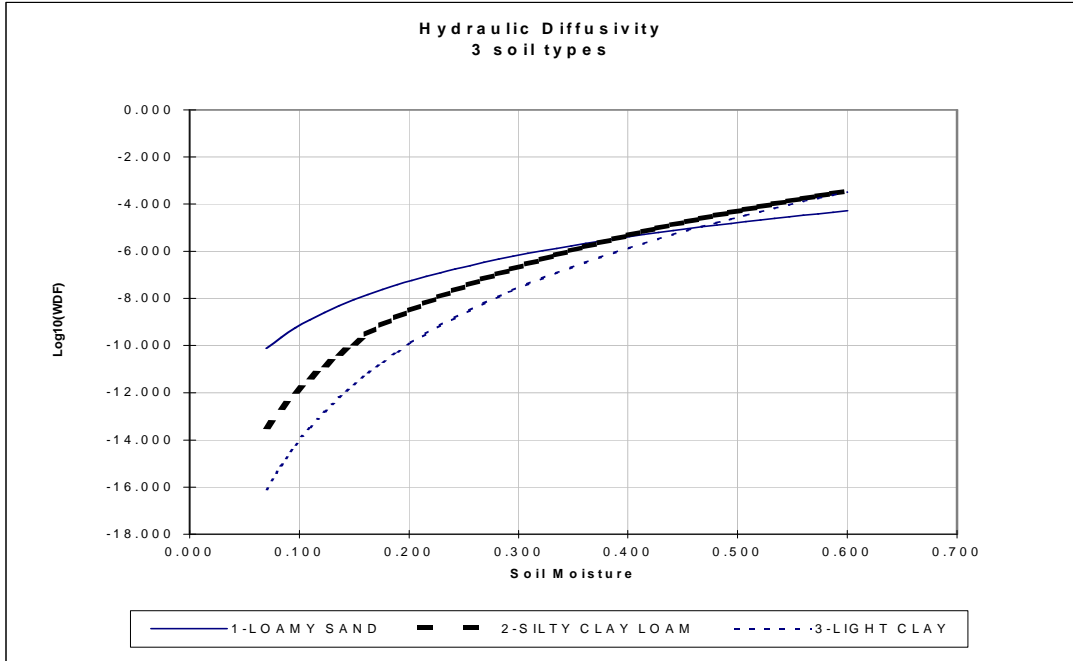
Figure 5-5 Hydraulic diffusivity D(θ) (logarithmic scale), for 3 soil types, as a function of soil moisture content (volumetric).
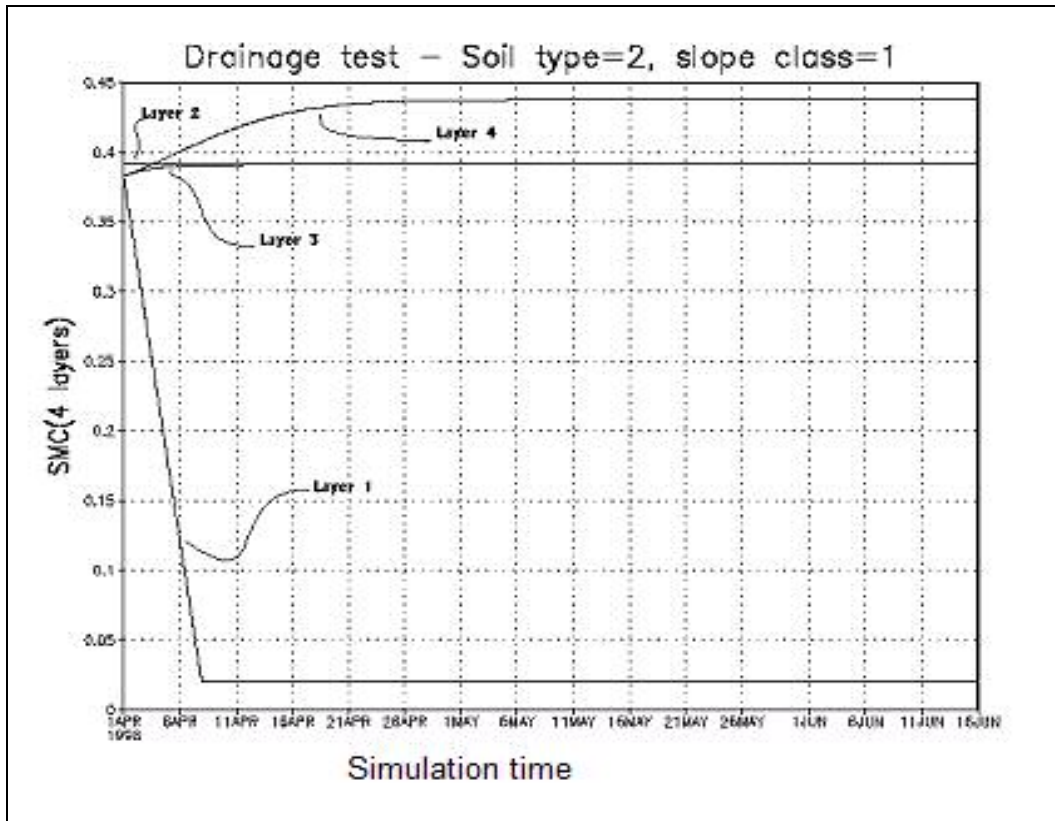
Figure 5-6 Drainage test with the old code, isolating the gravitational effects.
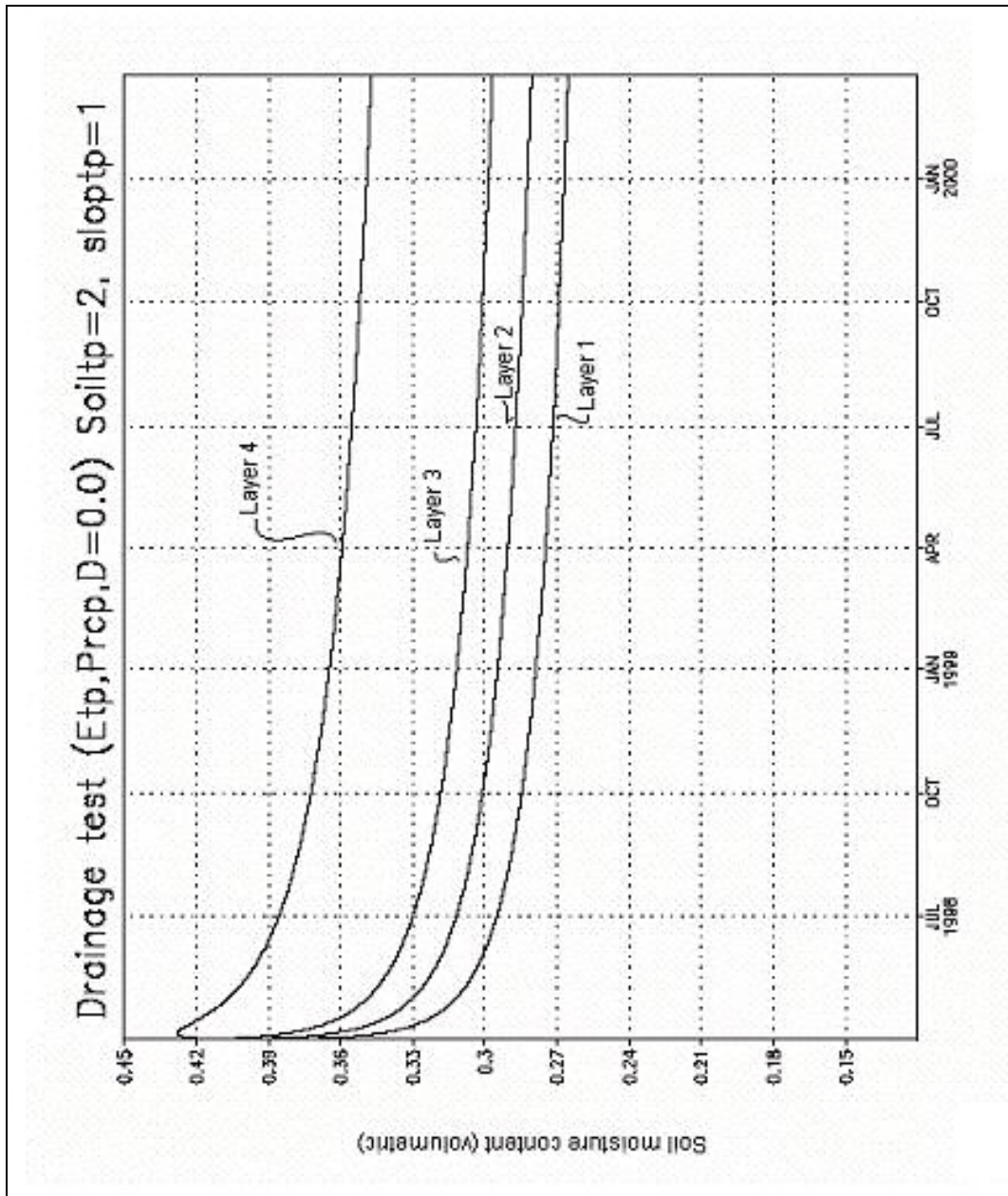
Figure 5-7 Drainage test with the corrected code.

5.1.2 Frozen soil state iteration

The subroutine FRH2O in the Noah LSM calculates the amount of water in the soil that remains unfrozen when the temperature is below the freezing point (supercooled liquid content due to adsorption of the water molecules to soil particles). It solves the following implicit equation (5.1) for θ_{ice} iteratively (from which one obtains $\theta_{liquid} = \theta_{total} - \theta_{ice}$) by the Newton method:

57

$$\frac{g\,\psi_s}{L}\,(1 + c_k\,\theta_{ice}\,)^2\,(\frac{\theta - \theta_{ice}}{\theta_s}\,)^{-b} - \frac{T}{T + 273.16} = 0 \qquad (5.1)$$

where

g   is the acceleration of gravity,

ψ_S is the soil water potential,

L   is the latent heat of fusion,

c_k is a parameter that accounts for the effect of increase in specific surface of soil minerals and ice-liquid water,

θ is θ_{total}, the total soil moisture content,

θ_s is the saturation soil moisture content,

b   is a parameter in Campbell's approximation [1974] for ψ, and

T   is the temperature in Celsius degrees.

       In the case of this function, the solution to F(x)=0 might be located in a region where the graph of the function is parallel to the abscissas, causing difficulties for the Newton solver. To overcome this problem, F(x) was substituted by L(x), a transformation of F(x) such that the solution to F(x) coincides with the solution to the transformation, L(x), for the useful range of x (θ_{ice}). The useful range of θ_{ice} is given as: $0 \le \theta_{ice} < \theta_{total}$ (frozen portion can only be positive and less than 100% of the total soil moisture). When the solution is negative ($\theta_{ice} < 0$, unphysical), it is interpreted as not having potential for any frozen content so it is equal to zero. The method's search for the solution equals locating the crossing of the abscissas by the function (see Figure 5-8). The function L(x) is obtained by putting (5.1) in the form:

$$\frac{g\,\psi_s}{L}\,(1 + c_k\,\theta_{ice}\,)^2\,(\frac{\theta - \theta_{ice}}{\theta_s}\,)^{-b} = \frac{T}{T + 273.16} \qquad (5.2)$$

and taking the logarithm from both sides of the equality, to obtain

$$\log\left[\frac{g\,\psi_s}{L}\,(1+\,c_k\,\theta_{ice}\,)^2\,(\,\frac{\theta\,\text{-}\,\theta_{ice}}{\theta_s}\,)^{-b}\right] = \log\left(\frac{T}{T+\,273.16}\right) \quad\quad (5.3)$$

which upon regrouping to obtain L(x)=0 yields

$$\log\left[\frac{g\,\psi_s}{L}\,(1+\,c_k\,\theta_{ice}\,)^2\,(\,\frac{\theta\,\text{-}\,\theta_{ice}}{\theta_s}\,)^{-b}\right] - \log\left(\frac{T}{T+\,273.16}\right) = 0. \quad\quad (5.4)$$

Figure 5-8 shows the graphs of the functions F(x) and L(x) illustrating how L(x) much better defines the solution by intercepting the abscissas in a much more vertical angle (the slope of L(x), given by $\dfrac{d\text{L(x)}}{dx}$, is further away from zero at the vicinity of the solution).
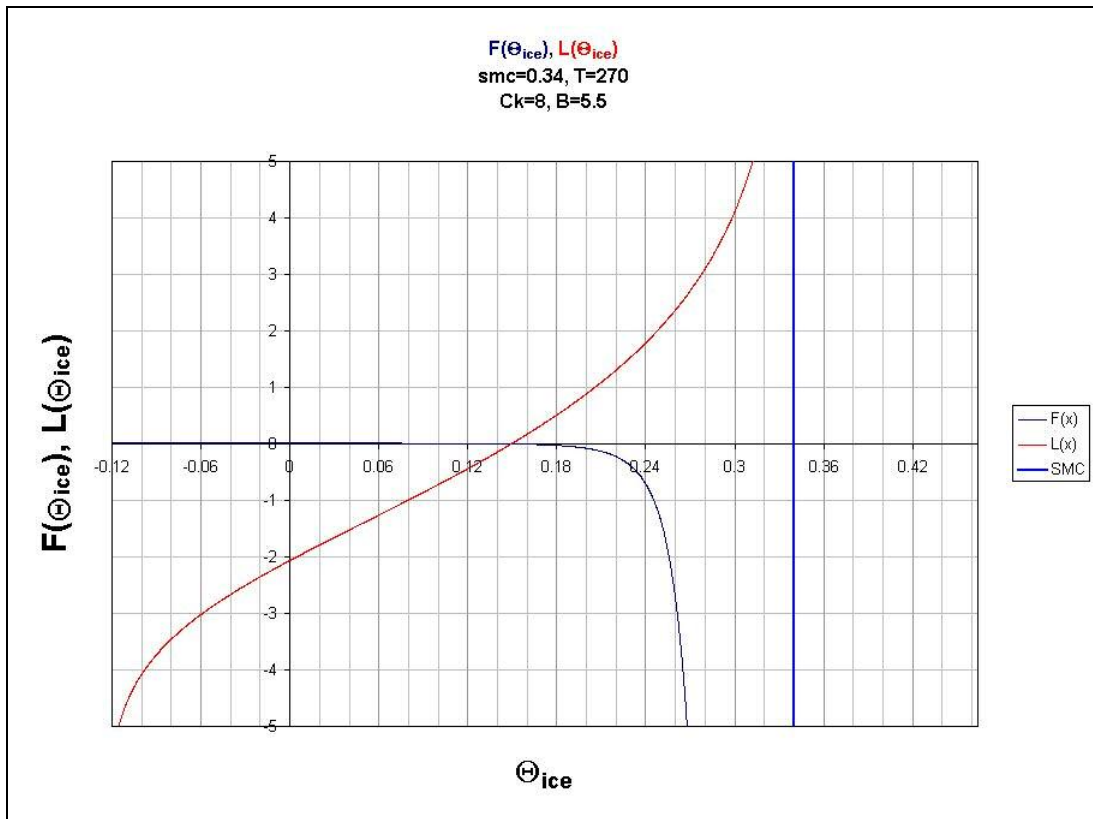
Figure 5-8 Graphs of the left hand sides of (5.1) and (5.4) as functions of frozen soil moisture content, F(θ_{ice}) and L(θ_{ice}), respectively. The vertical blue line (SMC) indicates the total soil moisture content ($\theta_{\text{total}} = \theta_{\text{liq}} + \theta_{\text{ice}}$), a line that θ_{ice} cannot cross.

Given experiences from users of the model that the convergence of the original FRH2O subroutine was slow the above solution was adopted. For comparative evaluation, results are shown here for the two methods while running the model over the year 1998 and illustrate the great reduction in computer time achieved. For a comparative evaluation, both the original and the new FRH2O subroutine were tested while the iterations required to solve the equation each time it is called (during a regular 1998 run) were recorded. First, using the original version, Figure 5-9 shows that temperatures closer to the freezing limit are more problematic owing to the issue of the solution being located in a region where the graph of F(x) was almost parallel to the abscissas.
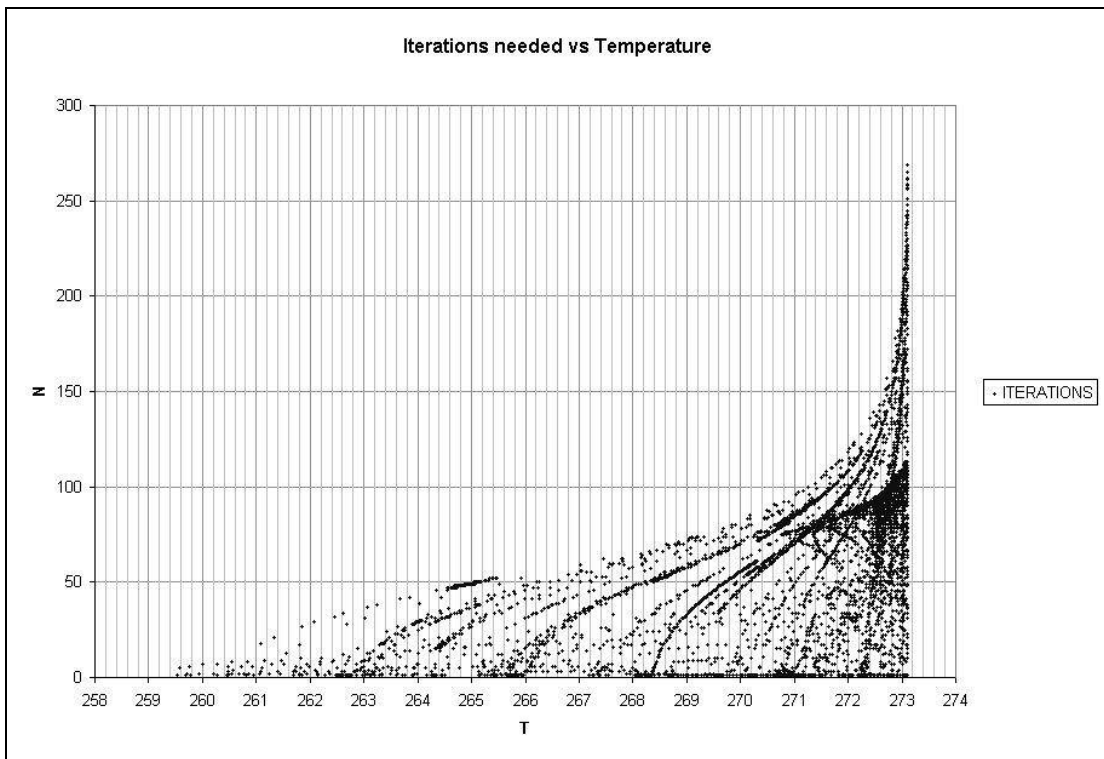
Figure 5-9 Collected events of the Newton solver calls during a regular 1-year simulation with the model and the number of iterations required for the solution organized by temperature given as input.

In a typical 1998 run, when the subroutine is called on more than 6000 events for a single location, it was commonplace for the old version to require in the range of 100

iterations to reach the solution (Figure 5-10). The new version is not only more reliable but it also reaches the solution in three iterations or less (Figure 5-11).
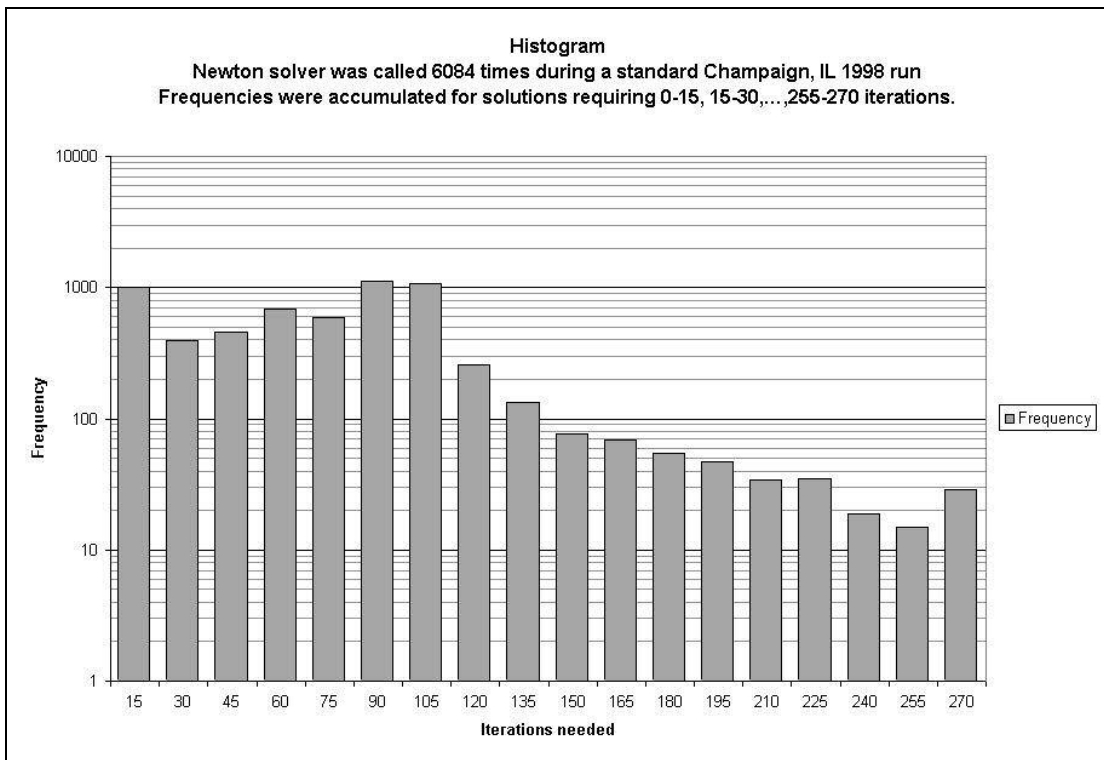
Figure 5-10 Event distribution (logarithmic scale) of all calls to the Newton solver during a regular 1-year simulation with the model by the number of iterations required for the solution.
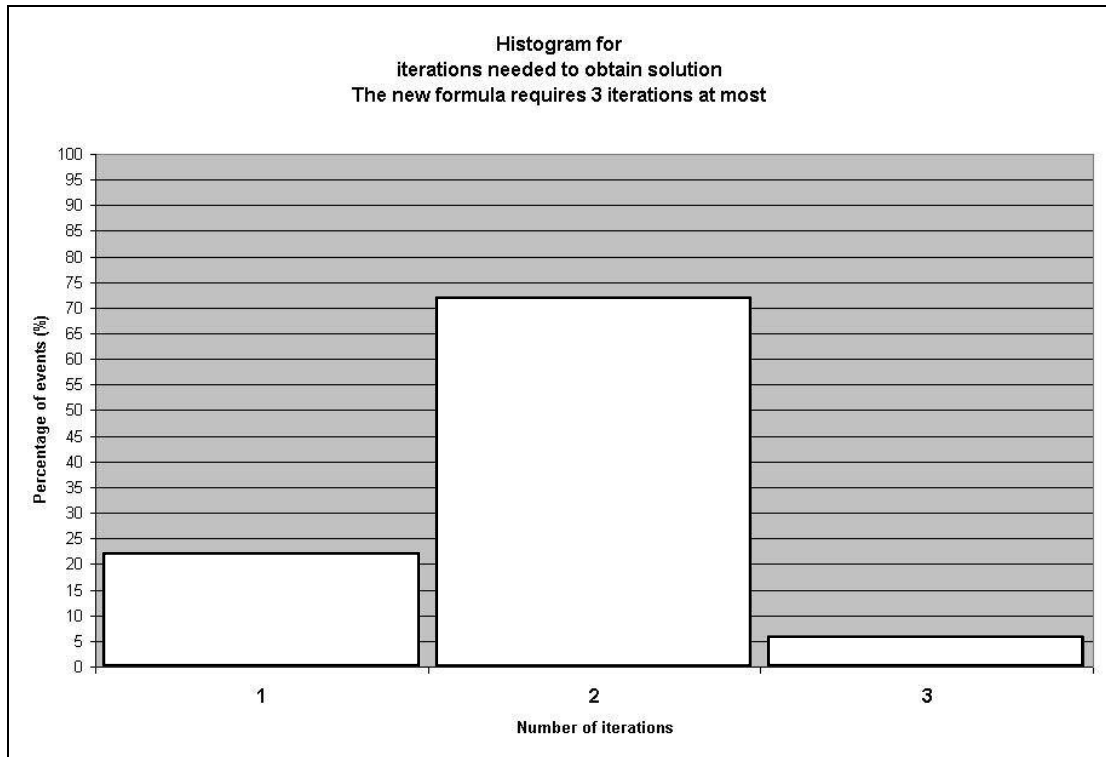
Figure 5-11 Percentage distribution of all calls to the Newton solver during a regular 1-year simulation with the model by the number of iterations required for the solution

5.2 Improved differentiability

The automatic differentiation tool TAMC (Tangent linear and Adjoint Model Compiler, Giering, R., 1997) was applied to the previous version of the model and the inadequacies of the code for automatic differentiation were corrected on that occasion, until the code was accepted and processed yielding its tangent linear and adjoint. That experience helped to develop some programming rules that are being followed in the present version. In some instances, certain functions of the code were modified to behave smoothly and to avoid non-defined derivatives, as exemplified next.

5.2.1 Example of singular behavior with certain functions in the tangent linear model, and proposed solution.

Problems were found in functions of the kind:

$$f(x) = [abs(x)]^p$$

which give rise, in the tangent linear version, to functions of this kind:

$$f'(x) = p[abs(x)]^{p-1} \cdot [abs(x)]'$$

For the above function, consider the two limits when x goes to zero from the positive side (0+) and the negative side (0-):

$$\lim_{x \to 0^+} f'(x) \qquad \text{and} \qquad \lim_{x \to 0^-} f'(x)$$

and the function $\quad abs(x) = \begin{cases} x, & x \geq 0 \\ -x, & x < 0 \end{cases}$

so, the first limit yields

$$\lim_{x \to 0^+} px^{p-1} = \begin{cases} +\infty, & p < 1 \\ 1, & p = 1 \\ 0, & p > 1 \end{cases} \quad ,$$

and the second limit yields

$$\lim_{(-x) \to 0^+} -p(-x)^{p-1} = \begin{cases} -\infty, & p < 1 \\ -1, & p = 1 \\ 0, & p > 1 \end{cases} .$$

In our case, the model was found to have functions where $p < 1$, depending on x which happens frequently to be zero, causing the derivative code (tangent linear and adjoint) to give a "division by zero" error because they require the computation of $f'(x)$, which diverges to $\pm\infty$ when $x \to 0^\pm$. Solutions to this kind of problem must take into account how $f'(x)$ is used in the derivative code, especially what is the expected value of the variables calculated using $f'(x)$ when $x = 0$ and also when x is near zero. The following illustrates one such function as an example and describes how to modify it in order to achieve a good approximation to the original while eliminating the singularities from its derivative within the actually used range of variation of x.

63

The function $E_c(W_c)$ in equation (3.4) can be written, for $n=0.5$ in the form:

$$F(x) = Cx^{1/2} \qquad (5.5)$$

where, $x = \dfrac{W_c}{S}$ has a range between 0 and 1.

$F(x)$ has no derivative for $x = 0$ (the graph of $F(x)$ is parallel to the ordinate axis at that point).

Consider the difference with using $y = x + \varepsilon$ instead of x as the input variable in the above mentioned $F(x)$, where ε is an arbitrarily chosen, small positive constant. The most important feature is that y cannot reach zero within the range of variation of x. In order for this function $F(y(x))$ to approximate our original $F(x)$, the difference between these two functions must be addressed.

This difference can be approximated by a first-order Taylor expansion of the original function. We have

$$F(x) = F(y - \varepsilon) \qquad (5.6)$$

and $F(y - \varepsilon) \approx F(y) - F'(y) \cdot \varepsilon = F_2(x)$. In this case,

$$F_2(x) = C \left[(x + \varepsilon)^{\frac{1}{2}} - \frac{1}{2} \frac{\varepsilon}{(x + \varepsilon)^{\frac{1}{2}}} \right] \qquad (5.7)$$

Unfortunately, the formula (5.7) does not meet the important requirement of matching $F(x)$ at $x = 0$, that is, does not satisfy $F(0) = 0$ which is true in (5.5). Instead, (5.7) at $x = 0$ yields

$$\boxed{F_2(0) = \frac{C}{2} \varepsilon^{\frac{1}{2}}}$$

therefore $F_2(0) \neq 0$, even though it approximates $F(x)$ in a very acceptable manner elsewhere. To solve this problem, F_2 is changed by the inclusion of a correction

factor. This must smoothly change the function to make it equal to zero when x=0 without producing much change in the rest of the *x* range. This correction factor, utilized here is $\left(1 + \dfrac{\varepsilon}{(x+\varepsilon)}\right)$, which multiplies the second term of F_2 (compare formula (5.7) to formula (5.8) and causes greatest effect when x=0 but tends to neutralize itself for greater values of x

$$F_2(x) = C\left[(x+\varepsilon)^{\frac{1}{2}} - \frac{1}{2}\frac{\varepsilon}{(x+\varepsilon)^{\frac{1}{2}}}\left(1 + \frac{\varepsilon}{(x+\varepsilon)}\right)\right] \tag{5.8}$$

This formula satisfies the constraint of having $F_2(0) = 0$ and fits the original formula very well elsewhere.

5.3   Vertical diffusion of soil water during freezing

On occasions during the freezing season, the original version of the Noah LSM would exhibit large vertical transfer of water from warmer soil layers with predominantly liquid water content to adjacent colder layers with significant frozen content. The magnitude and swiftness of these transfers prompted questions about the physical validity of those effects given the possibility that the vertical and temporal resolution set for the model could be too coarse to properly represent this process. The water diffusion/conduction scheme was examined. First, we know that the water diffusivity depends strongly on soil moisture content. Second, the current approach (Koren et al., 1999-A, hereafter referred to as VK) calculates the soil water diffusivity *D(θ)* in equation (3.1), denoted here as *WDF* for partially frozen soil using the same function as in the unfrozen case except that only the liquid (unfrozen) content is taken into account (5.9).

$$WDF_{VK} = WDF(\theta_{liq}) \quad \text{where} \quad \theta_{liq} = \theta_{total} - \theta_{ICE} \tag{5.9}$$

For the model four soil layers, that could represent a large vertical gradient of diffusivity because adjacent soil layers can have a very different fraction of frozen content, especially when one layer freezes while the others are still melt or vice-versa.

To limit the transfer in the presence of frozen soil, one of the tested alternatives, the "D" approach, formula (5.10),

$$WDF_D = \begin{cases} WDF_{VK} & for \quad \theta_{ICE\,max} < Threshold \\ WDF(0.2) & for \quad \theta_{ICE\,max} \geq Threshold \end{cases} \tag{5.10}$$

constrains severely the diffusivity coefficient when the frozen soil moisture content in any layer is greater that a small non-zero threshold by setting the diffusivity to the one corresponding to a soil moisture volumetric fraction of 0.2. This leads to the problem of an abrupt change (discontinuous first derivative in the function WDF_D) as soil moisture freezes and consequently spoils differentiability and arguably yields an overly strong departure from the expected behavior of a physically based simulation of the process. The final approach that was chosen (WDF_W - "weighted approach" in formulas (5.11)) uses both the original (WDF_{VK}) and the "D" (WDF_D) functions but weights them in a way that it matches the original approach in value and first derivative at the freezing threshold (Figure 5-15) and falls rapidly but smoothly towards the "D" calculated values as soil freezing increases (Figure 5-14). The formulations for these weights are given in formulas (5.12) and their respective graph is in Figure 5-12. The general behavior of the functions given by the three approaches can be seen in Figure 5-13.
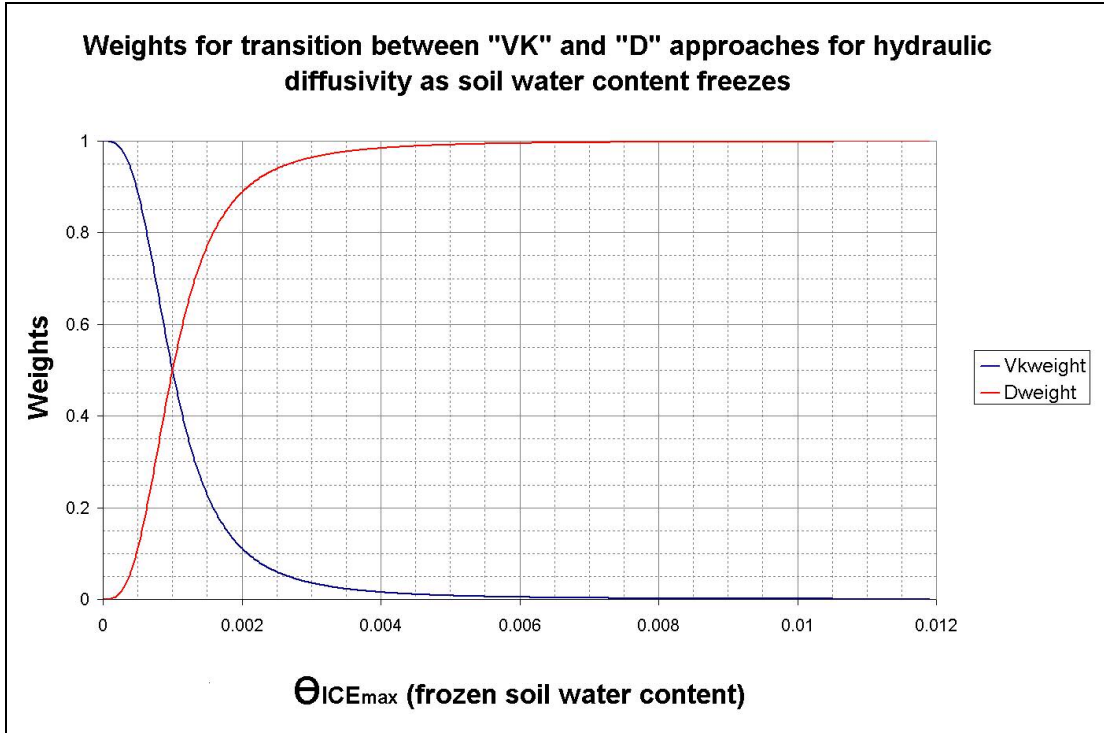
Figure 5-12 Weights for transition from the unfrozen to the partially frozen hydraulic diffusivity behavior as function of the presence of volumetric frozen soil water content.

$$WDF_w = \begin{cases} WDF_{VK} & for \quad \theta_{ICE\,max} = 0 \\ (VK_{weight}WDF_{VK} + D_{weight}WDF_D) & for \quad \theta_{ICE\,max} > 0 \end{cases} \tag{5.11}$$

$$VK_{weight} = \frac{1}{1 + (C_1 * Sice)^{p_1}} \tag{5.12}$$

$$D_{weight} = 1 - VK_{weight}$$

where C_1 and p_1 are constants chosen to manipulate the shape of the function.
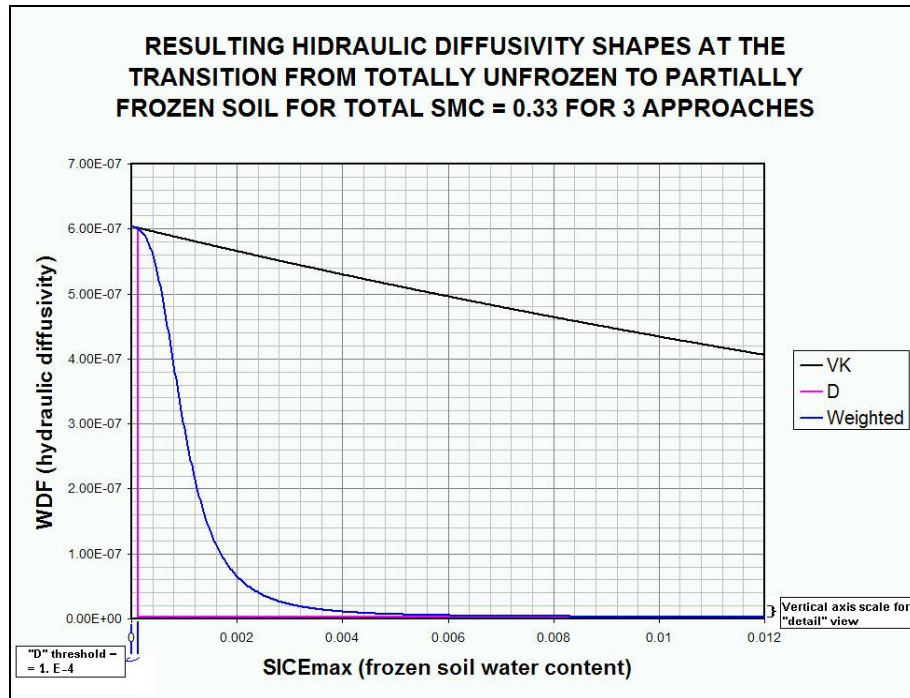
Figure 5-13 Resulting hydraulic diffusivity at the transition from unfrozen to partially frozen soil for the old (VK), step (D) and the new (Weighted) approaches.
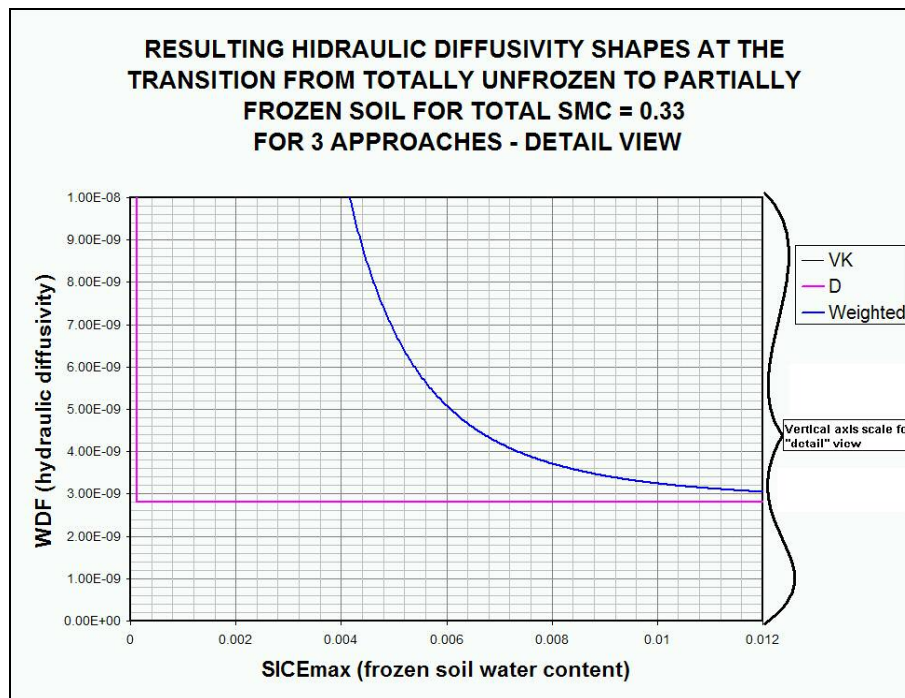
Figure 5-14 Magnification of the ordinates' axis of Figure 5-13 showing the strong adherence of the weighted approach to the magnitudes prescribed by the D approach as soil moisture content freezes.

68
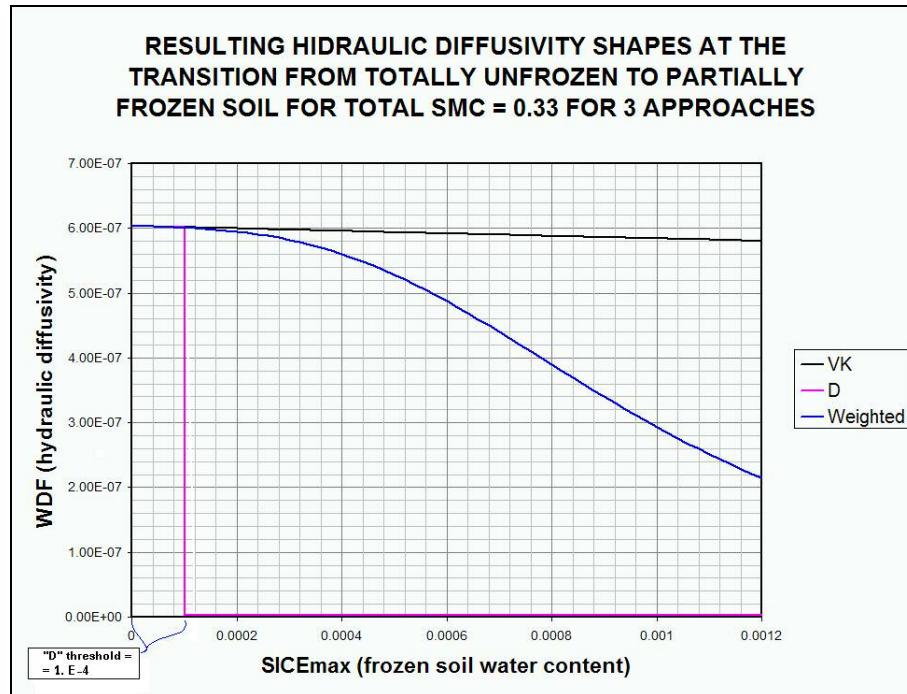
Figure 5-15 Magnification of the abscissas' axis of Figure 5-13 showing the weighted approach matching the old (VK) behavior in magnitude and first derivative (slope) at the transition from unfrozen to partially frozen soil moisture content.

5.4 Sensitivity to initial conditions

Early experiments were executed with the Noah LSM to demonstrate that an erroneous specification of the initial soil moisture content would have long term consequences in the simulation, even with correct atmospheric forcing. Running a five month simulation with the model for two different initializations of soil moisture, 0.250 and 0.350 (volumetric soil moisture content, SMC hereafter), it is observed that the differences introduced by the different initial conditions have a very long term impact even with correct atmospheric and precipitation forcing. Figure 5-16 to Figure 5-19 show the persistence of initialization-caused differences in the SMC for each one of the four layers of the soil model, respectively. Figure 5-20 shows the discrepancy in the latent heat flux that this difference in the initial SMC would produce during the first week of a forecast. These results emphasize the importance of a proper initialization of the soil moisture, discussed further in the next chapters.

69
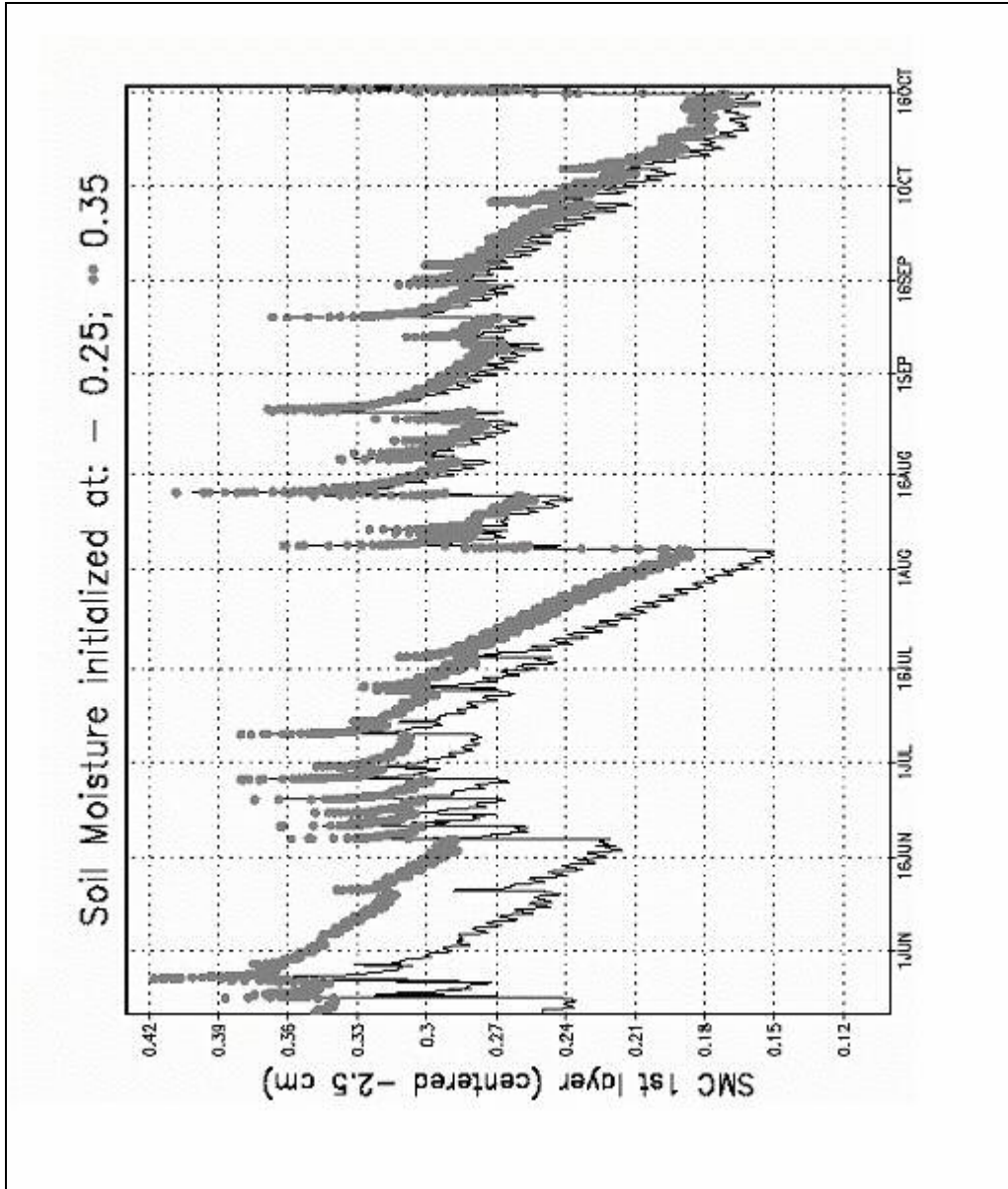
Figure 5-16 Volumetric soil moisture content (SMC) output from five months simulations using the model for two different initializations of soil moisture, 0.250 and 0.350 (volumetric). First layer.
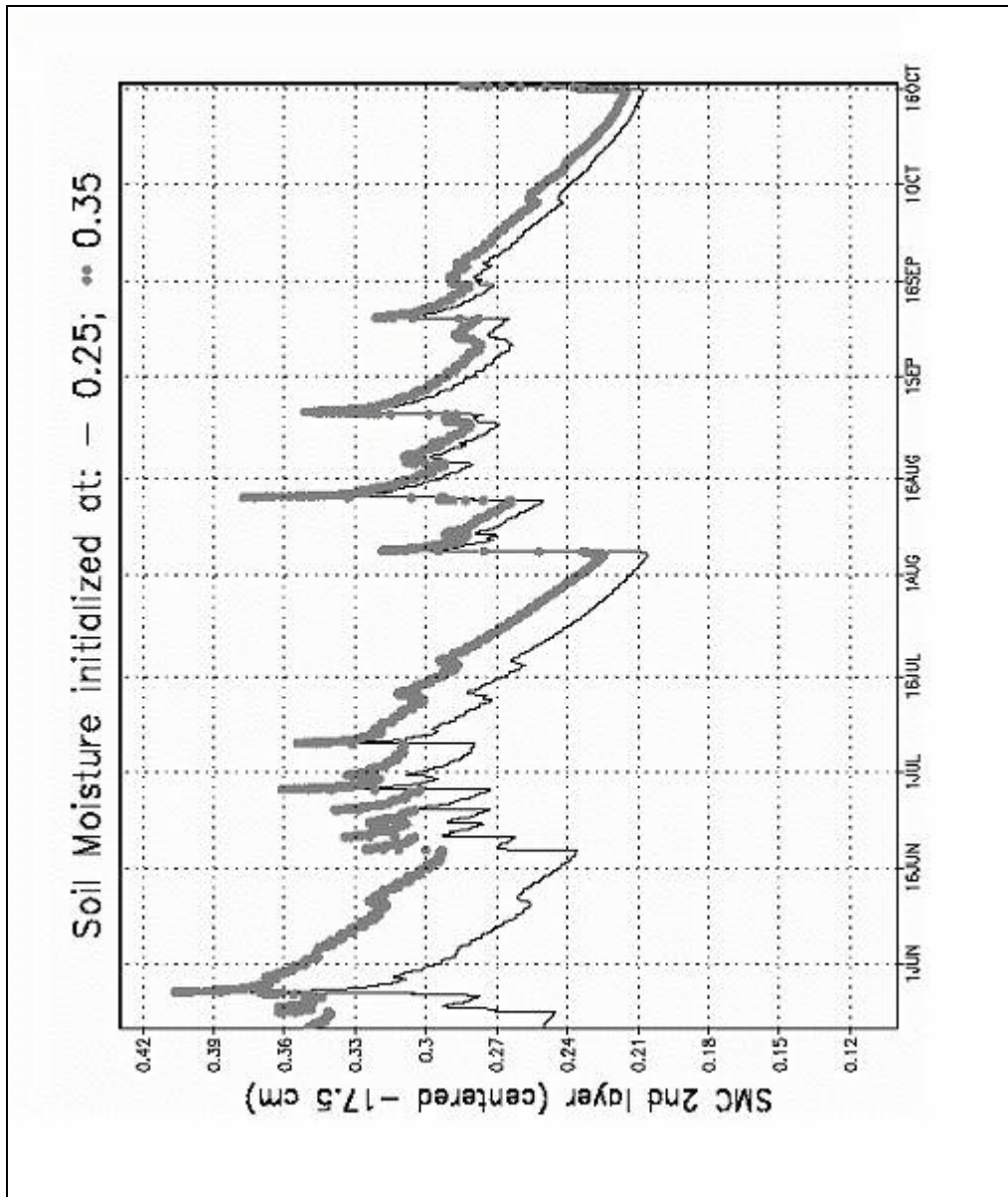
Figure 5-17 Volumetric soil moisture content (SMC) output from five months simulations using the model for two different initializations of soil moisture, 0.250 and 0.350 (volumetric). Second layer.
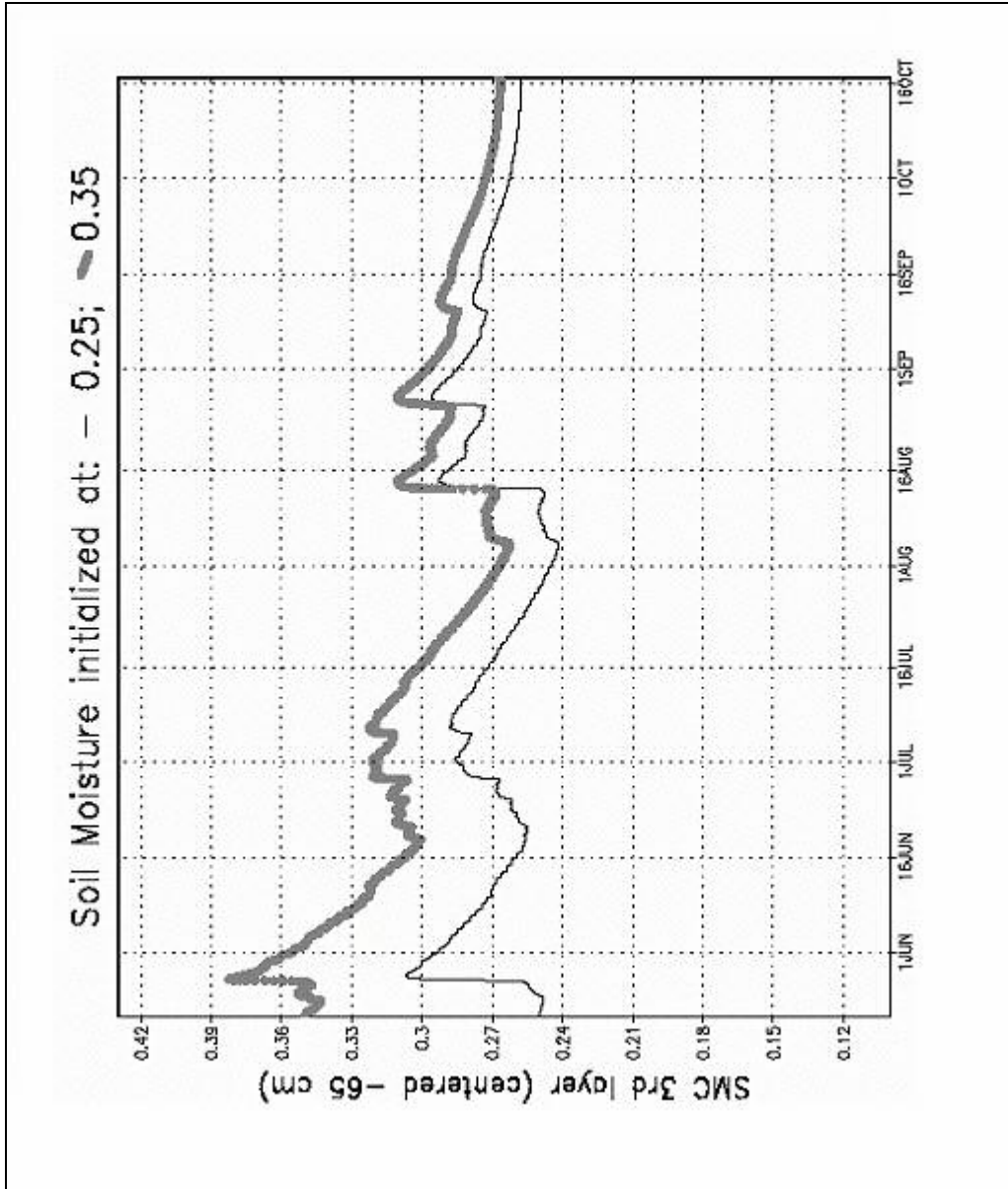
Figure 5-18 Volumetric soil moisture content (SMC) output from five months simulations using the model for two different initializations of soil moisture, 0.250 and 0.350 (volumetric). Third layer.
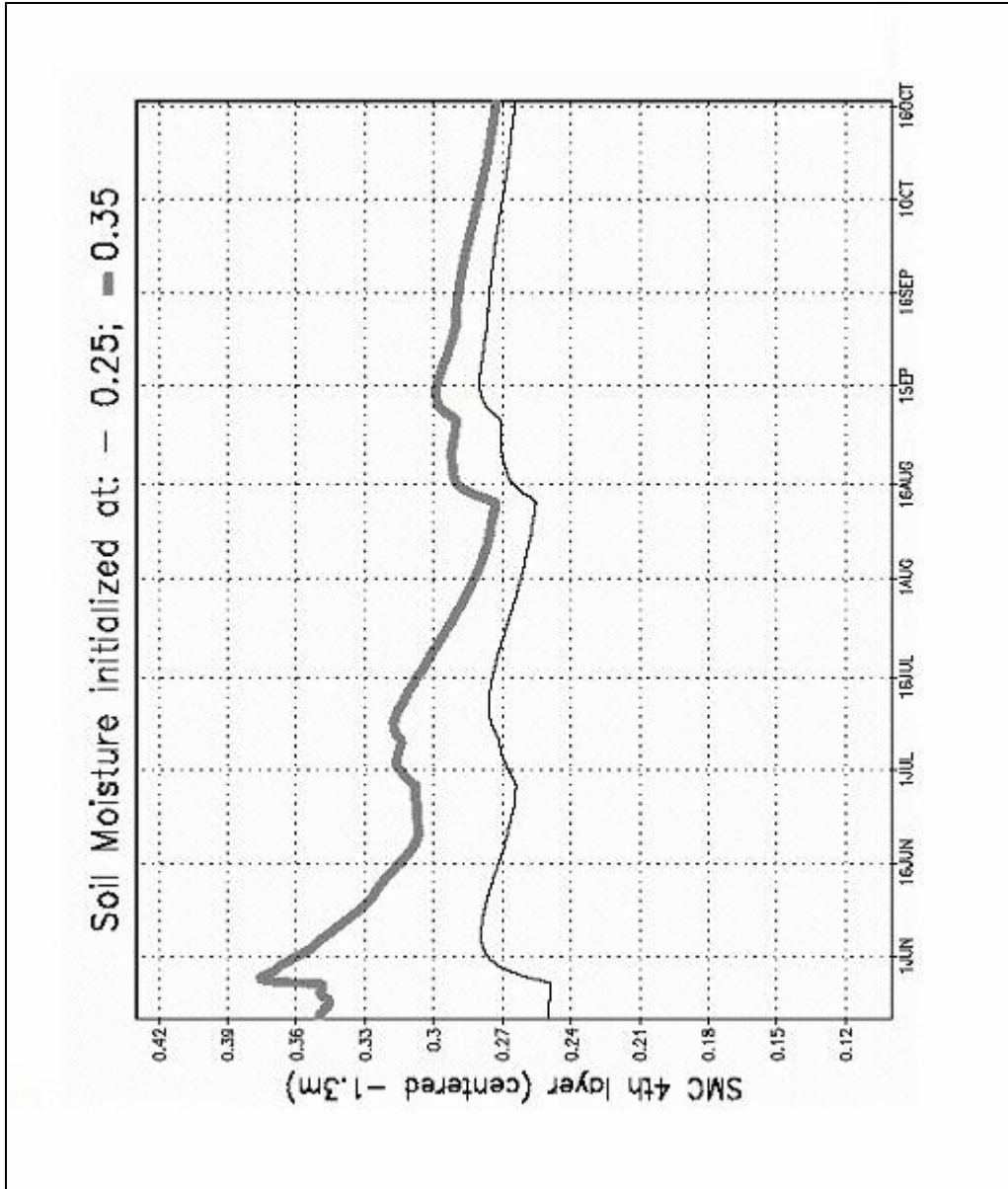
**Figure 5-19 Volumetric soil moisture content (SMC) output from a five months'
simulation of the model for two different initializations of soil moisture, 0.250 and 0.350
(volumetric). Fourth layer.**
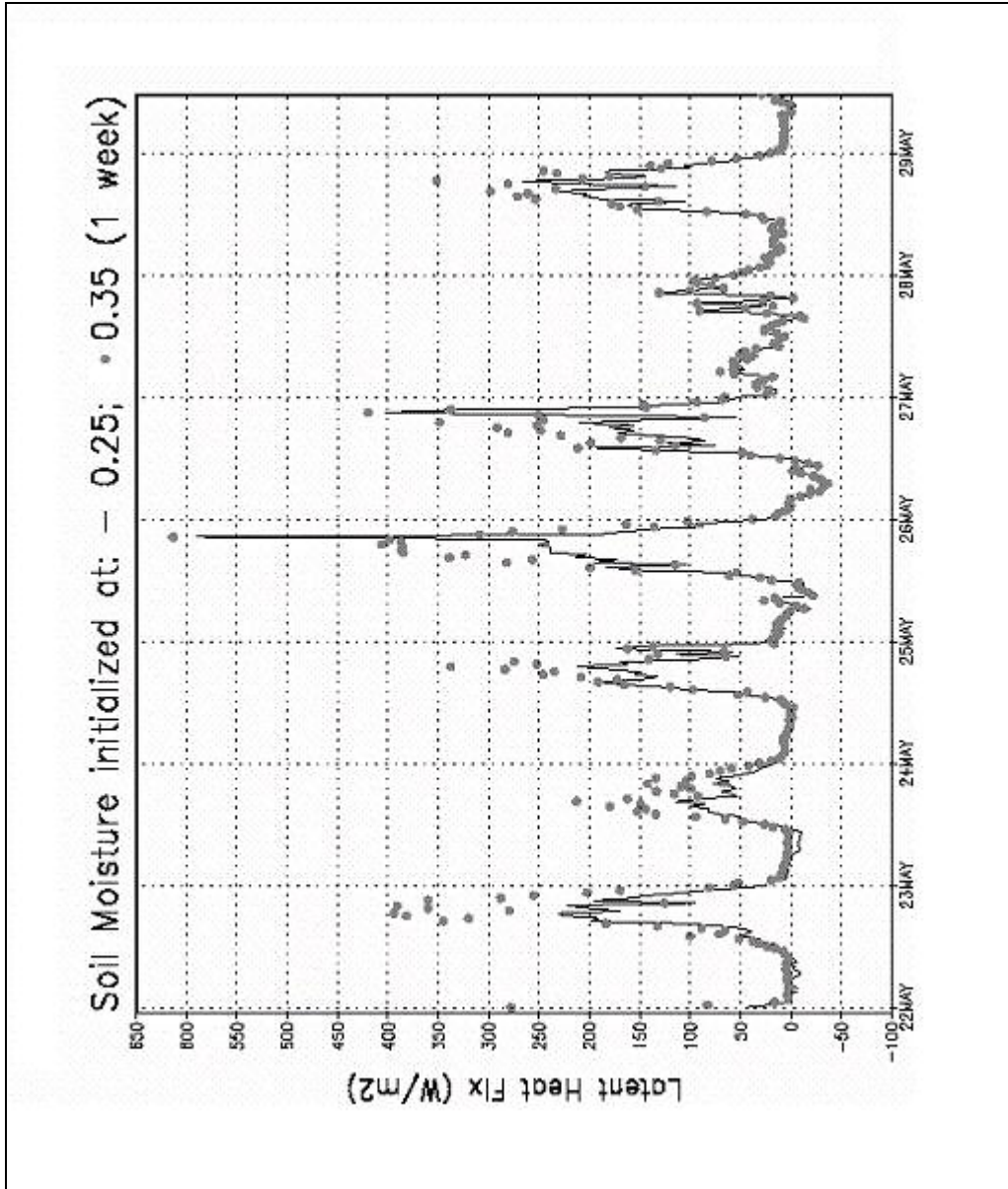
Figure 5-20 Impact of the initial soil moisture content for two different initializations of soil moisture, 0.250 and 0.350 (volumetric). Latent heat flux, 1 week.

Chapter 6
Generation and validation of the model control run.

The control run should be produced under the best possible conditions in order to yield an idealized trajectory. This is needed in order to be able to use this trajectory as reference in the evaluations of other runs. To accomplish this, we use the most physically consistent initial conditions available, as resulting from a previous spin-up adjustment under conditions prior to the actual run, plus forcing as accurate as possible which, in our case, is given by ground station observations.

6.1   Multi-year spin-up of initial land states

The main experiments in this work are studied against the background of a 1998 control run with a companion 1997 spin-up run (discussed below) because of the availability and quality of ground station verification and forcing data during those two years. The following was done to produce the initial conditions for the control run.

First, it is necessary to note that without proper spin-up, land surface simulations can be negatively impacted (Maurer and Lettenmaier, 2003; Cosgrove et al., 2003; Zhang and Frederiksen, 2003). The soil moisture initial conditions have a long term impact; an initialization severely departing from the model's climatology may affect the model's performance during years of simulation (Cosgrove et al., 2003).

The availability of ground-based observations of forcing data for 1997 in our test site allows the use of that year for spin-up runs to achieve a better initialization for 1998. We reasonably expect that running 1997 from acceptable initial conditions would lead to even more acceptable 1998 initial conditions (with the use of actual observed forcing and good model physics). The problem is that the exact initial conditions for 1997 are unknown. As in Cosgrove et al., (2003), our approach was to repeat the forcing from 1997 in a yearly cycle for 10 years; therefore 1997 is also

used as a proxy for the average conditions of the last several years leading to 1997. The spin-up "convergence" can be defined as a continuous run whose time length exceeds the longest memory processes in the system/model, making the arbitrary initial conditions used irrelevant.

The figures below show the results of the spin-up performed with the Noah model using station observed forcing data over the year 1997. It was noticed that a common equilibrium is reached within four to five years-cycle regardless of the extreme initial conditions imposed. The typical e-folding times for the decay of the initial departures from equilibrium were in the range of one year for the extremely dry initial soil moisture conditions and less than five months for the extremely moist case. Figure 6-1 shows the total model column volumetric soil moisture content evolving along the repeated 1997 forcing cycles in two runs; one starting from saturated soil moisture conditions (moist) and the other from dry conditions converging to a common equilibrium.
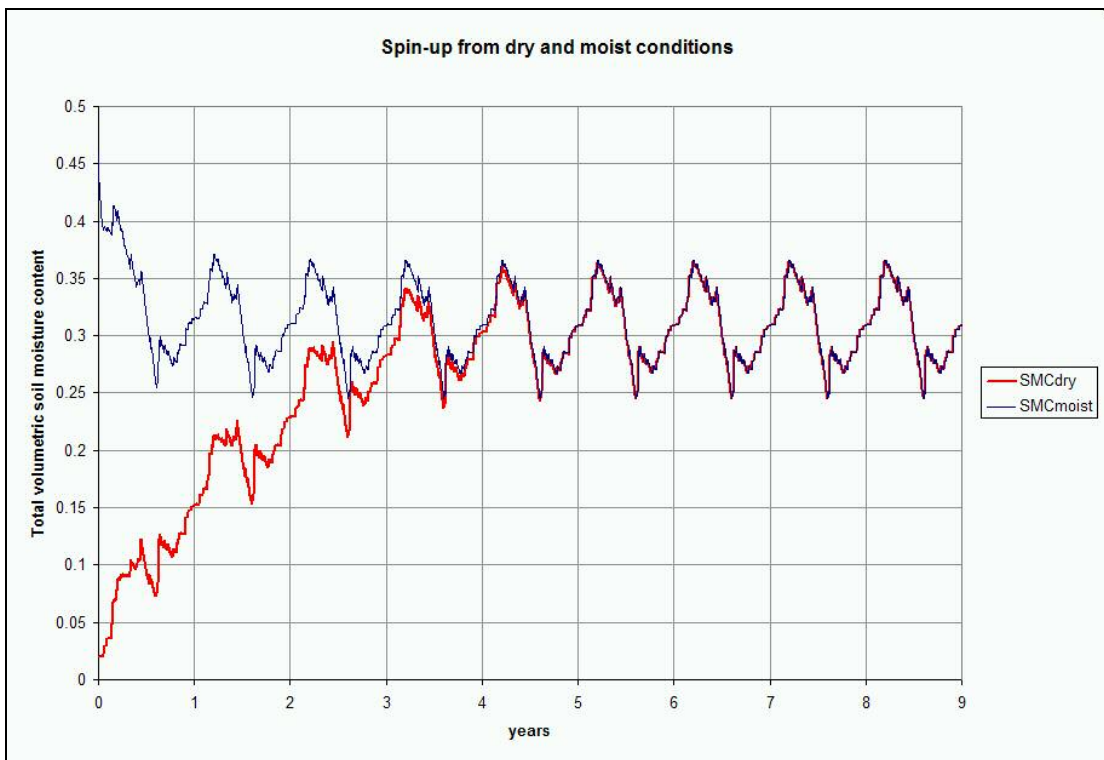
Figure 6-1 Convergence to a common equilibrium after a few years of spin-up cycling starting from the opposite extremes of soil moisture, dry and moist.

In figures Figure 6-2 to Figure 6-5 we see the RMS of the anomaly introduced by the extreme initial conditions with respect to equilibrium as they decay during the spin-up process and their respective exponential curves fit for both moist and dry extreme initial conditions cases. We also notice that, because the behavior is not exactly exponential, slightly different rates of decay are observed if only the beginning of the process is taken into account for the exponential fit.
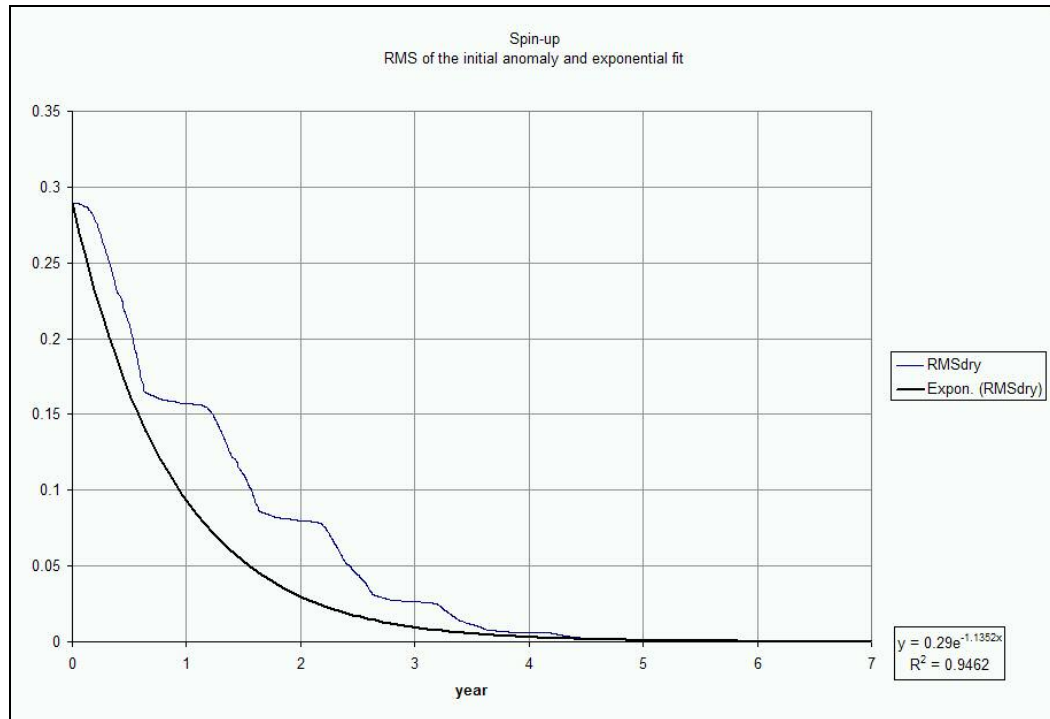
Figure 6-2 RMS of the spin-up from the dry extreme conditions with respect to equilibrium and its exponential fit based on the first seven years of adjustment.
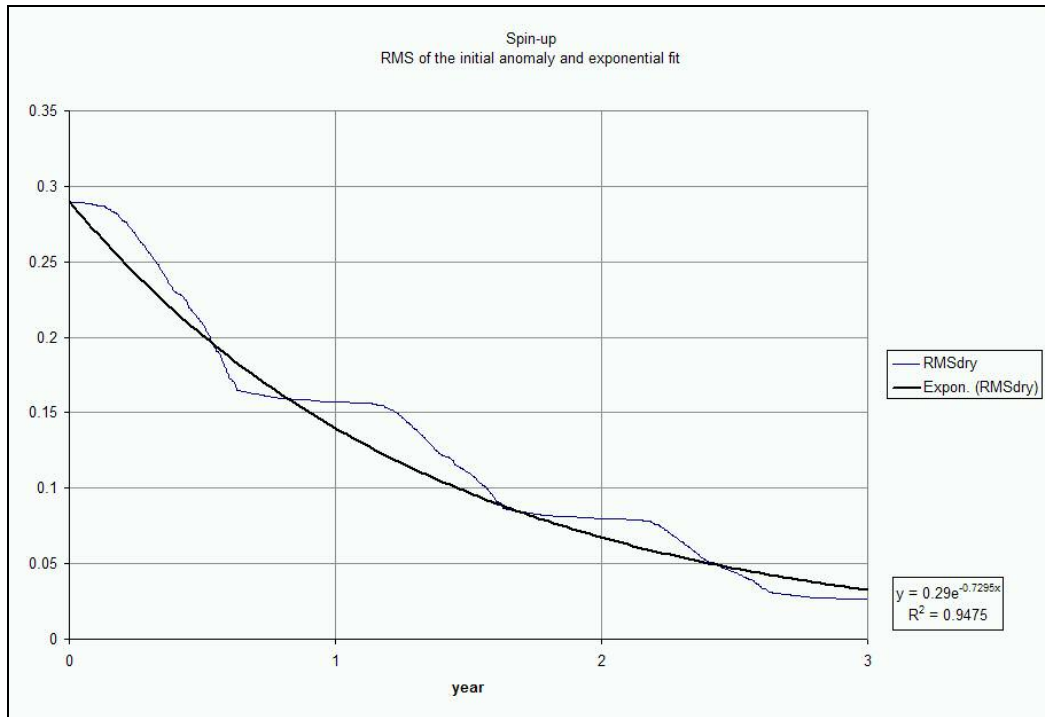
Figure 6-3 RMS of the spin-up from the dry extreme conditions with respect to equilibrium and its exponential fit based on the first three years of adjustment.
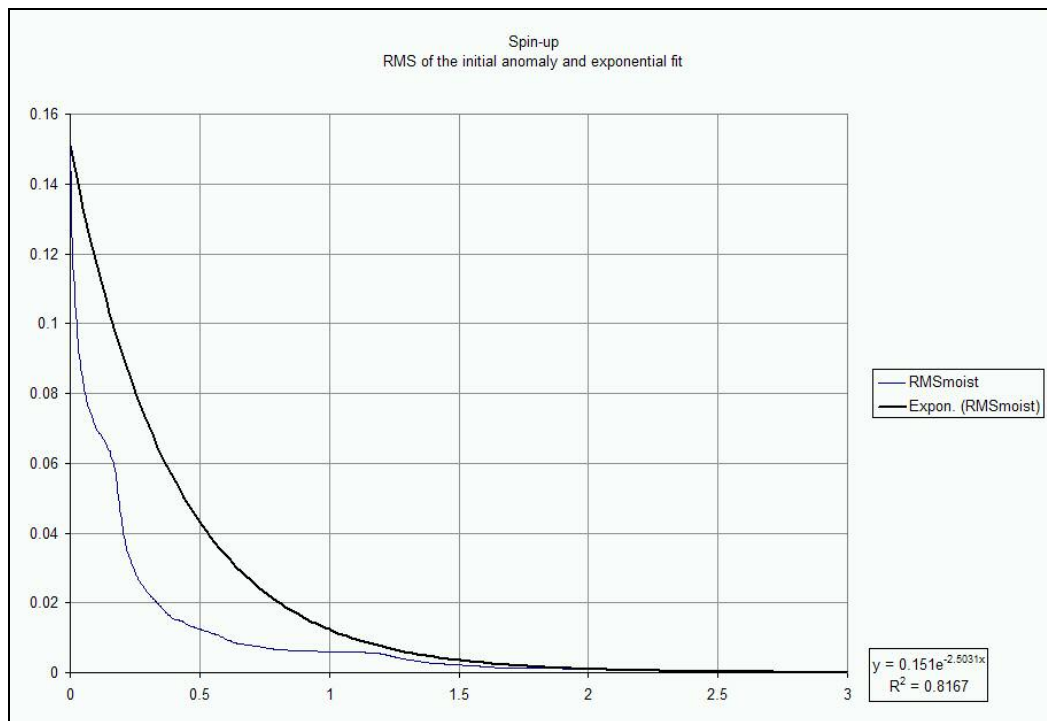
Figure 6-4 RMS of the spin-up from the moist extreme conditions with respect to equilibrium and its exponential fit based on the first three years of adjustment.
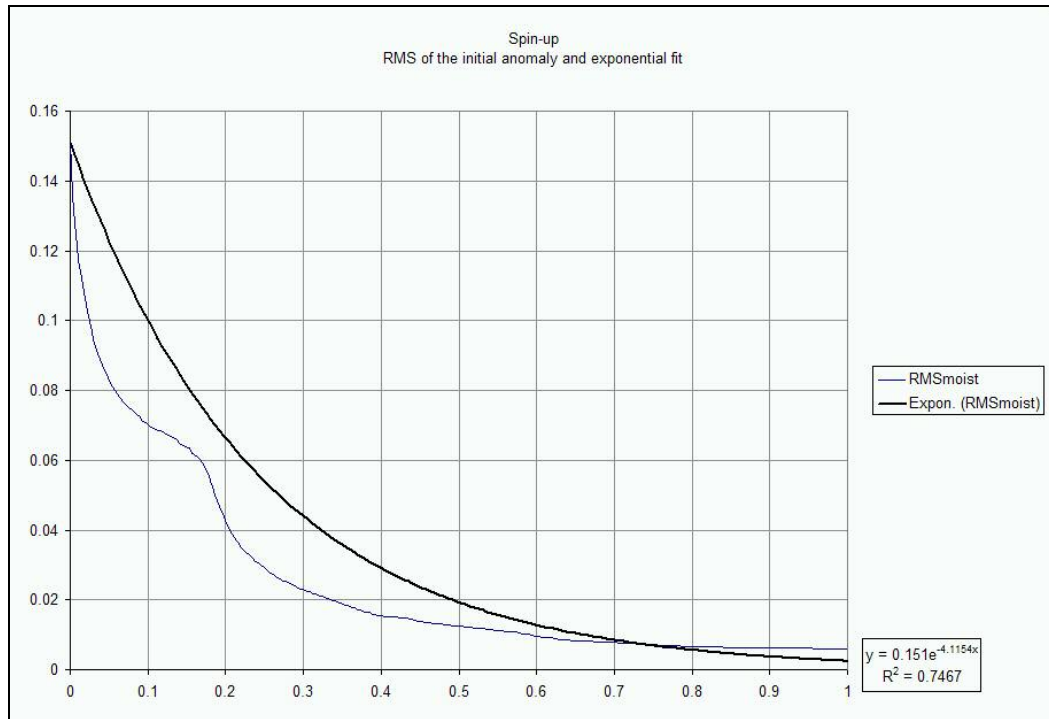
Figure 6-5 RMS of the spin-up from the moist extreme conditions with respect to equilibrium and its exponential fit based on the first year of adjustment.

Table 1 shows that in the exponential fit for the dry case, the e-folding time decreases if we take into account more years of spin-up, while in the moist case, the opposite happens. The difference in times and behavior is explained by the physical processes involved in each case; for the moist case, the strongly increased drainage at the beginning (from the strong relationship of the soil hydraulic coefficients with soil moisture), speeds-up the adjustment while the dry case depends on the occurrence of rain to fill-up its deficit. This is an important conclusion because it provides guidance on the approach to soil moisture initialization for regional models.

Table 1 Exponential decay e-folding time versus the length of spin-up used for the exponential curve fit and whether the initial conditions were on the moist or dry extremes.

Basis for e-fold calculation (years)	e-folding time (months)
dry 11	10.57
dry 7	11.01
dry 3	16.45
moist 3	4.79
moist 1	2.92

6.2 Validation against reference site flux station

The 1998 control run uses the idealized initial conditions given by the multi-cycle 1997 spin-up. The first time step of 1998 takes in the adjusted states from the last time-step of 1997 and is forced by observations. The fluxes produced by this run were checked against observations. The results are shown in Figures Figure 6-6 to Figure 6-11.
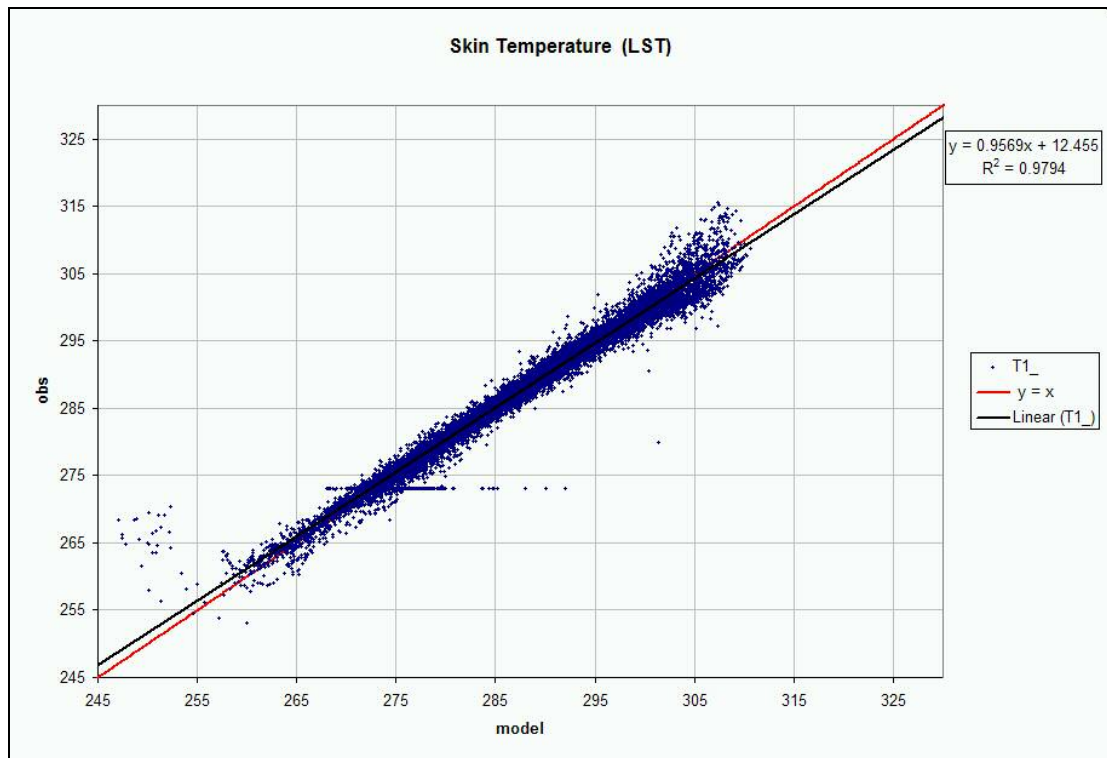
Figure 6-6 Land surface temperature from the model 1998 control run versus observations from the ground station and its corresponding least squares linear fit.

In Figure 6-6 we can see that the model land surface temperature stays quite close to the observations, given by the great concentration of points along the main diagonal (in red).
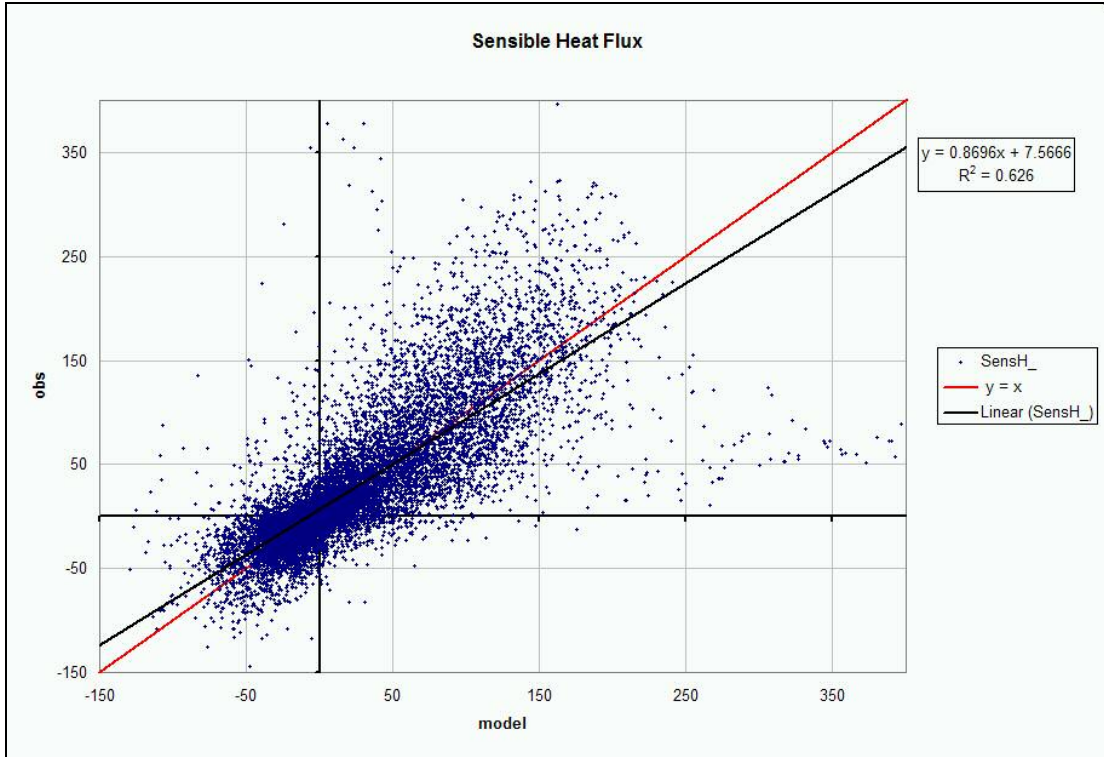
Figure 6-7 Sensible heat flux from the model 1998 control run versus observations from the ground station and its corresponding least squares linear fit.

The sensible heat flux (Figure 6-7) is well described by the model but with a larger dispersion around the main diagonal. The results seem acceptable given the many small scale random processes involved in the derivation of these fluxes from observations that are not captured in the model. The same remark applies to the latent heat flux (Figure 6-8).
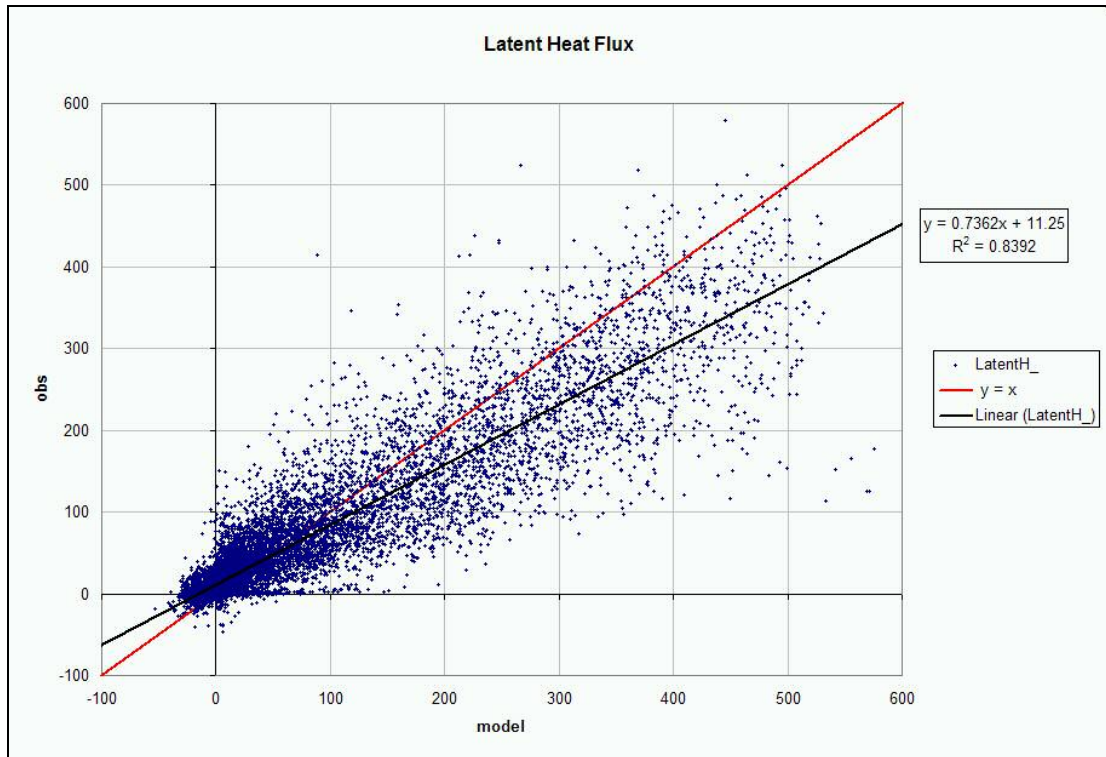
Figure 6-8 Latent heat flux from the model 1998 control run versus observations from the ground station and its corresponding least squares linear fit.

The ground heat flux (Figure 6-9) shows less agreement indicating the difficulties of modeling of the cold season processes, especially those related to freezing. This becomes clear in Figure 6-10 and Figure 6-11 that separate the results for the parts of the year with and without freezing. We can see from these two figures that the model is in much better agreement with observations during the non-freezing season, and that the two processes require different tuning. As a result, further refinements were made to the model including the handling of ground heat flux under partial snow cover but since they were incorporated after the main experiments presented in this work, they are not shown.
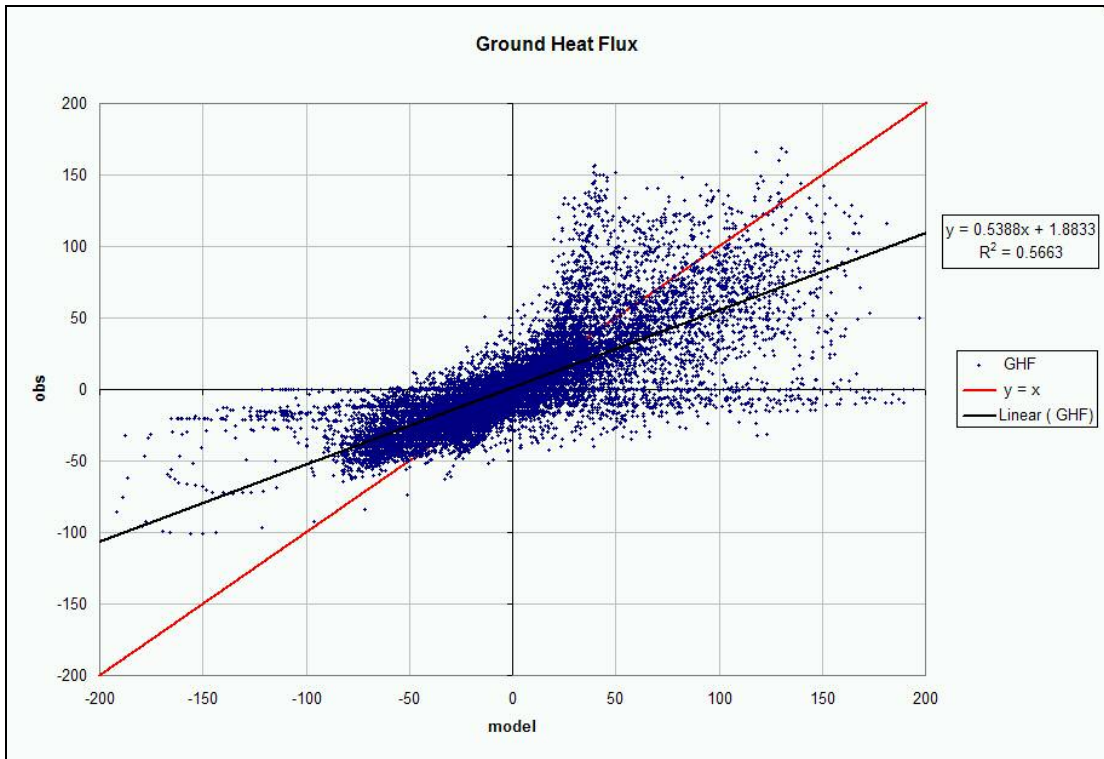
Figure 6-9 Ground heat flux from the model 1998 control run versus observations from the ground station and its corresponding least squares linear fit.
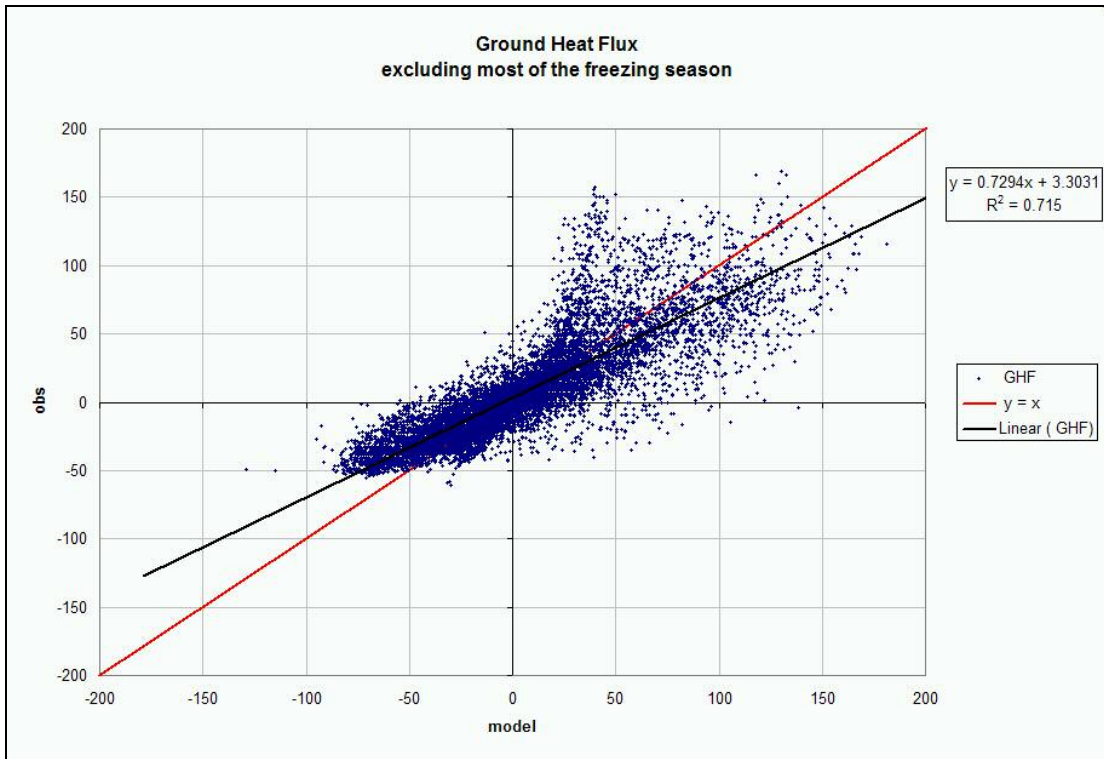
Figure 6-10 Same as Figure 6-9 but with the season in which freezing occurs removed.
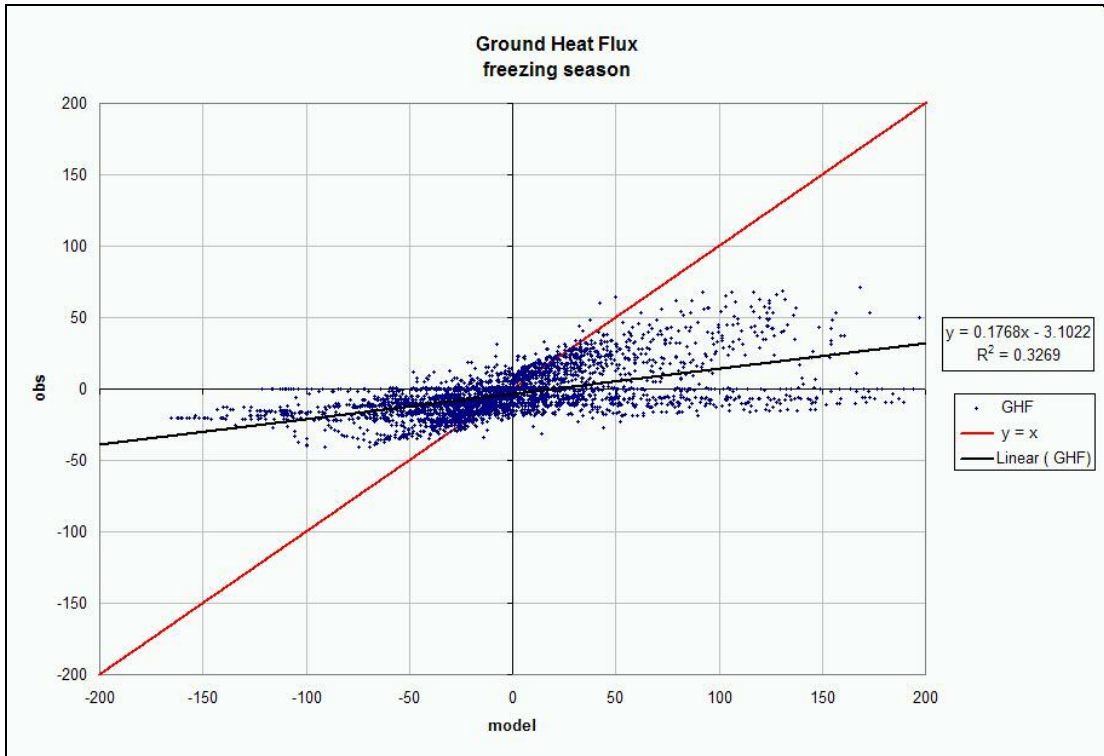
Figure 6-11 Same as Figure 6-9 but just for the season in which freezing occurs

84

Chapter 7
Data Assimilation Experiments

To test our basic assimilation approach, we performed experiments with the land-surface model in settings that will be described in the following sections.

The experiments involve running the Noah Land-Surface Model off-line, which means that the companion atmospheric model is not coupled to it and this required that forcing from the atmosphere be provided by other means. In our case, the required atmospheric variables are read from a file containing either ground station observations or data from the GCIP Land Data Assimilation System (LDAS) Project (Mitchell et. al., 1999-B) retrospective LDAS forcing files. We also perform an experiment using GOES satellite-based land surface temperature retrievals described in section 4.3. This LDAS forcing data is made to correspond to the same location, time period and temporal resolution via time and space interpolations.

This information read from a file (similar to what would be provided by the coupled atmospheric model in an "on-line" coupled setting), is regarded as "forcing" and required by the land-surface model at every time-step but not changed by the model (read-only). Given this forcing, the model updates the soil and land-surface variables to compute the land-atmosphere fluxes for every time-step. The soil and land-surface variables that are updated by the model time-integration scheme have to be initialized (initial condition) and are regarded as "state variables". There are also variables that the model calculates internally but are not given to the model externally in any case, these variables are collected at the end of each time-step, are regarded as "output" or "diagnostic" variables (for example, the computed fluxes, such as the ground, sensible and latent heat flux are in this category).

When observations are available and compared to either model state or output variables, they can be used for simulation verification. Since it is difficult to find observations on a continental scale that match land-surface models' state or output variables, it may be necessary to extend the model creating special output variables that could be related to a particular available observation for verification purposes.

Like forecast verification, variational data assimilation can only use observations that can be matched to state or output variables. The difference is that, in the data assimilation case, the verification of the skill of the system (model state or output variables versus corresponding observations) is a function that calculates a measure of error (within a chosen time window) that is related to the initial values of the state variables (initial conditions) or, in the case of model calibration, related to the parameters that are to be corrected in order to improve the model's skill. The problem of finding corrections for these initial conditions or parameters that minimize the error in the prediction of the observed variable during the assimilation window is only part of the problem. The ultimate desired result is actually to obtain forecast improvements after the end of the assimilation time window. When considering possible forecast improvements, one should bear in mind that some land surface model state variables are strongly driven by the forcing and may carry little memory of the initial state after a short period of time; on the other hand, other variables could be very persistent and indicative of a more fundamental underlying condition. The latter variables are more useful in improving the model's simulation after the assimilation time window (forecast). In this category, soil moisture is the most important variable and a single correction of its initial state can impact the forecast for months.

In the case of a multi-layer soil moisture model (accounting for the vertical distribution), one can choose the control variable to enhance the response at longer time-scales, since deeper layers have longer time-scales. Alternatively, taking advantage of the model's physics, which are trustworthy, one can reduce the size of the control variable to facilitate the solution of the optimization problem. For example, relying on the good quality of the model soil hydraulics, the variational data assimilation can use a cost function dependent on a uniform correction for all layers (total soil moisture correction) which, as discussed in previous chapters, has a much better defined minimum than one dependent on corrections for each individual layer (in addition to the problem of the size of the space to search for solutions and multiple minima).

The initial conditions for all the runs are provided by a spin-up run using forcing data from the surface station site (section 4.1) corresponding to the year previous to the actual test runs (1997 is cycled several times to provide initial conditions for 1998). This procedure provides good quality initial conditions for the starting point of Jan 1, 1998 as necessary for the actual experiments that use forcing data corresponding to the entire year of 1998.

The first four experiments are designed to test whether we can recover initial soil moisture information from land surface temperature (LST) observations within a "perfect model" scenario known as an "identical twin" experiment. For this purpose we consider the control run as "truth", and perform a model integration with a forcing that has been degraded from the "true" run, for example by reducing precipitation. In the degraded run we assimilate LST provided by the "true" run during several episodes, and check whether the soil moisture after a period of assimilation is closer to the "true" soil moisture of the control run, and how long does the influence of these changes persist.

In last four experiments (except no. 7), we abandon the perfect model scenario and use real LST observations, and forcings from either the surface station (experiment 5) or the Land-surface Data Assimilation System (experiments 6, 7 and 8). Because we are not using a perfect model, the biases between model variables and observed variables yield, not surprisingly, considerably worse results than in the identical twin experiments 1-4. We estimate the impact of longer assimilation windows, and are able to identify cases in which the use of observed temperatures in the data assimilation results in soil moisture corrections of the wrong sign.

Tables 2 and 3 below summarize the data assimilation experiments to be explained and presented in the following sections.

Table 2: Schematic table of identical twin (perfect model) experiments.

Experiment	Reference run ("truth")	Forcing for DA run	Assimilated variable	Figures
1. Original MOIST conditions, assimilation run is drier	Control: 1997 spin-up flux station observed forcing.	Flux station but precip reduced -30%	Control run LST	Figures 7-1 to 7-5
2. MOIST conditions, assimilation run is moister	Reference 2: Station observed forcing but precip. reduced by about 10% (still moist)	Flux station	Reference 2 run LST	Figures 7-6 to 7-7
3. DRY conditions, assimilation run is drier	Reference 3: Dry (50% precipitation reduction)	Flux station but precip reduced -70%	Reference 3 run LST	Figures 7-8 to 7-12
4. DRY conditions, assimilation run is moister	Reference 4: Dry (70% precipitation reduction)	Flux station but precip reduced -50%	Reference 4 run LST	Figures 7-13 to 7-14

Table 3: Schematic table of non identical twin experiments.

Experiment	Reference run ("truth")	Forcing for DA run	Assimilated variable	Figures
5. Assimilating reference site ground station (T. Meyers) LST	Control	Flux station but precip reduced -30%	Flux station LST observations	Figures 7-15 to 7-18
6. NLDAS forced run. Assimilating reference site ground station (T. Meyers) LST	Control	NLDAS	Flux station LST observations	Figures 7-19 to 7-21
7. NLDAS forced run. Assimilating LST from the control run	Control	NLDAS	Control run LST	Figures 7-22 to 7-26
8. NLDAS forced run. Assimilating LST from the GOES satellite	Control	NLDAS	GOES LST observations	Figures 7-27 to 7-32

7.1 Assimilating ideal synthetic data: Identical Twin Experiments

Our identical twin experiments consists of having a first or "reference" run with ideal forcing and initial conditions, and a second run where the forcing is arbitrarily degraded. In our first run, the model is expected to reproduce the ground-station observed fluxes as accurately as possible, and hence this is our "control" run or reference ("true") trajectory. In the second run, the forcing data from 1998 is artificially degraded (to simulate some of the inaccuracies that could happen when the forcing is provided by a companion atmospheric model) and the data assimilation scheme is introduced to correct the trajectory of the land surface model as it deviates from the reference trajectory due to inaccurate forcing. The data assimilation scheme uses only the land surface temperature (LST) from the control run (as a proxy for land surface temperature observations) to derive corrections to the soil moisture state trajectory.

In order to be able to correct the soil moisture states based only on the behavior of the LST over a period of time, *it is necessary that the soil moisture and LST have a physical connection in which a change in soil moisture causes a change in LST behavior*. The physics of this connection in the model was presented in section 3.2.1. In the experimental setting, this was shown in Figure 2-2 where changes in the initial soil moisture given to the model (abscissas) are responsible for changes in the value of a cost function computed from the squared differences of the model LST with respect to a recorded reference-state LST.

7.1.1 Degradation of precipitation forcing

As a first test to the data assimilation system, in experiment 1, following the spin-up year (1997), we degraded the forcing throughout 1998 by imposing a of 30% reduction to all moderate or large amounts in the 30-minute precipitation forcing. The form of the reduction applied to the precipitation forcing, only used in experiment 1, is as follows: for precipitation equivalent to 5mm/day or less, there is no reduction, between 5mm/day and 50mm/day, the reduction increases linearly from 0 to 30%,

and the reduction remains at 30% for precipitation intensities above that mark. As this run tends to depart from the reference trajectory given by the control run, the data assimilation system uses the land surface temperature (LST) from the control run to correct the soil moisture states.

Other experiments followed to further test the system in different situations such that four possible situations were covered, two in a predominantly moist state of soil moisture and two in a predominantly dry state. In each of these states (moist year, dry year), the data assimilation run would be made drier and then moister than the reference run. Therefore, throughout the four cases, the data assimilation system would have to correct the soil moisture content from moist to dry and vice versa. To achieve some of these conditions, artificially dry, alternative reference runs ("truth") were generated and used in place of the control run. These runs were called Reference 2, 3 and 4 to differentiate from control, which can be regarded as our Reference 1.

The Reference runs 2 to 4 were generated from the same initial conditions as control but some precipitation reduction was imposed. The three alternative reference runs plus the original control run aim to cover two moist situations and two dry situations for the first four data assimilation experiments. Our original experiment, using the control run, can be classified as being in a predominantly moist soil moisture state with a data assimilation run that tends to be drier than control.

The more generic formula (used only in experiments 2, 3 and 4) to achieve different degrees of reduction to the original 30 minutes precipitation data is of the form:

$$P_{out}(P_{in}) = (P_{in} + 1)^b - 1 \qquad\qquad (7.1)$$

where

P_{out} is the reduced precipitation.

P_{in} is the original (input) precipitation.

b is an exponent between 0 and 1.

This formula was chosen to have the output precipitation, P_{out} match the input P_{in} at near zero precipitation, and to have the reduction more severe for higher precipitation input, P_{in} and for small b.

7.1.2 Assimilating the LST of the control run

The assimilation of land surface temperature from the control run is done by reading those values and using them as observations. In the cost function, the model is run over a particular period of time (data assimilation window) taking as input the magnitude of the change, *"x"*, made to the soil moisture content at the beginning of this data assimilation window. This produces a time series of land surface temperature (LST_x) while at the same time the LST values stored from the reference ("truth") run are read (LST_{obs}). LST_x and LST_{obs} correspond to the same period in time. The data assimilation window, in our case, is of 3½-day unless otherwise noted. The cost function adds the squared differences between the time series LST_x and LST_{obs} over this period (plus a background term proportional to x^2, to penalize great changes and creating a default minimum at $x=0$ in case of lack of other influences).

The data assimilation scheme may run the cost function repeatedly over this time period making changes only to the input in search of the values of *"x"* that minimize the cost function. Here it is noted that the time series LST_x is affected by x.

The figures labeled "soil moisture content evolution" show the results of the data assimilation runs versus their reference run from May to November 1998. During this time there are four data assimilation events, the red marks indicate the beginning and end of each data assimilation window. The corrections to the soil moisture occur at the beginning of each window and the correction to the soil moisture affects LST_x in a direction that diminishes the differences in land surface temperature produced by the test run, LST_x (under the tentative soil moisture correction) and control run (LST_{obs}) over the time window.

For the identical twin model simulations, the data assimilation events are very successful in bringing the test run states closer to control. Note that the intervals between data assimilation events were set to be long enough to allow the effects of

91

incorrect forcing in the test run to cause it to diverge significantly from the reference trajectory (labeled "control" in the figures).

The figures illustrate the effects of data assimilation in two forms. First, the two time series of a single soil moisture level for the reference ("true") run and the data assimilation run, and later, the soil moisture profiles at each data assimilation event, before and after the correction to be compared to the profile of the reference control run at that time. The time series shown are usually of the third soil layer because its slow time scale allows easier visualization of the data assimilation effects.

Experiment 1 is the original twin experiment; the control run is intended to be as accurate as possible in terms of initial conditions and forcing, the data assimilation run received precipitation reduced up to 30% when moderate or severe according to the first part of section 7.1.1 above. In Figure 7-1 (the moisture content evolution for soil layer 3) we see that the soil moisture corrections derived at each data assimilation event were very successful at bringing the state close to that of the control run. The data assimilation events' profiles, Figure 7-2 to Figure 7-5 show that the first correction (mid May) was the most accurate while the others that followed had a slight propensity to overestimate the soil moisture state. The beneficial impact of the assimilation of LST on the moisture lasted for several weeks.
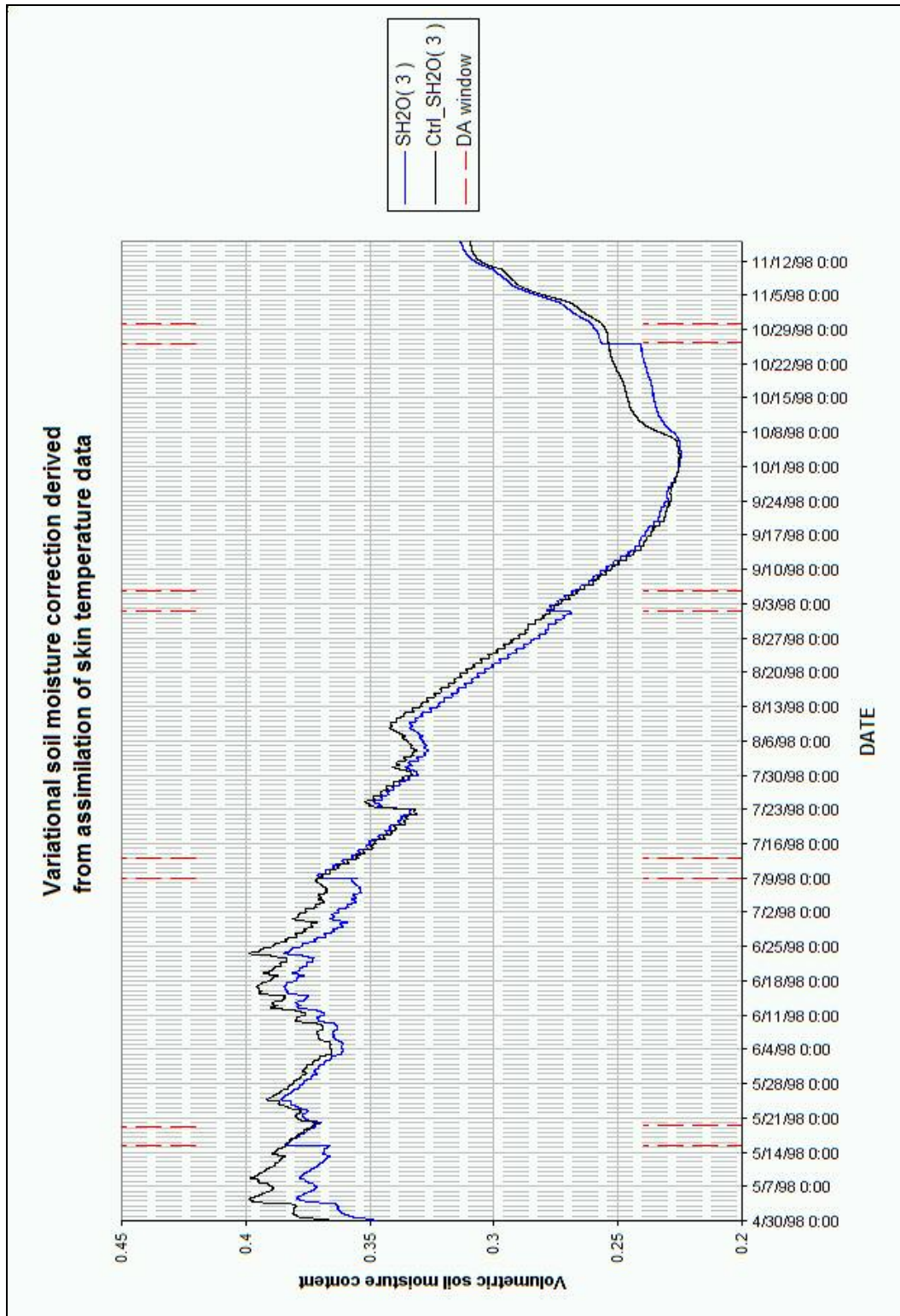
Figure 7-1 Experiment 1. Soil moisture content evolution for the control run (black line) and data assimilation run (blue line). Third soil layer.

Figure 7-2 Experiment 1. Soil moisture profiles before (blue) and after (black) data assimilation event 1 (mid-May) versus control ("truth" in red). Soil layer 1 is from the surface to 10 cm deep, soil layer 2 is from 10 cm to 40 cm deep, soil layer 3 is from 40 cm to 1 m deep and soil layer 4 is from 1 m to 2m deep. Plant roots are present in layers 1 to 3.
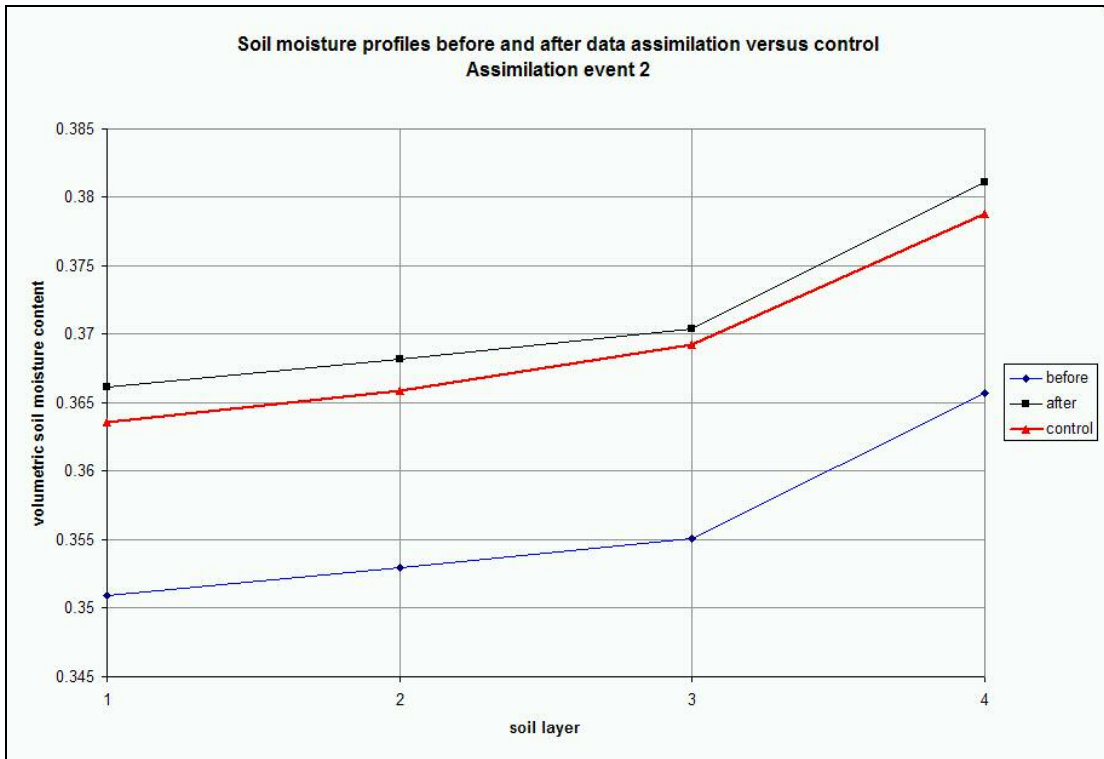
Figure 7-3 Experiment 1. Same as Figure 7-2, for data assimilation event 2 (July).
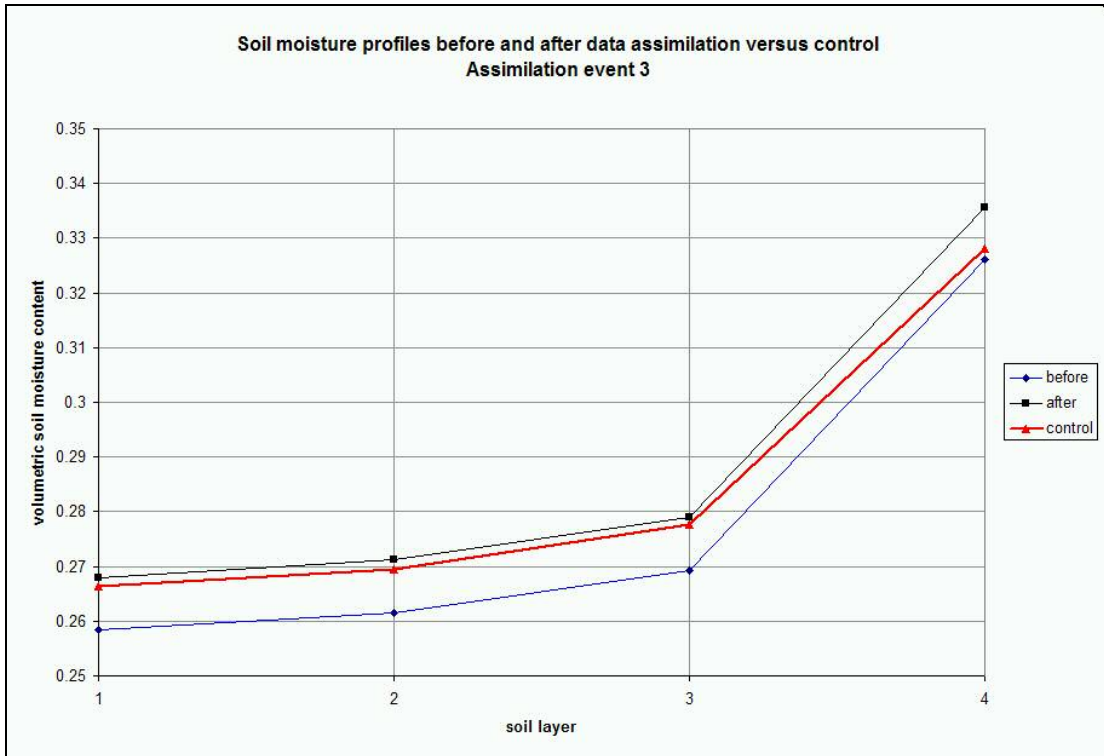
Figure 7-4 Experiment 1. Same as Figure 7-2, for data assimilation event 3 (September).
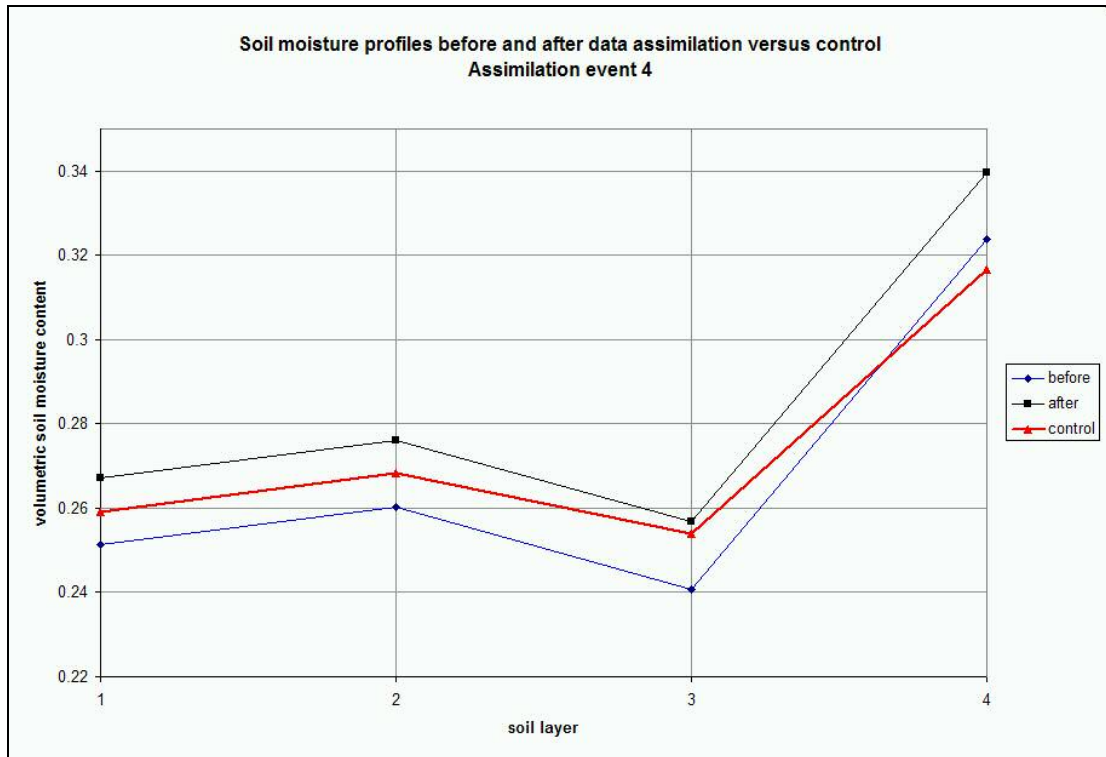
Figure 7-5 Experiment 1. Same as Figure 7-2, for data assimilation event 4 (end of October).

Experiment 2 consists of the data assimilation run being moister than control with the soil moisture state for both runs being on the moist side (as the conditions observed for 1998 actually prescribe). Specifically, the differences with experiment 1 are that the data assimilation run receives the 1998 precipitation as observed by the reference site ground station without reduction and the reference run ("truth") is made artificially drier by imposing about 10% reduction on precipitation through formula in (7.1) of section 7.1.1. Figure 7-6 shows that the corrections derived from the data assimilation events were most effective on events 1 (mid-May) and 3 (September) but little change (still in the right direction) was produced on the other two events. This could be due to uncertainties inherent in the minimization scheme or can arise from lack of sensitivity (see Figure 2-3) on given conditions allowing a greater influence of the background term. The soil moisture profiles before and after the correction are

shown for data assimilation event 1 (Figure 7-7), the resulting profile after data assimilation came very close to the profile of the control run, as desired.

Figure 7-6 Experiment 2. Soil moisture content evolution for the reference 2 run (black line, considered as truth) and data assimilation run (blue line). Third soil layer.

Figure 7-7 Experiment 2. Soil moisture profiles before and after data assimilation event 1 (mid-May) versus reference.

Experiment 3 consists of the data assimilation run being drier than the reference or truth and the soil moisture state for both runs being significantly drier than the conditions presented in experiments 1 and 2. Specifically, the differences of experiment 3 with respect to 1 are that both the reference 3 run and the data assimilation run receive the 1998 precipitation forcing greatly reduced by formula (7.1), but the data assimilation run is the driest of the two runs. Precipitation reductions were in the range of 50% (in reference or "truth" run) and 70% (in data assimilation run). Figure 7-8 shows that the corrections derived from the data assimilation events were successful in bringing the state of the test run very close to the "truth", also illustrated by Figure 7-9 to Figure 7-12, the soil moisture profiles before and after the corrections for each event. They also indicate that the state of layer 4 (the deepest layer, which in our setting, has no plant roots) has little weight in the determination of the correction.

Figure 7-8 Experiment 3. Soil moisture content evolution for the reference 3 run (black line) and data assimilation run (blue line). Second soil layer.
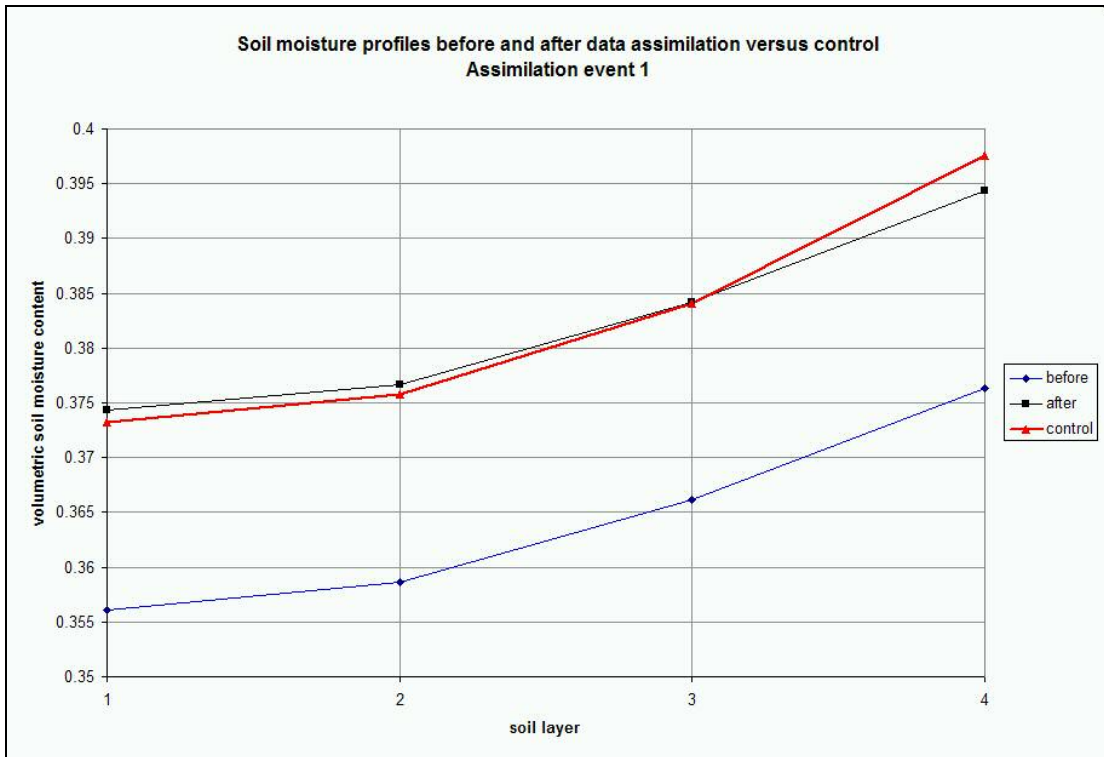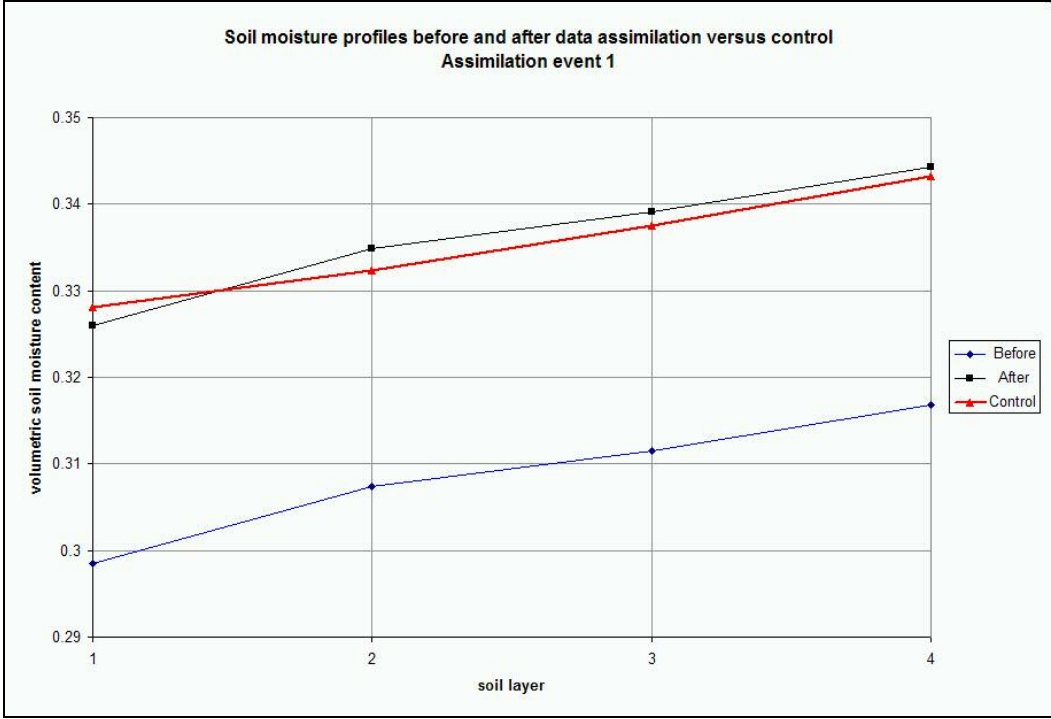
Figure 7-9 Experiment 3. Soil moisture profiles before and after data assimilation event 1 (mid-May) versus reference (red).
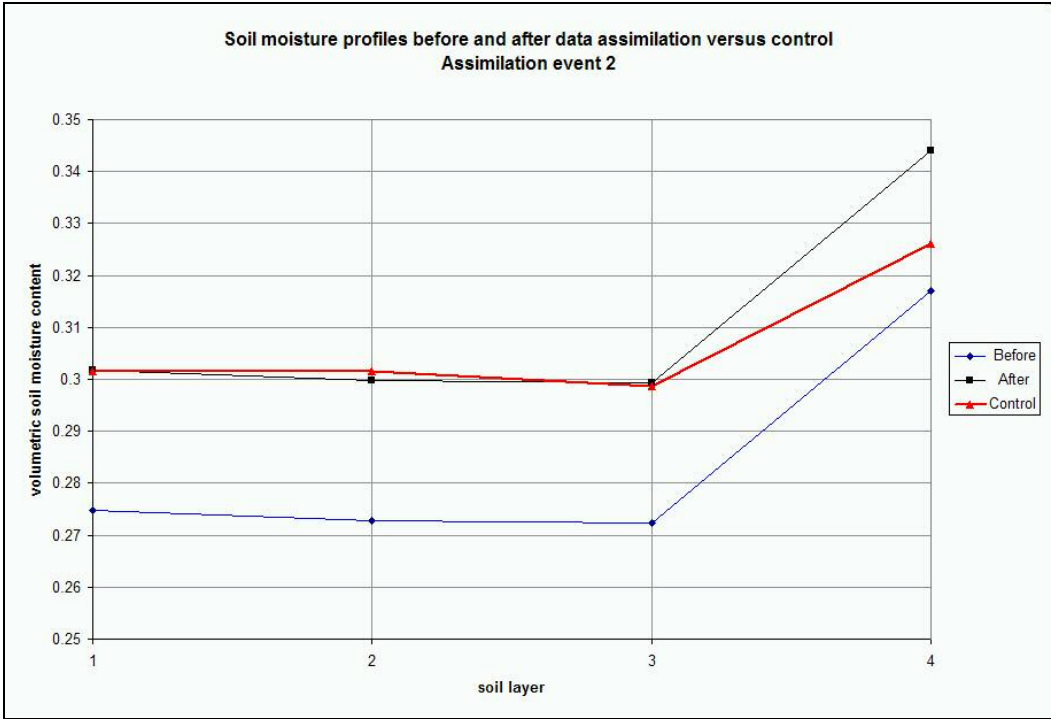
Figure 7-10 Experiment 3. Soil moisture profiles before and after data assimilation event 2 (July) versus reference (red).
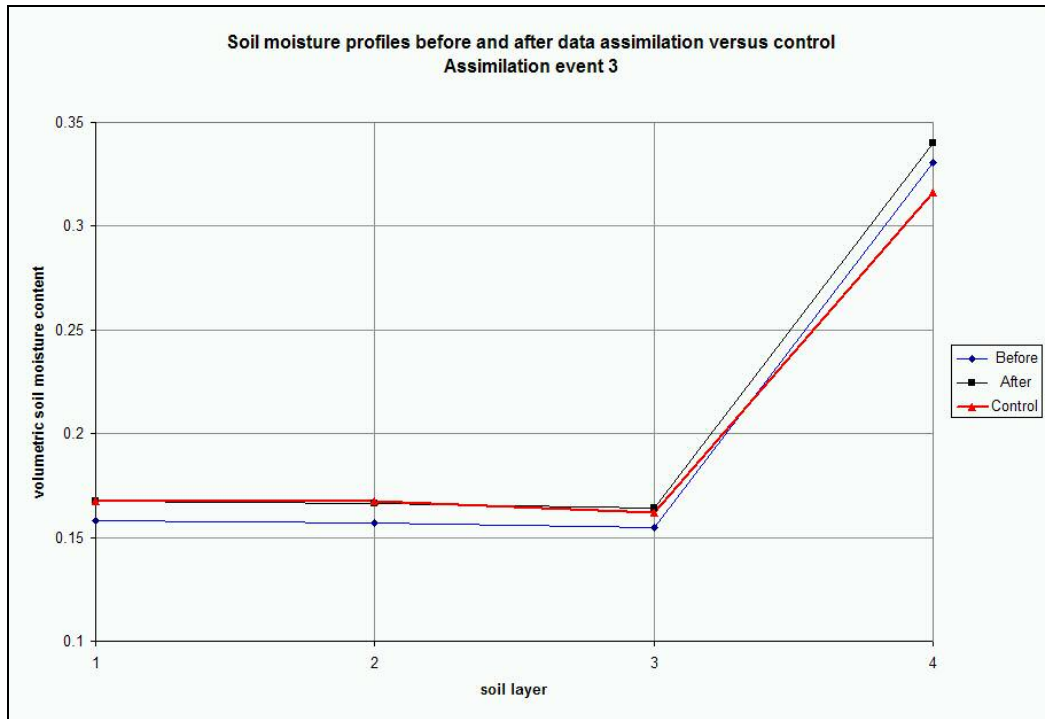
Figure 7-11 Experiment 3. Soil moisture profiles before and after data assimilation event 3 (September) versus reference (red).
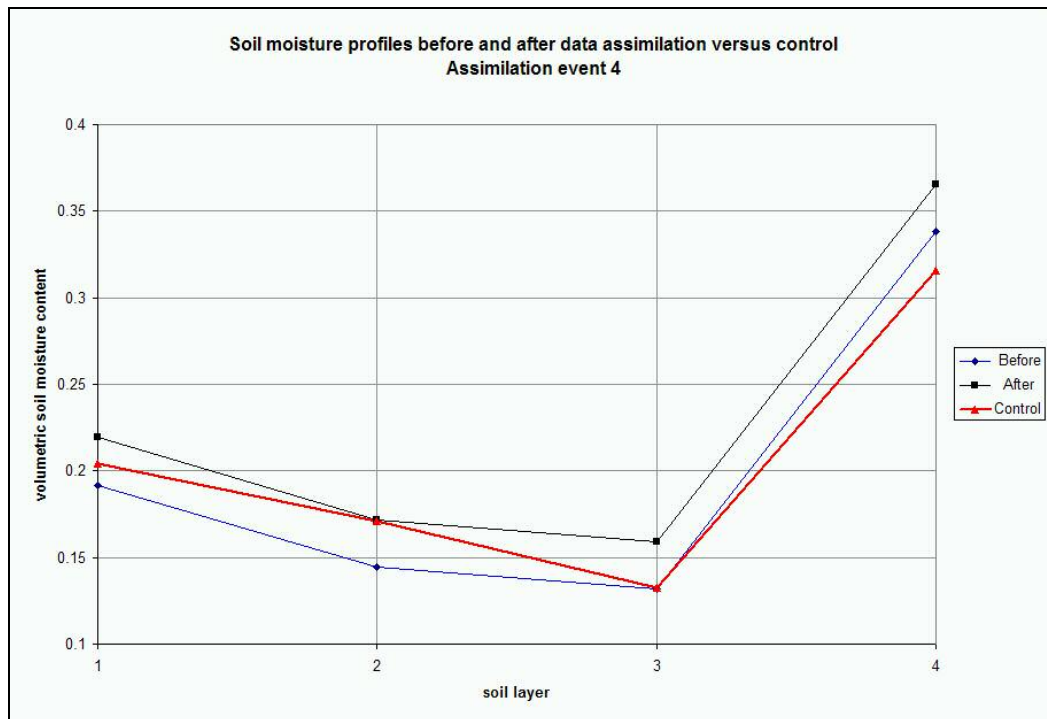
Figure 7-12 Experiment 3. Soil moisture profiles before and after data assimilation event 4 (end of October) versus reference (red).

Experiment 4 is similar to 3 except that consists of the reference ("true") run being drier than the data assimilation run. As in experiment 3, the soil moisture state for both runs is significantly drier than the conditions presented in experiments 1 and 2. The differences of experiment 4 with respect to 3 are that the 1998 precipitation forcing reductions by formula (7.1) are set so that the reference run is the driest one. Precipitation reductions were in the range of 70% ("truth") and 50% (data assimilation). Figure 7-13 shows that the first three corrections derived from the data assimilation events were successful in bringing the state of the test run very close to the true state (reference) but no significant change occurred from data assimilation event 4. Figure 7-14 shows the change produced in the soil moisture profile after data assimilation event 1, bringing the state very close to the one from control
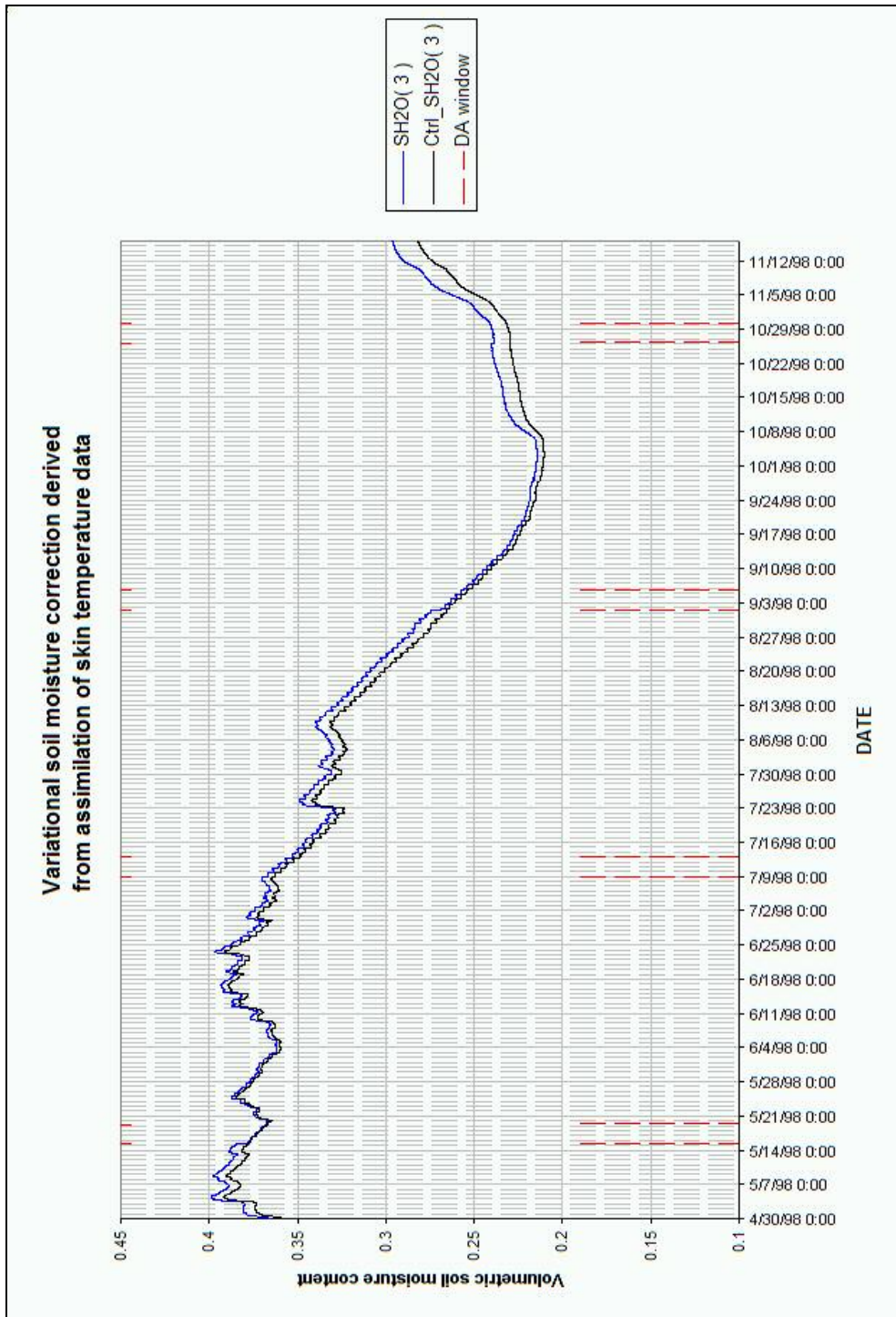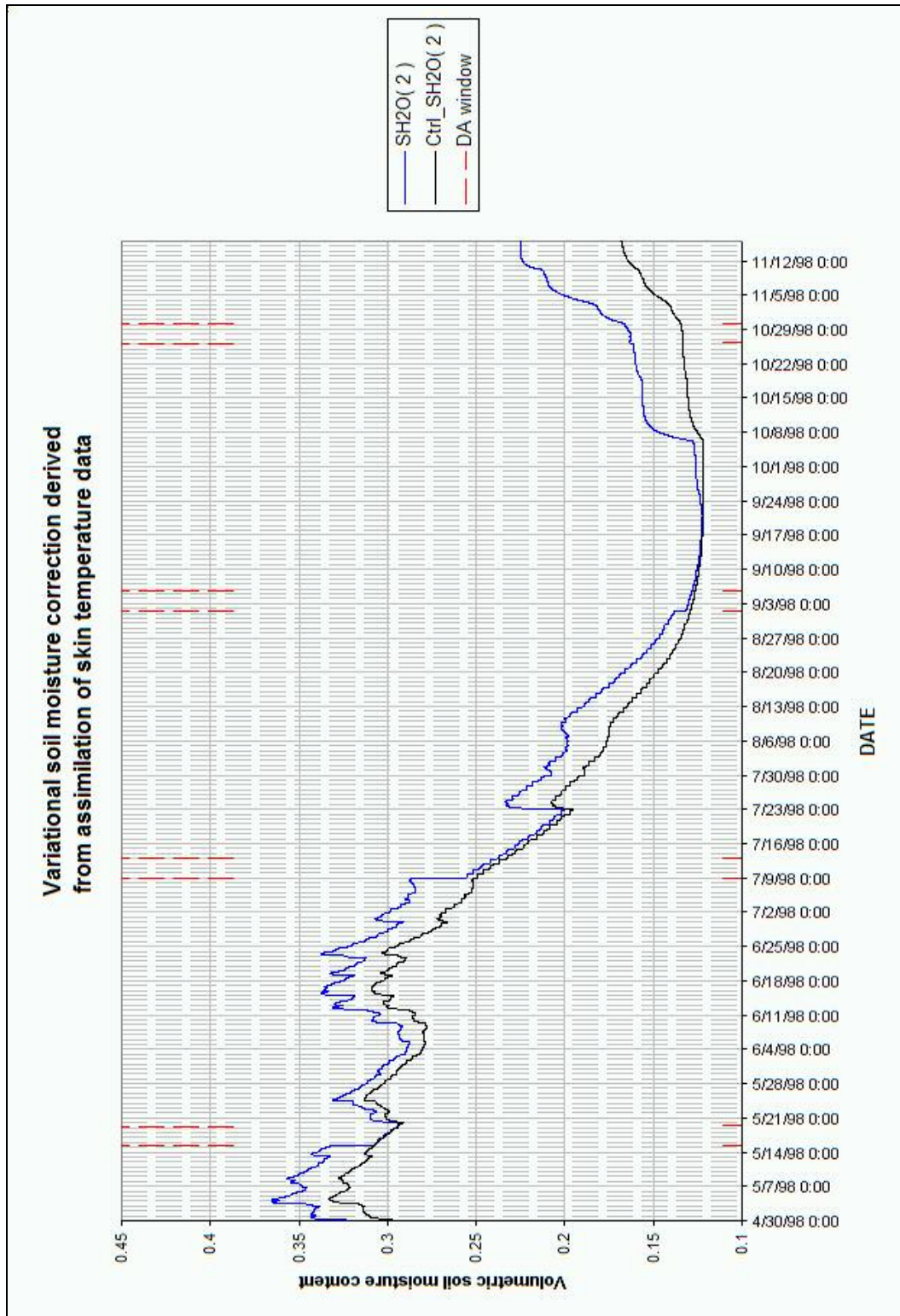
Figure 7-13 Experiment 4. Soil moisture content evolution for the reference 4 run (black line) and data assimilation run (blue line). Second soil layer.

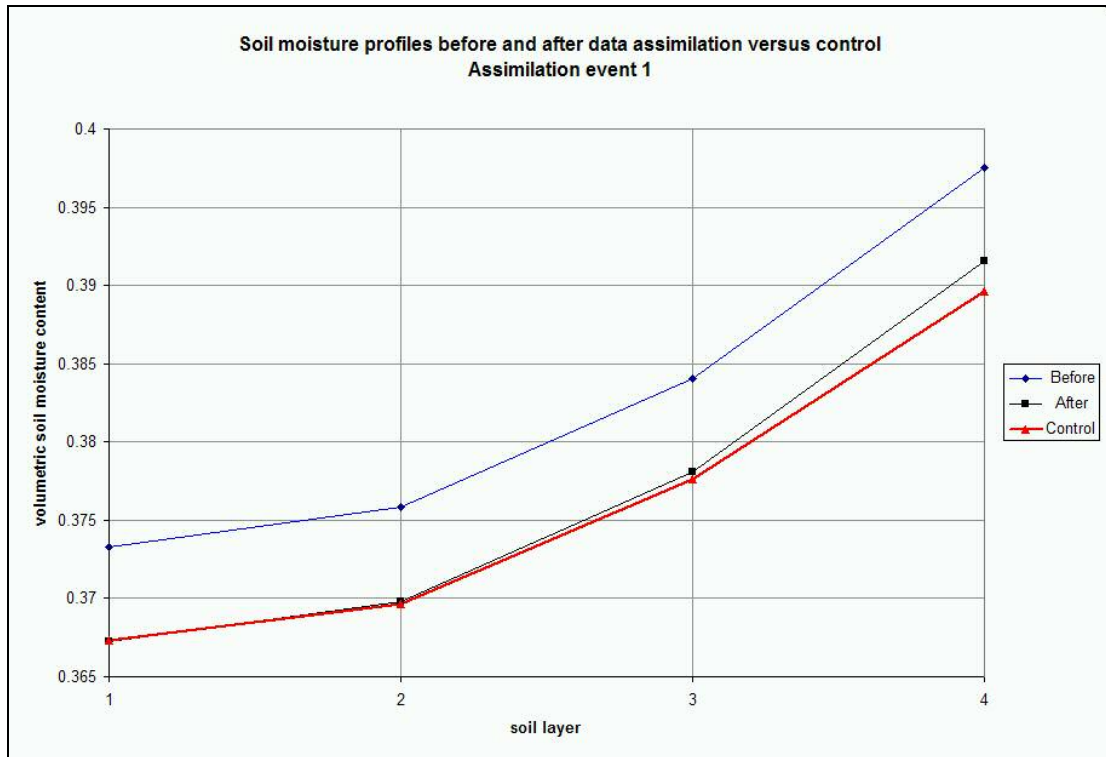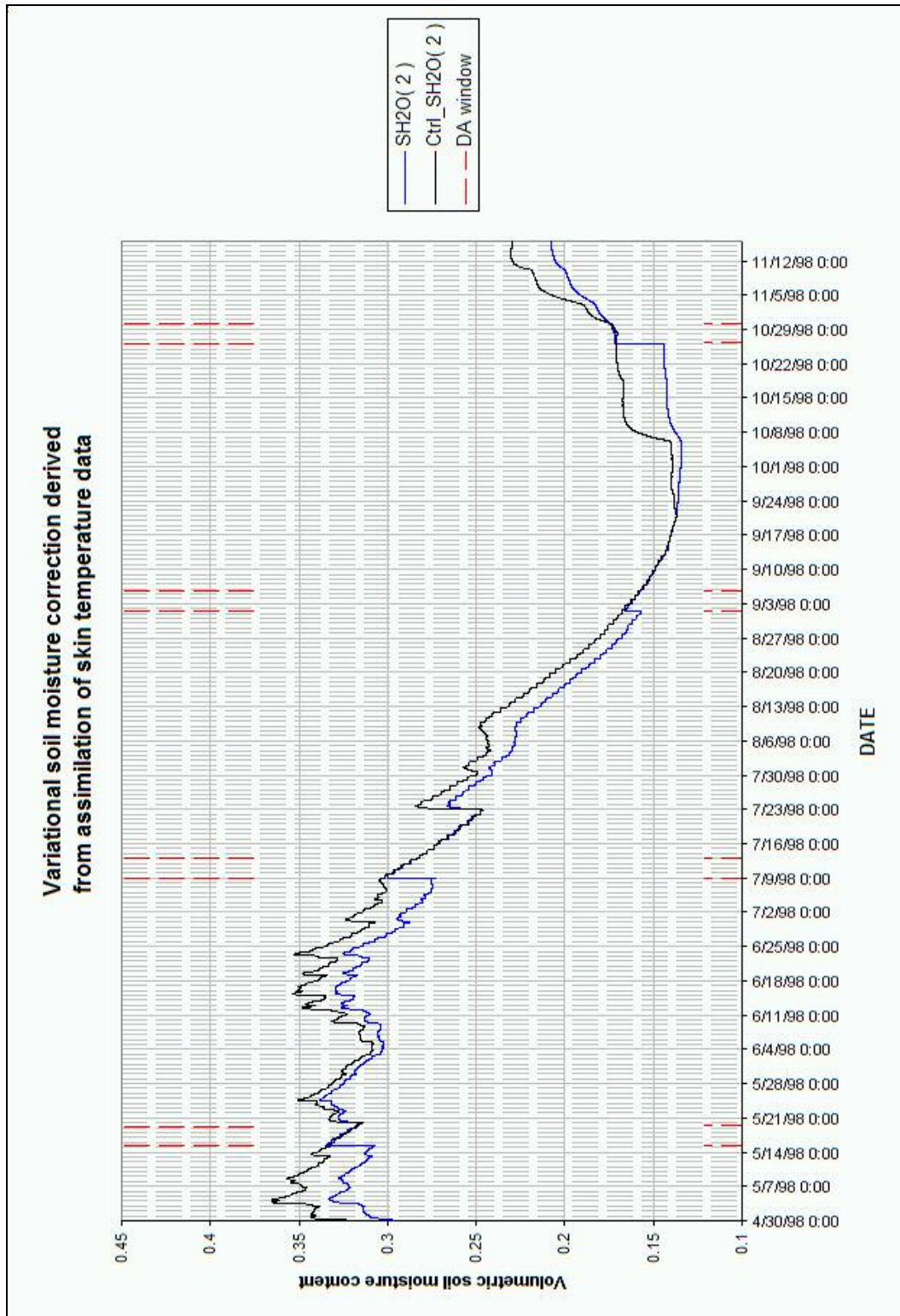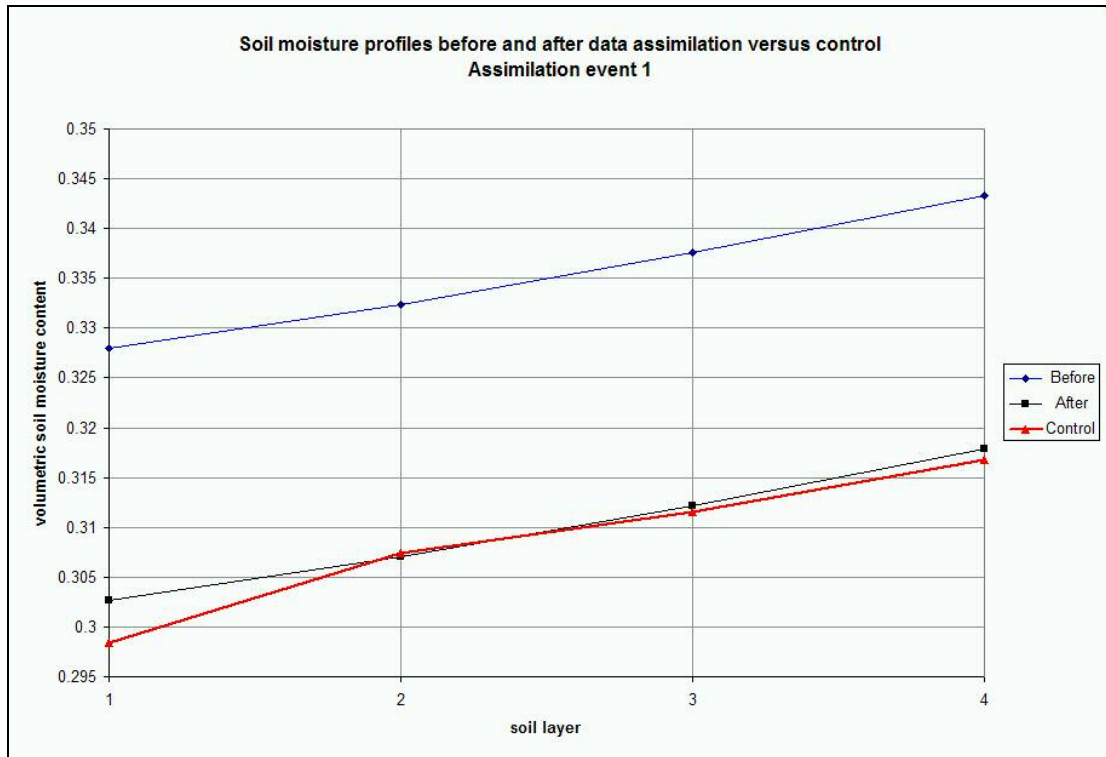**Figure 7-14 Experiment 4. Soil moisture profiles before and after data assimilation event 1 (mid-May) versus reference (red).**

7.2 Assimilating real data

The experiments that assimilate observed real data have the added challenge of the presence of differences between the model control run (taken as reference for the state variables' trajectories) and observations. That means that the exact correspondence between variables as given by the reference model run simulating nature ("truth") is no longer present ("perfect model" assumption no longer valid). The impact of the differences between the control run and nature, can be reduced if the differences are largely unbiased, as such unbiased differences tend to cancel out as the data assimilation time window is increased, otherwise biased differences can compromise the results.

7.2.1 Assimilating LST from the reference site station

Experiment 5 goes back to the original setting of experiment 1 (wherein an unaltered 1998 control run is compared with a data assimilation run that received up to 30% less precipitation) but the data assimilation events in Experiment 5 use the land surface temperature (LST) observed at the reference site ground station rather than the control run LST. Since the data assimilation run is receiving 30 percent less precipitation than the control run, its soil moisture will tend toward being too dry and its LST too warm during the day, so one expects the assimilation of LST to moisten the soil and lower the diurnal LST. Figure 7-15 shows the time evolution of the soil moisture content in model layer 3 for the data assimilation and control run. Only the third and fourth data assimilation periods (beginning of September and end of October) yielded the expected positive increase in soil moisture, while the first assimilation event (in May) had an unexpected impact of the opposite sign.

Taking into account the good correlation of the LST between the reference station and control run (Figure 6-6), the above experiment was repeated using a longer data assimilation window. The idea is that, from Figure 6-6, we expect to find relatively small uncertainties between the behavior of the LST from the control run and the reference site station and that those uncertainties would be almost unbiased. Therefore, on a longer time scale, the impact of the unbiased uncertainties should be reduced or canceled. Figure 7-16 shows the result of this second version of experiment 5, using a data assimilation window of almost 12 days. This longer assimilation window resulted in a marked diminution but not elimination of the unexpected soil moisture decrease in event 1 (mid-May) and great improvement on events 3 and 4 (September and end of October, respectively). Figure 7-17 shows, for this case, the soil moisture profiles before and after data assimilation event 1, when the correction was in the unexpected direction of reducing soil moisture hence increasing the difference with respect to the control run.

The unexpected soil moisture drying in event 1 (mid-May) suggests that the LST simulated in the degraded run during this period was not warmer that the LST observed by the ground station. Hence the apparent absence of bias inferred when

comparing the entire year scatter plot of LST from the control run and reference site station (Figure 6-6) likely masks the presence of significant temporary biases that change direction during the year. Indeed, Figure 7-18 shows the observed and simulated LST during the 3 ½ days of data assimilation event 1 and demonstrates that the LST from the reference site observations is warmer than that simulated by the control run, so its assimilation will act to reduce the soil moisture rather than correct (raise) the lowering of soil moisture from the imposed reduction of precipitation. This is the opposite to what happened in identical twin experiment 1, which assimilated LST from the control run (which has lower diurnal LST than the test run) and resulted in increasing (correcting) the soil moisture.
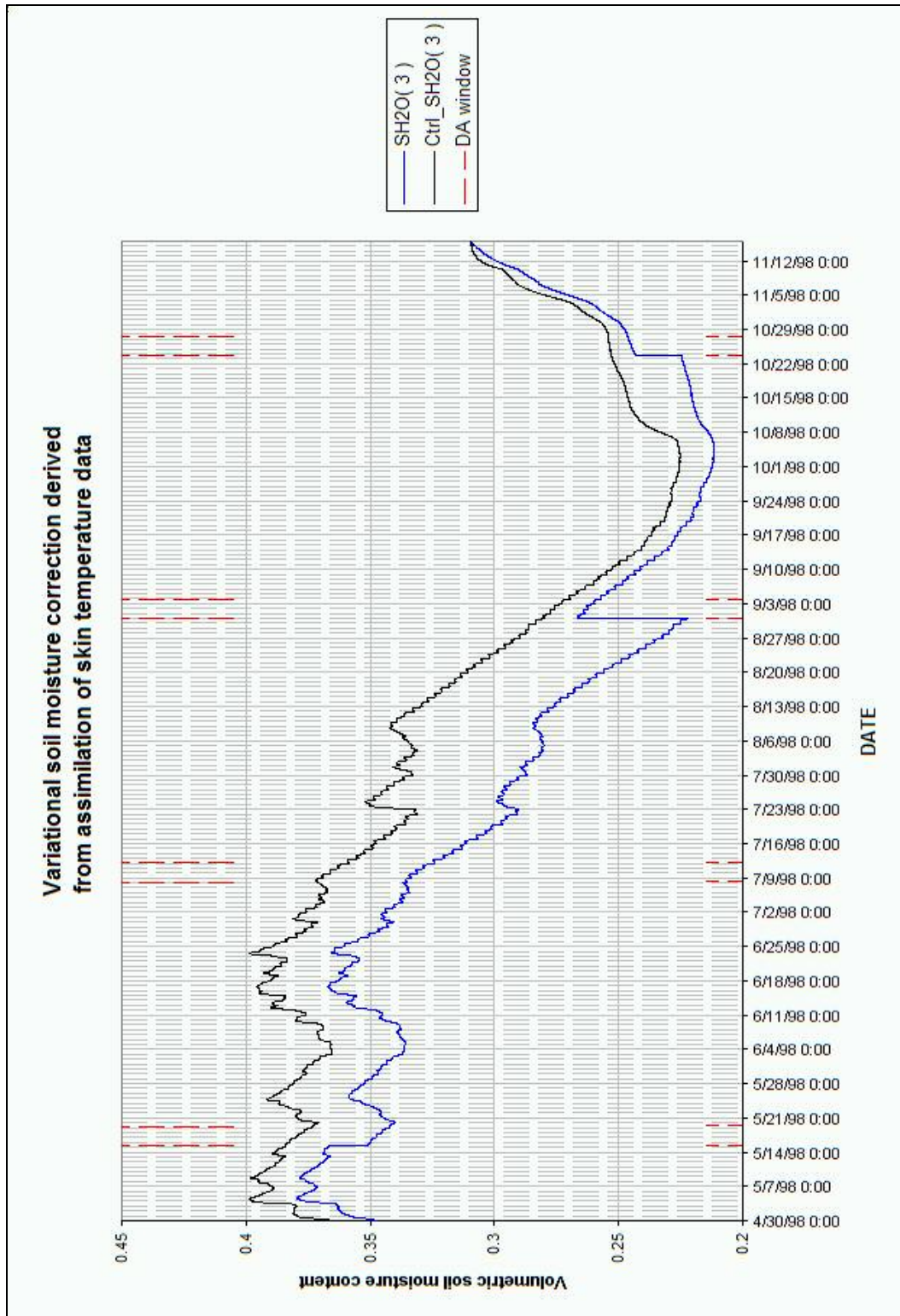
Figure 7-15 Experiment 5. Using a cost function of 3 ½ days. Soil moisture content evolution for the control run (black line) and data assimilation run (blue line). Soil layer 3.
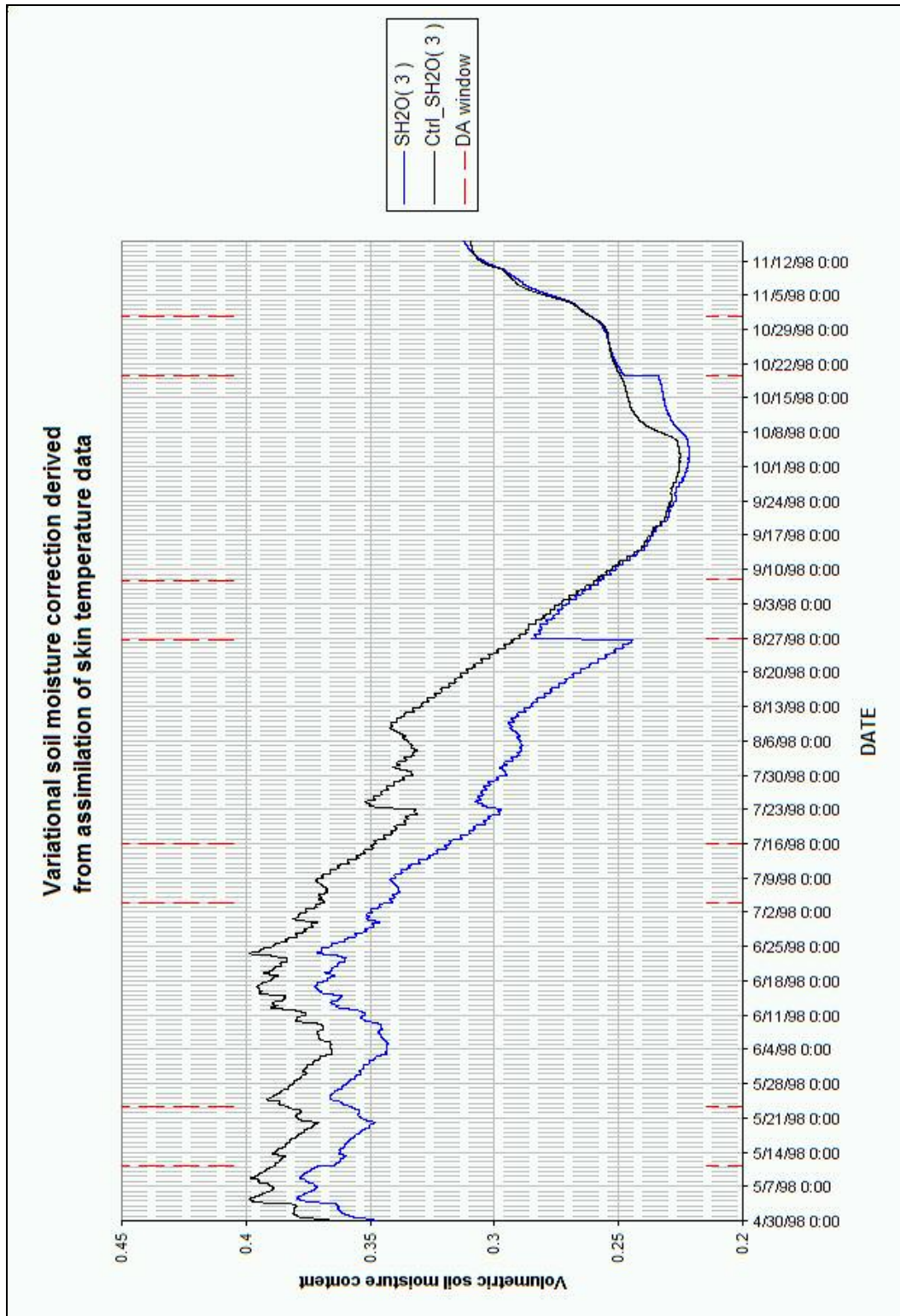
Figure 7-16 Experiment 5. Using a cost function of 11 days 20 hrs. Soil moisture content evolution for the control run (black line) and data assimilation run (blue line). Soil layer 3.

Figure 7-17 Experiment 5. Soil moisture profiles before and after data assimilation event 1 (mid-May) versus control.
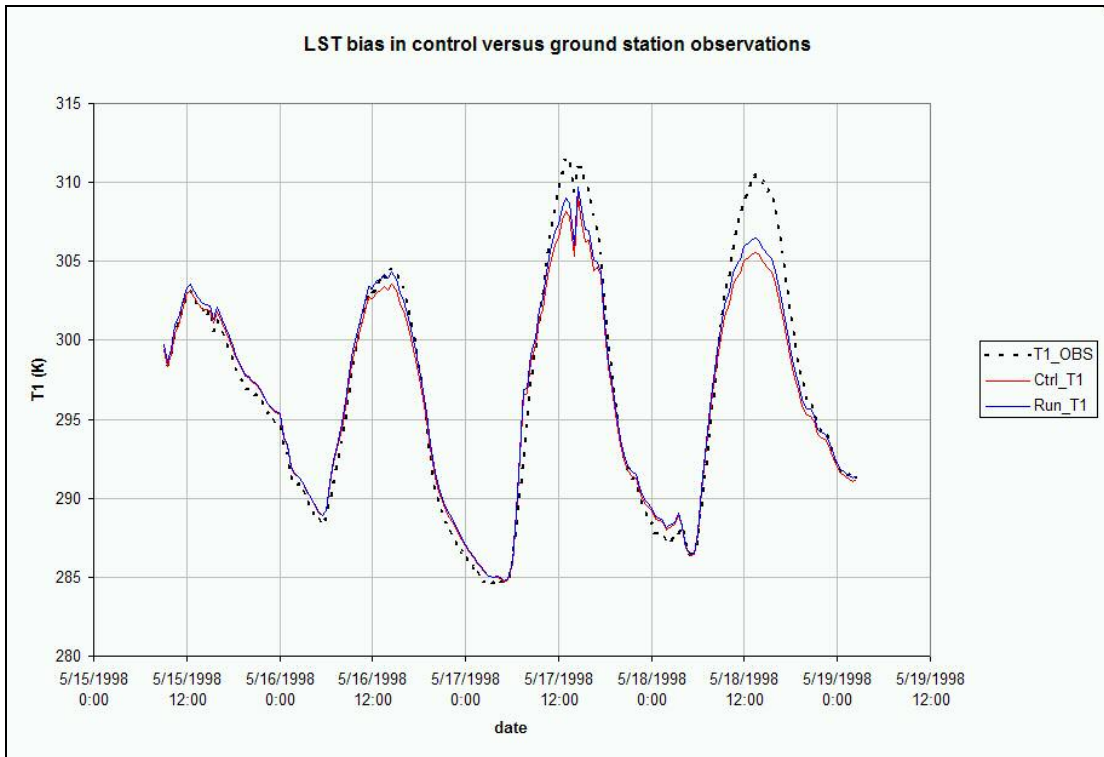
Figure 7-18 Experiment 5. Land surface temperature (LST, K) as 1) observed by ground station (dotted), 2) simulated by control run (red) and 3) simulated by run assimilating the ground station (blue)

7.2.2 Surface forcing from the North American Land Data Assimilation System (NLDAS)

In experiments 6 and 7 in this section and experiment 8 in section 7.2.3 the first run, taken as truth, is the original control, which over the year 1998, reproduced reasonably well the station LST observations (Figure 6-6). The forcing used for the assimilation runs in experiments 6, 7 and 8 instead of being different from that in the control run only in the precipitation, contains differences from the control in all the forcing fields, which are also expected to cause this run to depart from the reference trajectory. Specifically, the 1998 forcing data is taken from analyses that combine atmospheric observations and background states from runs of a mesoscale atmospheric model (see Mitchell et al., 2004 for an overview of the NLDAS project and references to companion papers). This NLDAS data was interpolated spatially from its nearest four grid points to the reference site location and temporally from 1-

hour resolution to the 30 minutes resolution matching the reference site station data. **The added challenge then for experiments 6, 7 and 8 is that not only the precipitation is different from the control but <u>all</u> the seven forcing fields differ (and by <u>either</u> <u>sign</u>) from what is used for the control run (see section 4.1 for a listing of the required forcing fields).**

Experiment 6 is the first of the NLDAS forcing experiments examined here. The assimilated observation used in the data assimilation run for experiment 6 is the LST from the reference site ground station, as in experiment 5 (longer assimilation window case). Figure 7-19 shows the time evolution of the soil moisture in model soil layer 3 for these runs.
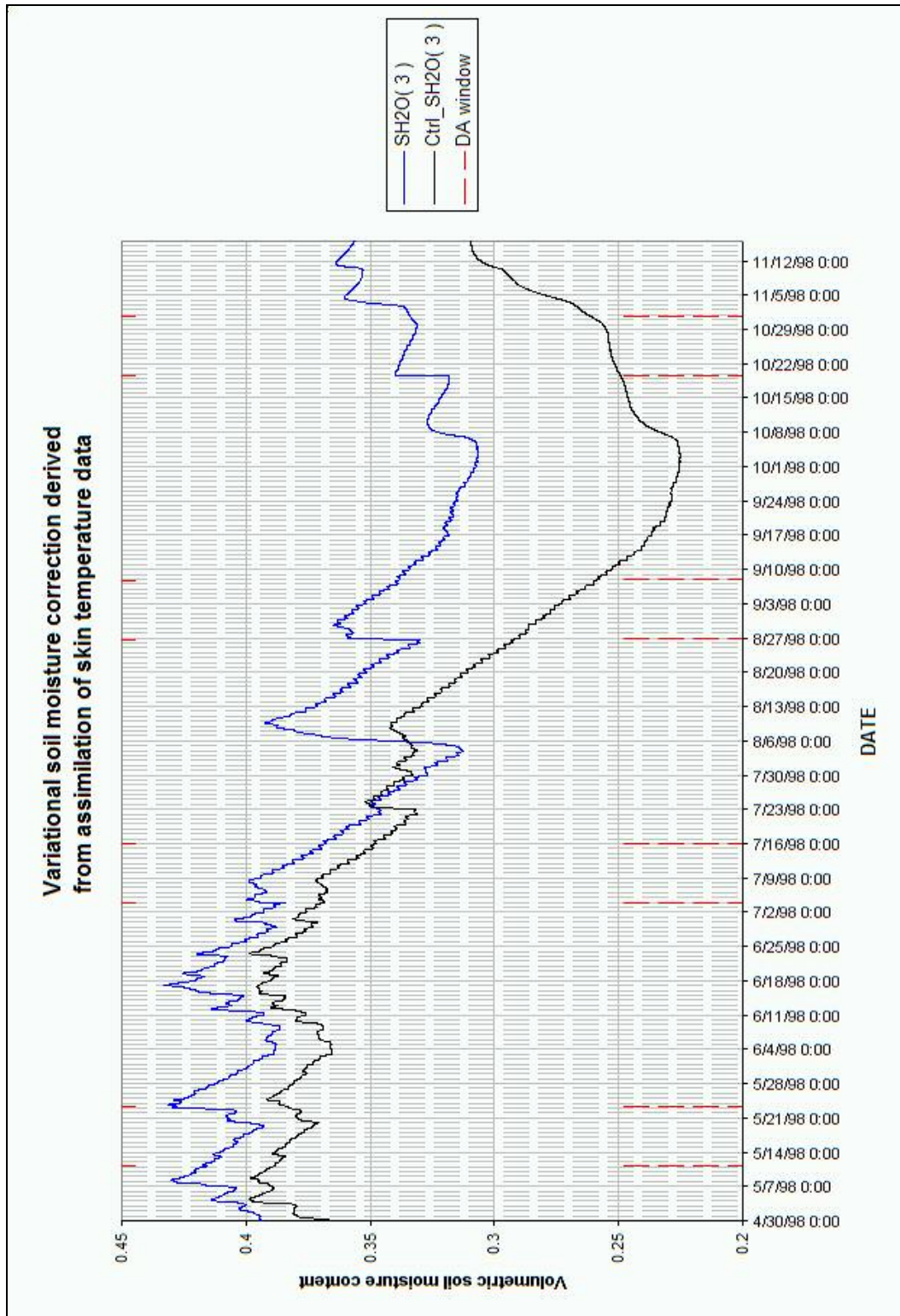
Figure 7-19 Experiment 6. NLDAS forced run with assimilation of LST from the reference site ground station. Soil layer 3 moisture content evolution.

Assimilation event 1 had almost no impact and, event 2 produced a small change. Inspection of the early August period (a non-assimilating period) of the assimilation run in Figure 7-19 reveals a big departure (of increasing soil moisture) away from the control run. The magnitude and quickness of the departure strongly suggests a large precipitation event in the NLDAS forcing that was mostly absent from the control forcing. Following this early August departure, the subsequent assimilation events 3 and 4 in late August and October produced strong changes in the wrong direction, also depicted in the profiles (Figure 7-20 and Figure 7-21). Given this undesired result, it was deemed wise to test again the assimilation of LST from the control run, which was the object of experiment 7, described next.
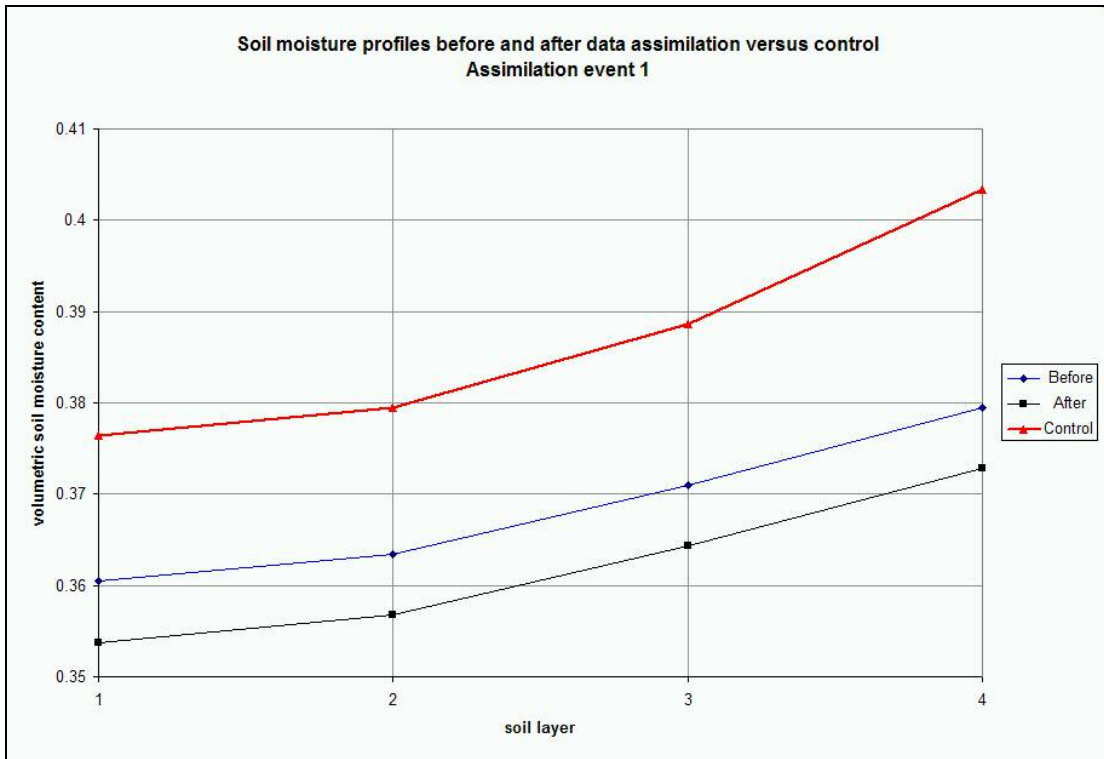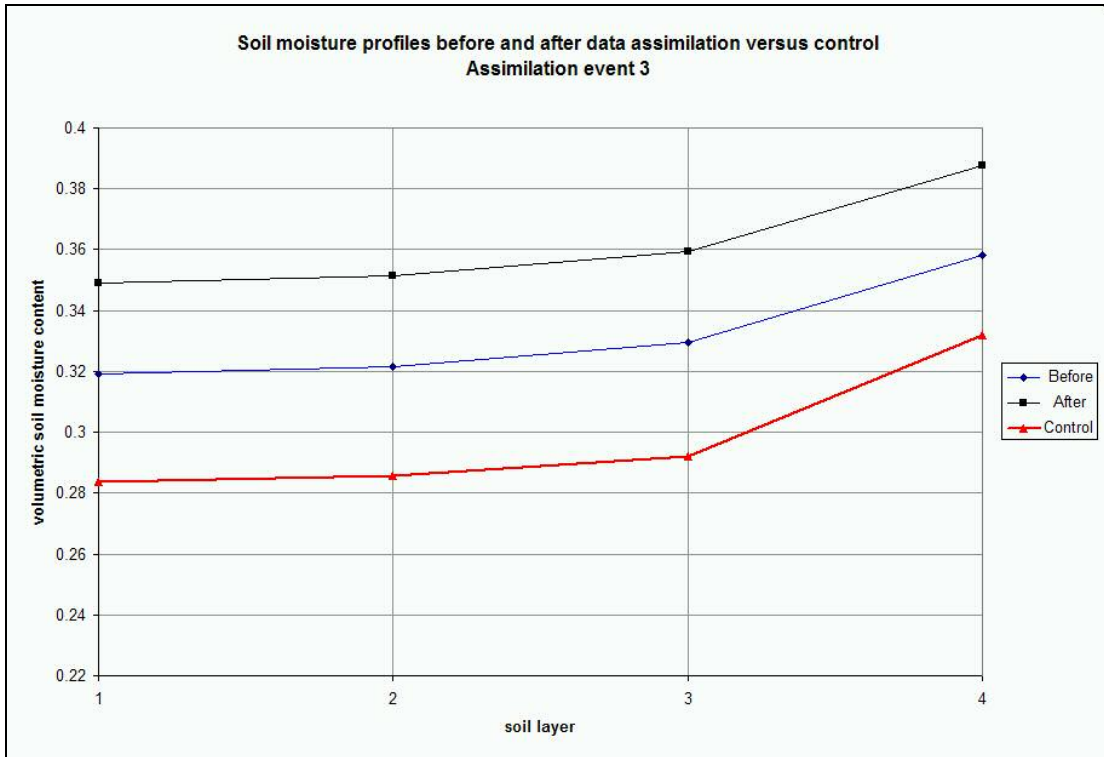

Figure 7-20 Experiment 6. Soil moisture profiles before and after data assimilation event 3 (September) versus control.
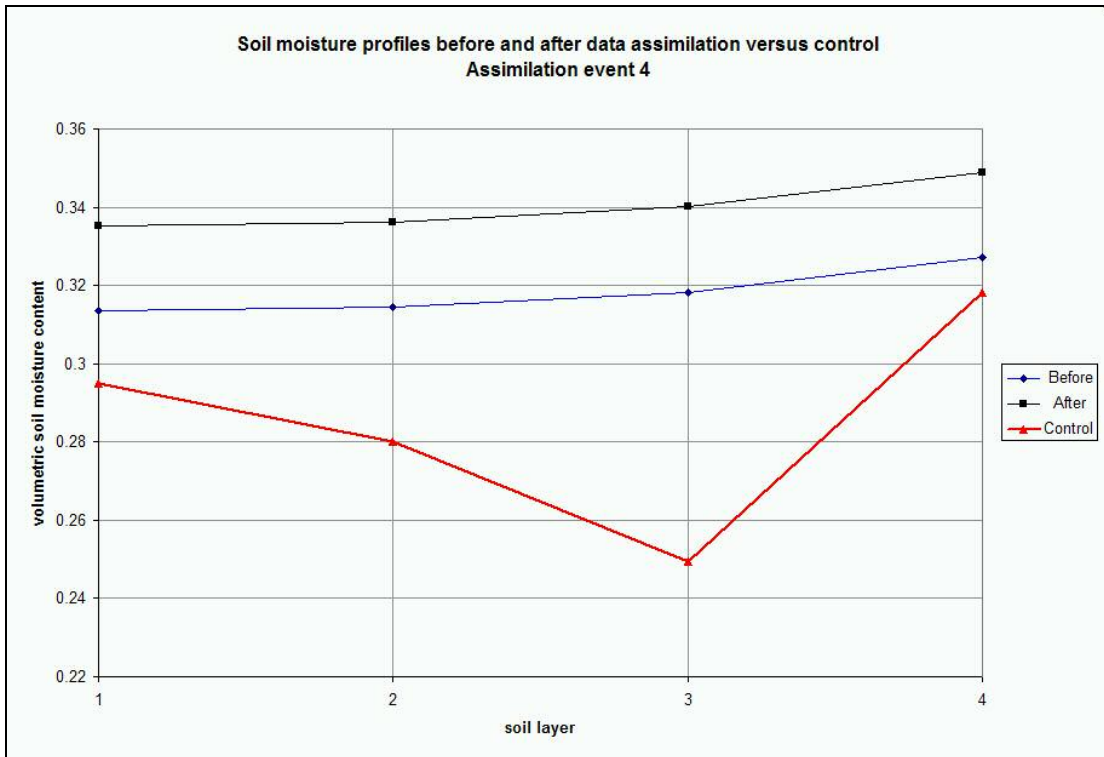
Figure 7-21 Experiment 6. Soil moisture profiles before and after data assimilation event 4 (end of October) versus control.

Experiment 7 is similar to 6 in which the data assimilation run is an NLDAS forced run, but control run LST (rather than ground station observed LST) is assimilated to derive soil moisture corrections. The time evolution for the soil moisture in layer 3 (Figure 7-22) and the soil moisture profile for data assimilation event 1 (Figure 7-23) indicate that the corrections derived are still in the wrong direction.

This result seems to contradict the idea that in a "perfect model" situation, assimilating data from the control ("true") run would be sufficient to bring the soil moisture states trajectory closer to that of the control run. However, we must remember that the NLDAS run has completely different forcing from that of the control run, including not only precipitation but also radiation, wind, air temperature, pressure and humidity. The data assimilation scheme can find the soil moisture states that make the test run's land surface temperature be closest to that of the assimilated

114

LST over the data assimilation window, but since the test run LST is also responding to a very different direct forcing error (such as radiation), that does not mean making this run's LST closer to that of the control run and consequently, does not mean finding a soil moisture state closer to that of the control run. This is to say that in experiments 6 and 7 the error in simulated LST may be arising not from soil moisture error due to wrong precipitation, but from other forcing error. If, for example, the radiative forcing is overestimated, this will tend to produce a warm LST in the model, and if we force a correction using only the soil moisture, the soil moisture will be incorrectly increased in order to cool the LST to counteract the warming of LST from high radiation forcing.

To illustrate this, Figures 7-24 to 7-26 below show (for a time interval within assimilation event 1) the model LST behavior with respect to different types of forcing error compared to the control. First, Figure 7-24 shows the LST time series of the assimilation run of experiment 7, along with the control run, corresponding to the two runs given by the red and black curves of Figure 7-23. Figure 7-24 shows that the LST of the two runs agree closely, despite significant differences (of order .05) in their soil moisture. Hence, the LST of the control run and the NLDAS-forced assimilation run of experiment 7 do not differ much despite non-trivial difference in their soil moisture states. This indicates that the data assimilation scheme has succeeded in modifying the soil moisture so that the assimilated run has an LST very similar to that of the observations (control or "truth"). Therefore, the assimilation run in experiment 7 provides a case where an error in soil moisture is not accompanied by a significant error in skin temperature. The latter result means that other sources of LST error besides soil moisture error are operating in the NLDAS-forced runs. As a reverse confirmation of the latter conclusion, Figure 7-25 shows cooler LST in the control run than in a <u>non-assimilating</u> test run whose <u>only</u> difference from the control is the application of slightly less precipitation forcing (and hence less soil moisture, which results in lower surface latent heat flux and thus warmer LST than the control).

A further illustration of error that emerges in simulated LST due to forcing errors unrelated to precipitation error, and its attendant soil moisture error, is given in Figure 7-26. This figure shows warmer LST in the control run compared to a <u>non-</u>

assimilating test run in which the only difference from the control is a 30% reduction of the surface solar insolation. The figure demonstrates that the radiation reduction alone reduced the LST. Such non-precipitation forcing errors will disrupt and distort the determination of soil moisture corrections from the contrast between model and observed LST. In the case of Figure 7-26, an attempt to assimilate the warmer control run LST into the test run would erroneously decrease the soil moisture in order to reduce the surface latent heat flux and cause an increase in the simulated LST. This important result from non-precipitation forcing errors is illuminated further in Section 7.3
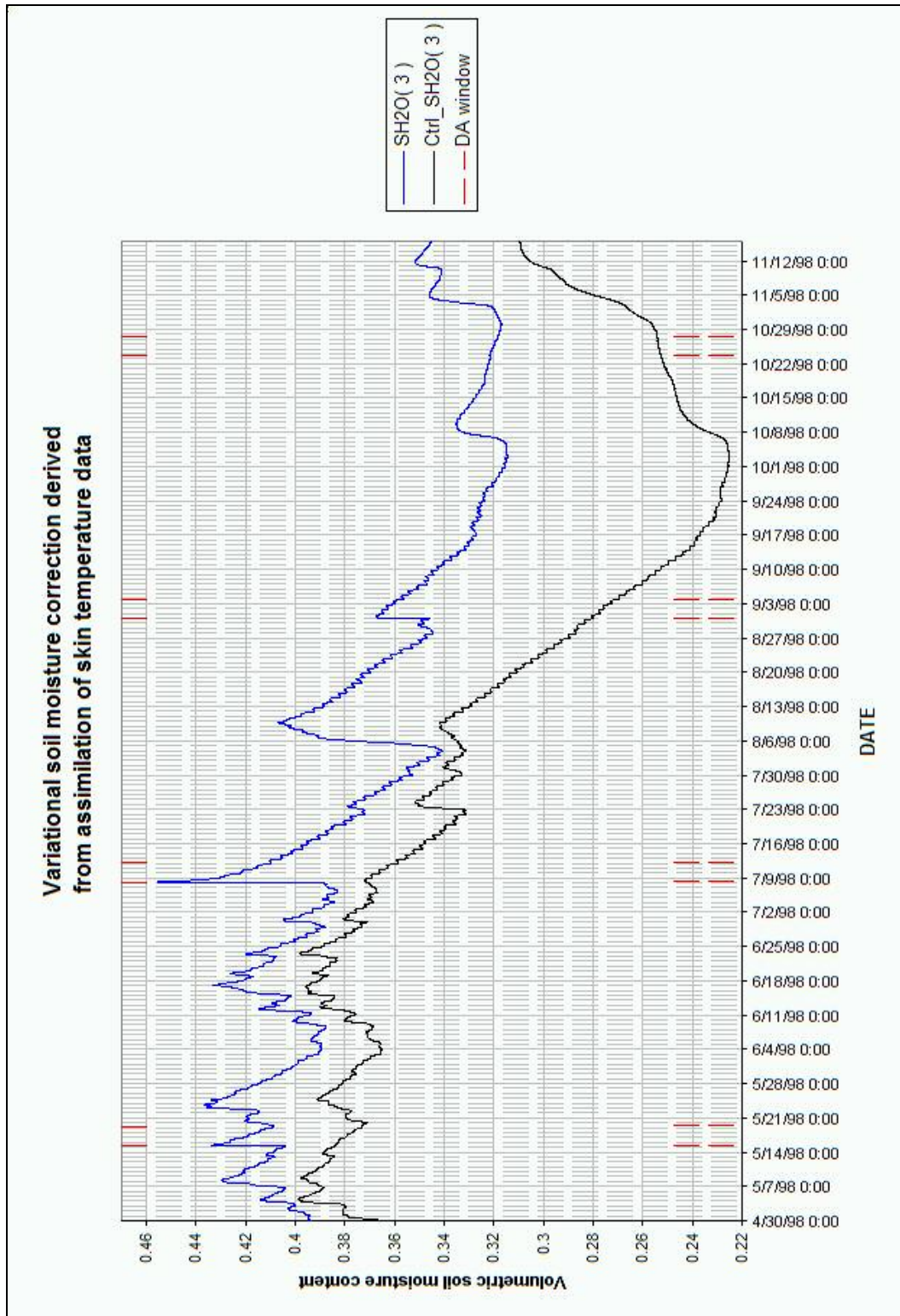
Figure 7-22 Experiment 7. NLDAS forced run with assimilation of LST from the control run. Soil moisture evolution for model soil layer 3.

Figure 7-23 Experiment 7. Soil moisture profiles before and after data assimilation event 1 (mid May) versus control.
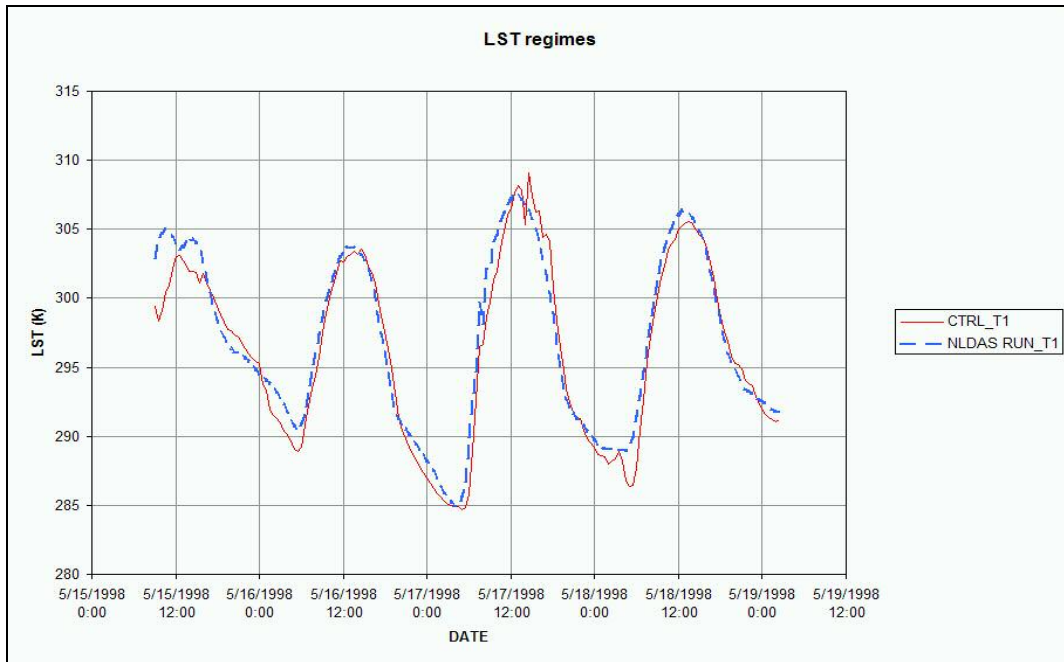
Figure 7-24 Experiment 7. Land surface temperature (LST) diurnal cycles during the time window of data assimilation event 1. Shown here are control (red) and NLDAS forced run (blue dashed line).
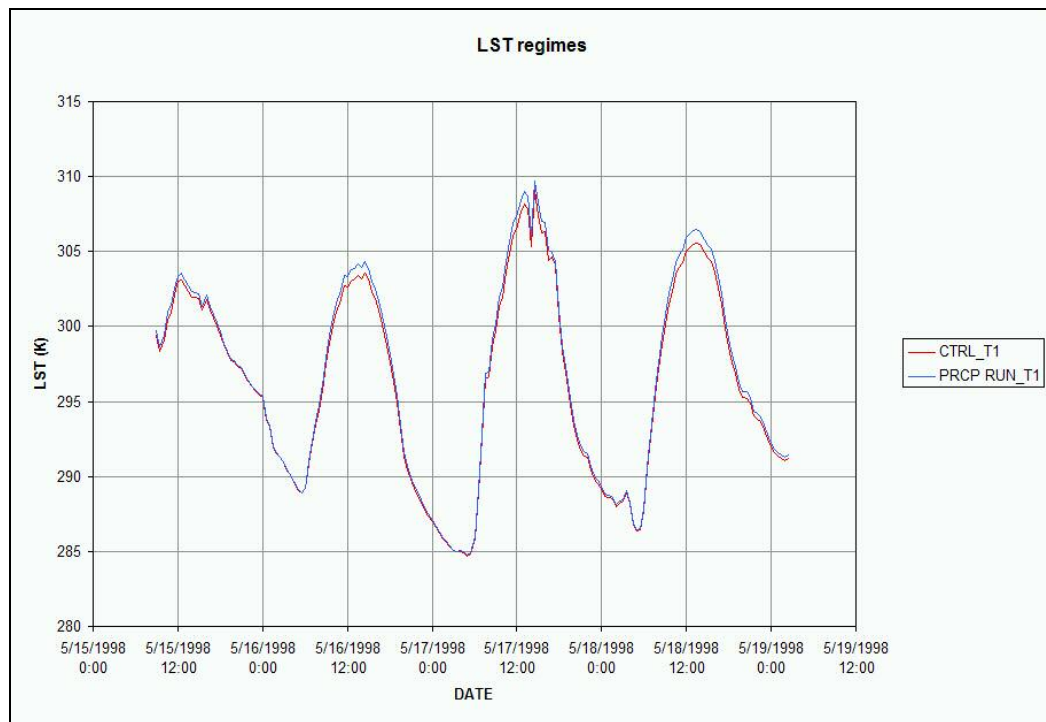
Figure 7-25 Soil moisture effect on land surface temperature diurnal cycle by comparison between model runs in which one of them (blue line) received less precipitation.

The precipitation reduced run (blue line) shows greater LST amplitude due to its reduced soil moisture content.
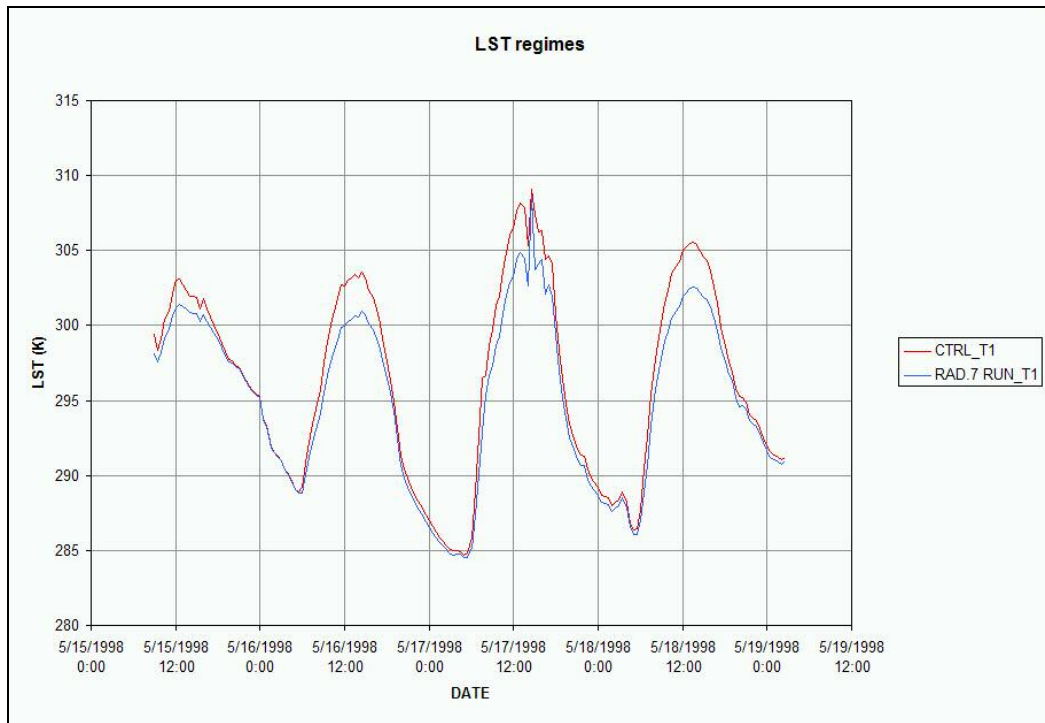
Figure 7-26 Solar radiation effect on land surface temperature (LST) diurnal cycle by comparison between model runs in which one of them received less solar radiation forcing (70%). The radiation reduced run (blue line) shows smaller LST amplitude.

7.2.3 Assimilating LST from the GOES satellite

GOES satellites provide the feasibility of retrieving hourly LST on a continental scale as discussed in section 4.3.. This would make possible the assimilation of LST in order to correct soil moisture initial condition in land surface models.

Experiment 8 differs from 7 and 6 by the fact that the assimilated LST comes from the GOES LST retrieval of section 4.3 temporally and spatially interpolated in the same form to the reference site as it was done with the NLDAS forcing. Also, since the temporal availability of this GOES LST data is sparse, data assimilation events were restricted to situations when at least six consecutive hours of GOES LST

data were available and the data assimilation time windows were restricted to this availability. In this data set, the longest time series of consecutive hourly GOES LST was 11 hours. Such data assimilation windows are too small to be visualized as two different marks signaling the beginning and end in a figure depicting a yearly time scale. Thus each mark labeled "DA event" in Figure 7-27 are actually two marks (representing the beginning and end of the data assimilation window).

In experiment 8 the evolution third layer soil moisture (Figure 7-27) shows that the data assimilation events alter the trajectory of the data assimilation run (blue line) considerably in the direction of the control run (black line), as can be seen by comparison with the NLDAS forced run without data assimilation (dotted red). Nevertheless, the assimilation run (blue line) quickly departs from the control run (black line) in between data assimilation events during the moisture charged, rainy part of the year (April-May) suggesting the strong differences in forcing and the limited memory of the system under these conditions. The presence of 1-2 degrees Kelvin warm biases (not shown) in the GOES land surface temperature are, to a certain extent, offset by the high surface solar insolation biases (not shown) imposed on the model land surface temperature under NLDAS forcing, causing the soil moisture corrections to be in the right direction (before and after profiles Figure 7-27 to Figure 7-32).
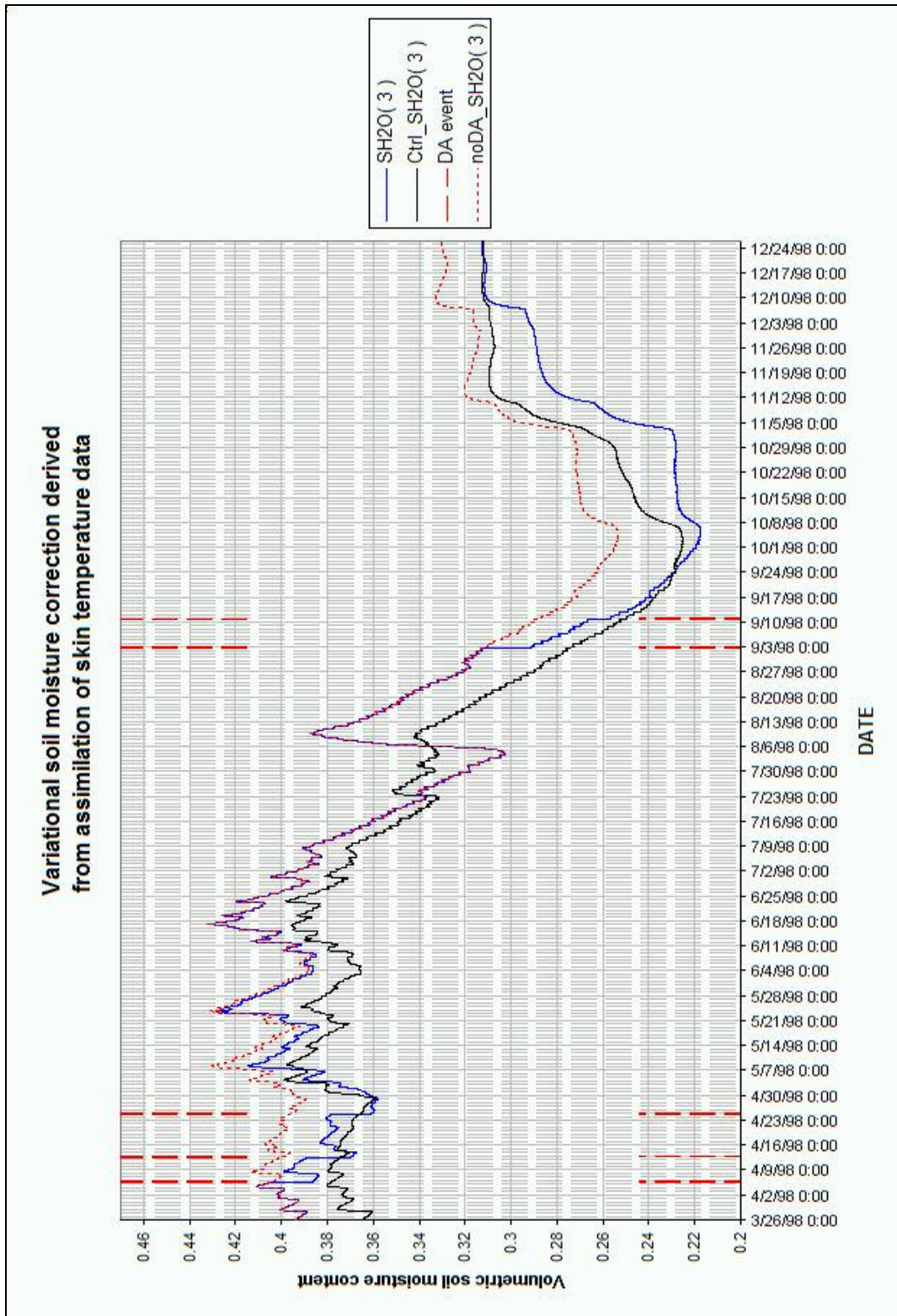
Figure 7-27 Experiment 8. Soil moisture content evolution for the control run (black), the NLDAS forced GOES LST data assimilation run (blue) and the NLDAS forced run without data assimilation (dotted red). Third soil layer.
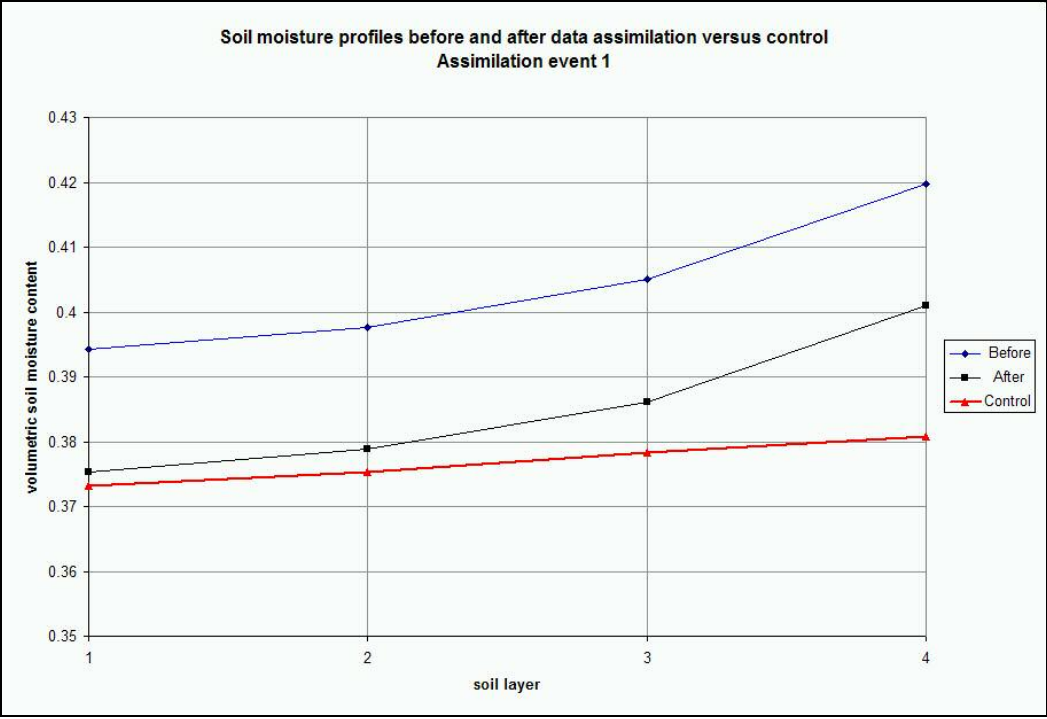
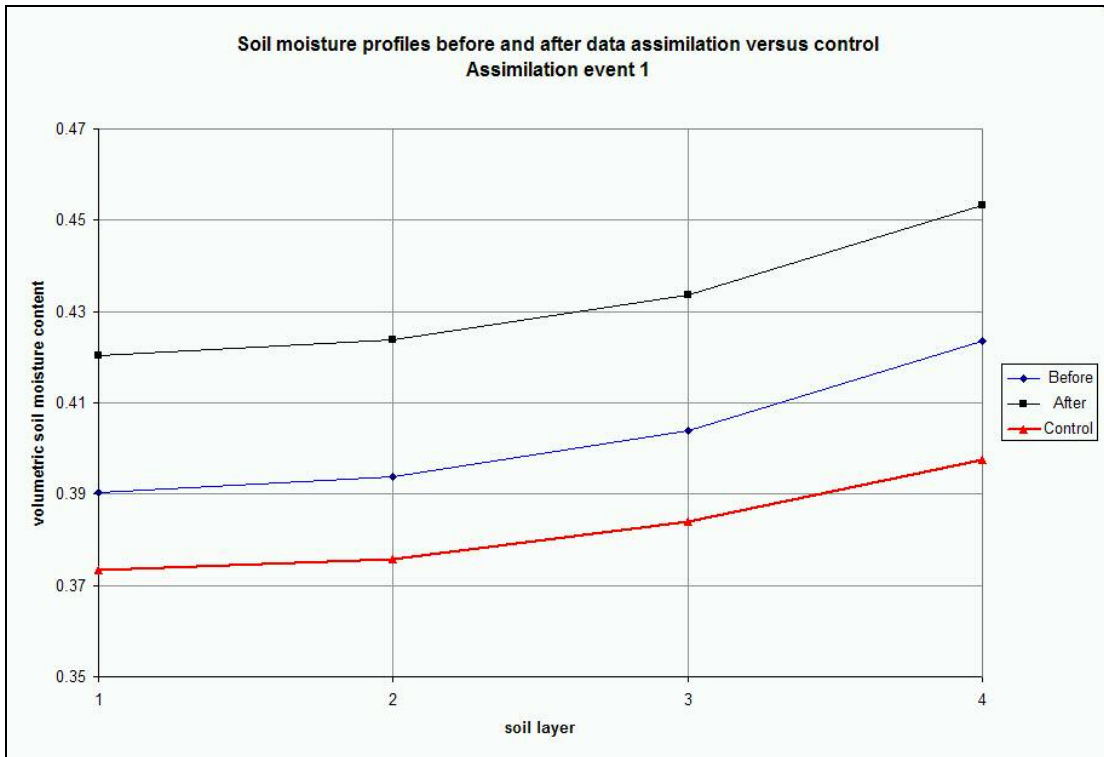**Figure 7-28 Experiment 8. Soil moisture profiles before and after data assimilation event 1 (early April) versus control.**
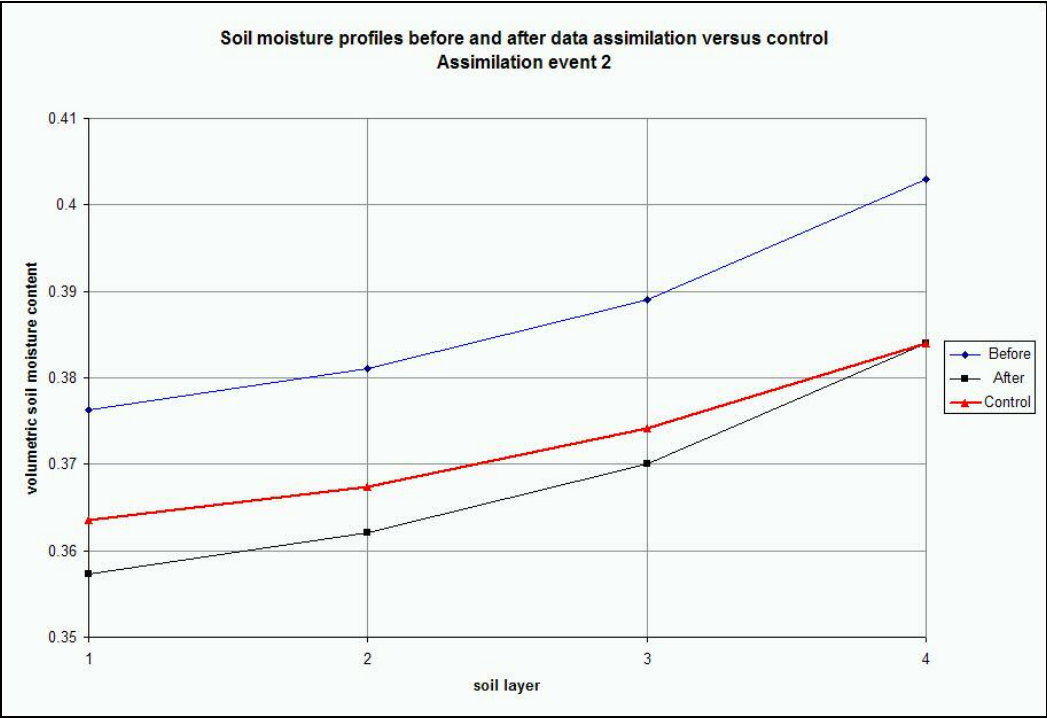

Figure 7-29 Experiment 8. Soil moisture profiles before and after data assimilation event 2 (mid April) versus control.
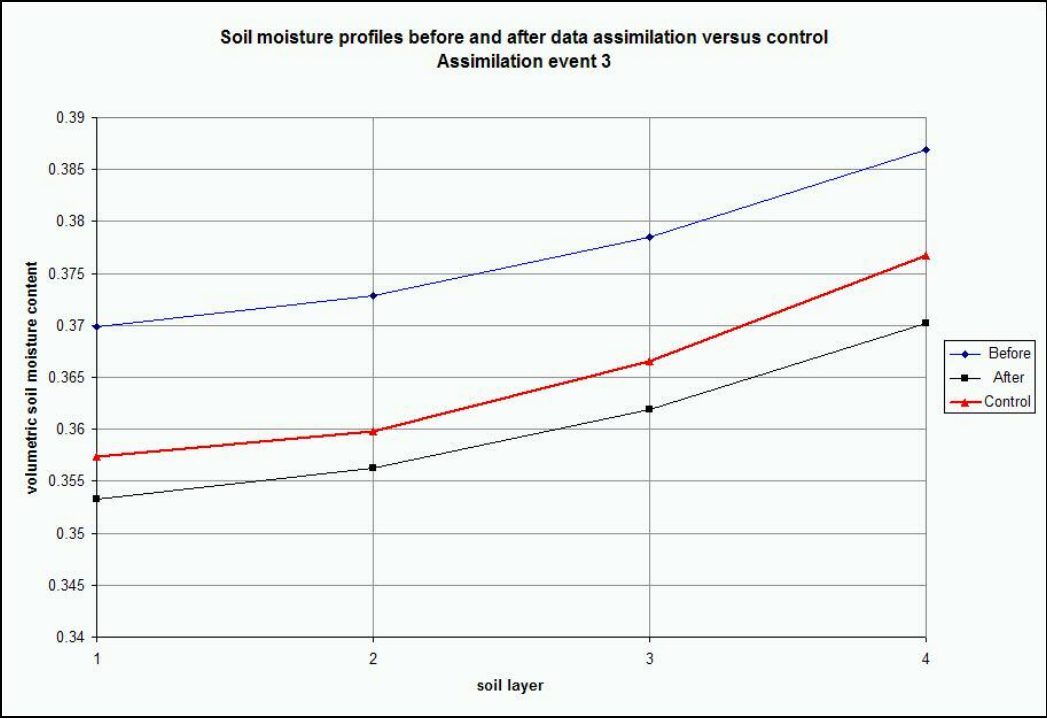
Figure 7-30 Experiment 8. Soil moisture profiles before and after data assimilation event 3 (late April) versus control.
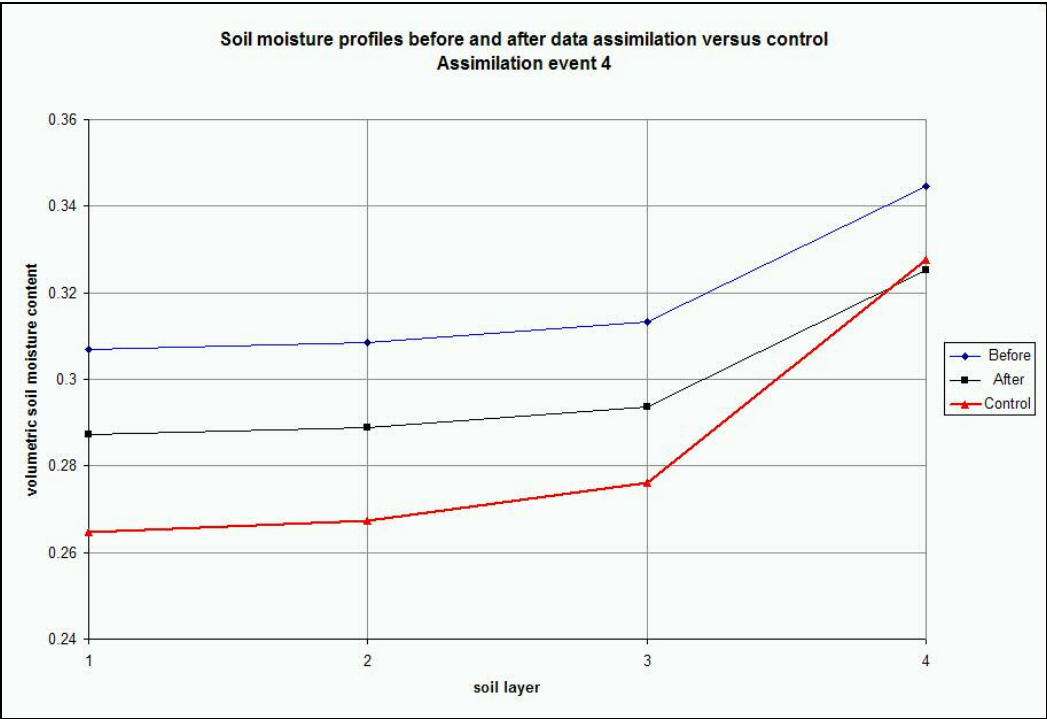
Figure 7-31 Experiment 8. Soil moisture profiles before and after data assimilation event 4 (early September) versus control.
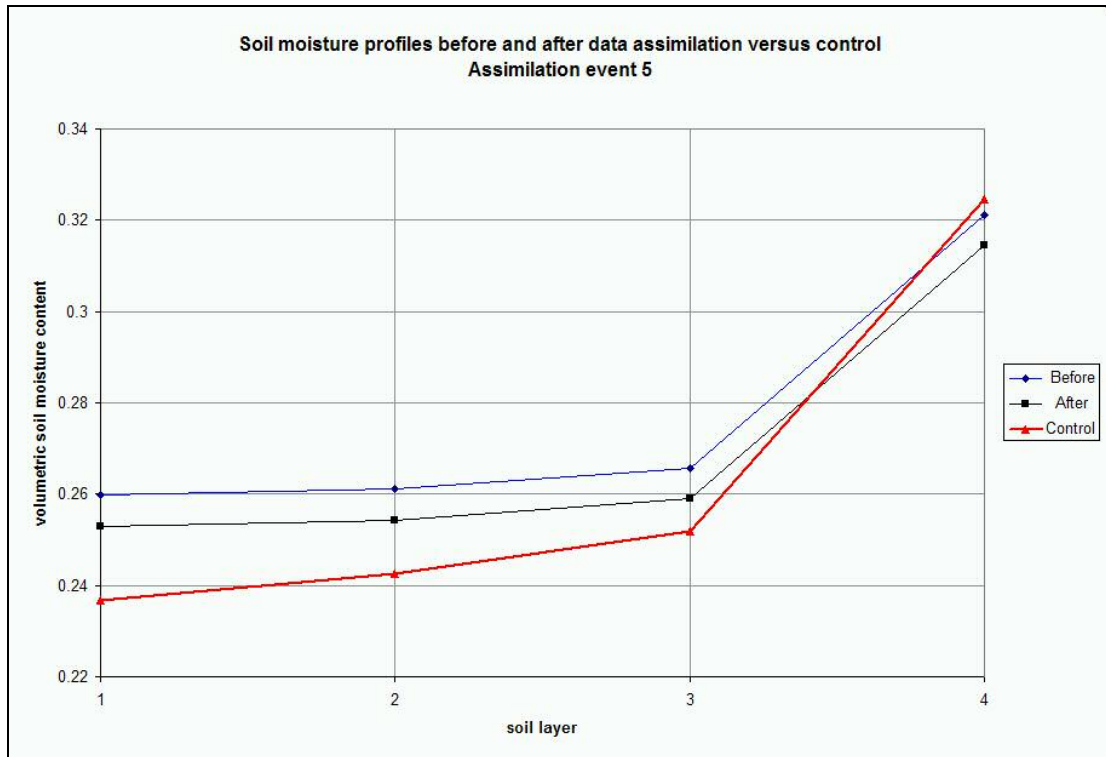
Figure 7-32 Experiment 8. Soil moisture profiles before and after data assimilation event 5 (mid September) versus control.

7.3 Conclusions from the ideal and real data assimilation experiments.

In summary, we have shown that the assimilation of LST (a variable that in principle can be observed from geostationary satellites and/or from ground stations) to improve the initialization of soil moisture (a variable that is generally unobserved but which influences the forecasts) is feasible if the surface forcings other than precipitation are known with great accuracy and the model is not biased.

With a realistic model and detailed observations of surface forcing, we were able to generate realistic LST and soil moisture for a given station. With this model, and accurate forcing besides precipitation, we did succeed in improving substantially the initial soil moisture by assimilating LST, even if the precipitation driving the soil model was either substantially overestimated or underestimated.

However, when we used surface forcing estimated from NLDAS, which have substantial uncertainties and probably significant biases, in both precipitation and non-precipitation forcing like radiative fluxes, we found that the results were not good (Experiment 7). Essentially, the assimilation system, as designed, was able to change the model LST in order to reproduce the assimilated LST by modifying the soil moisture. In this case, however, the origin of the LST error in the model was not the precipitation forcing and soil moisture but the non-precipitation forcing. This indicates that the problem of soil moisture initialization is not sufficiently constrained by the observations of LST alone. Possible approaches to deal with this important problem are briefly discussed in the final chapter.

Chapter 8

Conclusions

Land surface models are used to compute energy and water fluxes between the land and the atmosphere. A very important requirement of these models is the initial values of soil moisture, which is difficult to measure over large areas. Good quality soil moisture measurements for the above purposes involve planting devices into the soil at several depths between 0 and 1 meter or more. The problems are the large areas needing measurement and the spatial and temporal variations of soil moisture.

Through physics (Chapters 2 and 3), land surface models couple the soil moisture with other variables (such as low-level air temperature and relative humidity, land surface temperature, and sensible, latent and ground heat fluxes at the surface). Some of those (like land surface temperature) are easier to remotely measure than the soil moisture itself. Variational techniques allow the solution of the inverse problem of using land surface models to determine the soil moisture content from information on other variables (Chapter 2). The land surface model quality is important. We showed in Chapter 5 and in section 6.2 the several components of this project that led to improvements in either the model or in its numerical properties, leading to more efficient minimization algorithms.

The main results of assimilating LST in order to estimate the initial soil moisture were presented in Chapter 7. The "perfect model" scenarios (such as the twin experiment, section 7.1) work very well (Figure 7-1) when only errors in the soil moisture content are affecting the observed variable (LST). In this sense, the methodology has succeeded: if the other surface forcings are accurate, the assimilation of LST succeeds in substantially improving the soil moisture.

However, when we used surface forcing fields that would be available operationally, such as those from the NLDAS, the results were not good. This is because when other factors (such as radiative fluxes) influence the observed variable (LST), the influence from the soil moisture content is not easily recovered. The method successfully modifies the soil moisture in such a way as to make the model

LST follow the observed LST during the assimilation window, but this may not be desirable when the errors in the non-precipitation forcings are large enough to impact the LST at least as much as the errors in the soil moisture.

Future developments suggested by this work indicate the need to observe and use more variables in combination leading to isolating the effects of the soil moisture content on this new set of observations. Variational techniques can also be used to optimize the model (e.g. model parameters) but need reliable observations related to model output in order to adjust the model to reproduce their behavior. There have been recent developments in data assimilation that also offer considerable promise for attacking this problem. In particular, a new method known as 4-Dimensional Ensemble Kalman Filter (Hunt et al, 2004) has several advantages of both 4D-Var and Ensemble Kalman Filter (EnKF). Like other EnKF approaches, it does not require the linear tangent or adjoint models, and it solves the assimilation problem directly, not iteratively. EnKF would allow a simple inclusion of error correlations between different variables and forcings, thus reducing the problem of spurious corrections of soil moisture to account for errors due to other forcings that we found when using real data. EnKF can also be modified to estimate model deficiencies. 4D EnKF shares the ability of 4D-Var of assimilating observations at their correct time within an assimilation window, at the end of which the system provides not only an analysis but also an analysis error covariance. We believe that the combination of using more observations and such a flexible approach can achieve the desired goal of initializing soil moisture more accurately and thus improving forecasts.

Appendices

Appendix A: Limitations to the convergence of a finite-difference approximation scheme to the derivative in the presence of round-off errors.

A finite-differences estimate of the first derivative of a function calculated with a certain computer precision carries two major sources of error: the truncation error and the condition error (Gill et al., 1981). It will be shown that in this case, the truncation error cannot be arbitrarily diminished by decreasing the differences interval, h, because the uncertainties in the function computation are being magnified by a factor of $\frac{1}{h}$ in the finite differences formula.

The truncation error from a finite-differences estimate of the first derivative can be derived from the Taylor series expansion

$$f(x+h) = f(x) + hf'(x) + \frac{1}{2}h^2 f''(\xi)$$

yielding

$$f'(x) = \frac{f(x+h) - f(x)}{h} - \frac{1}{2}h^2 f''(\xi)$$

indicating that the error in the approximation,

$$f'(x) \approx \frac{f(x+h) - f(x)}{h}$$

will be in the magnitude of $\frac{1}{2}h \left| f''(\xi) \right|$, where ξ is between x and $x + h$.

The condition error is calculated from the rounding errors in the evaluation of the function f itself at machine precision in the numerator of the finite differences formula, this rounding error is of the order of $\left| f(x) \right| \varepsilon$, where ε is the relative

precision of the computer calculation of f so, the condition error in the finite differences formula will be of the order of $\dfrac{|f(x)|\varepsilon}{h}$, and this becomes arbitrarily large if h becomes arbitrarily small. Therefore, the finite differences approximation error cannot be arbitrarily reduced by reducing the difference interval arbitrarily when the function being differentiated is computed with round-off errors.

Bibliography

Baer, F., and Simons, T.J., 1970: Computational stability and time truncation of coupled linear equations with exact solutions. *Monthly Weather Review*, Vol. 98, 665-679

Bastidas, L. A., H.V. Gupta, S. Sorooshian, W.J. Shuttleworth and Z.L. Yang "Sensitivity Analysis of a Land Surface Scheme using Multi-Criteria Methods", *Journal of Geophysical Research*, Vol. 104, No D16, p. 19,481-19,490, 1999.

Bastidas, L. A., H. V. Gupta, and S. Sorooshian, Bounding parameters of land surface schemes with observational data, in Observations and Modeling of the Land Surface Hydrological Processes*,* V. Lakshmi, J. Albertson & J. Schaake, Editors, Water Science and Application Volume 3, p. 65-76, American Geophysical Union, 2001.

Bastidas, L. A., H. V. Gupta, and S. Sorooshian, Parameter, Structure and Performance Evaluation for Land Surface Models, in Advances in the Calibration of Watershed Models, Q. Duan, H. V. Gupta, S. Sorooshian, A. Rousseau, and R. Turcotte, Editors, AGU, 2002.

Beljaars, A. C. M., Viterbo, P., Miller, M.J., Betts, A., 1996: The Anomalous Rainfall Over The United States During July 1993: Sensitivity To Land Surface Parameterization And Soil Moisture Anomalies. Monthly Weather Review, Vol. 124, No. 3, March 1996.

Bell, S., 1994: Mesoscale Assimilation Of Moisture Parameters. Hirlam 3 Workshop On Analysis, Initialization And Data Assimilation. Norrkoping 23-24 February 1994.

Berbery, E. H., K. E. Mitchell, S. Benjamin, T. Smirnova, H. Ritchie, R. Hogue and E. Radeva 1999: Assessment of land surface energy budgets from regional and global models*. J. Geophys. Res.,* **104**, D16, 19,329-19,348.

Berbery, E. H., Y. Luo, K. E. Mitchell, and A. K. Betts (2003), Eta model estimated land surface processes and the hydrological cycle of the Mississippi basin, J. Geophys. Res., 108(D22), 8852, doi:10.1029/2002JD003192.

Betts, A. K., Ball, J.H., 1995: The Fife Surface Diurnal Cycle Climate. Journal Of Geophysical Research, Vol. 100, No. D12, 25,679-25,693, December 20, 1995.

Betts, A. K., Ball, J.H., Beljaars, A. C. M., Miller, M. J., Viterbo, P., 1996: The Land Surface-Atmosphere Interaction: A Review Based On Observational and Global Modeling Perspectives. *Journal of Geophysical Research,* Vol. 101, No. D3, 7209-7225.

Betts, A. K., Hong, S.-Y., Pan, H.-L., 1996: Comparison Of NCEP-NCAR Reanalysis With 1987 Fife Data. Monthly Weather Review, Vol. 124, No. 7, July 1996.

Betts, A. K., Ball, J.H., 1997: Fife Surface Climate and Site-Average Dataset 1987-89. Journal of the Atmospheric Sciences, Vol. 55, No. 7, pp. 1091–1108.

Betts, A. K., Chen F., Mitchell, K.E., Janjic, Z., 1997: Assessment of the Land-Surface and Boundary-Layer Models in Two Operational Versions of the NCEP Eta Model Using Fife Data. *Monthly Weather Review*. Vol. 125. 2896-2916.

Betts, A. K., Viterbo, P., Wood, E., 1997: Surface Energy And Water Balance For The Arkansas-Red River Basin From The ECMWF Analysis. Submitted To Journal Of Climate.

Betts, A. K., Viterbo, P., Beljaars, A. C. M., 1998: Comparison Of The Land-Surface Interaction In The ECMWF Reanalysis Model With The 1987 Fife Data. Monthly Weather Review, Vol. 126, 186-198, January 1998.

Bouttier, F., 1994. Soil Moisture Assimilation At Meteo-France. Hirlam 3 Workshop On Analysis, Initialization And Data Assimilation. Norrkoping 23-24 February 1994.

Bouttier, F., J.-F. Mahfouf, J. Noilhan, 1993-A: Sequential Assimilation of Soil
Moisture from Atmospheric Low-Level Parameters. Part I: Sensitivity and
Calibration Studies. *Journal of Applied Meteorology*, Vol. 32, 1335-1351.

Bouttier, F., J.-F. Mahfouf, J. Noilhan, 1993-B: Sequential Assimilation of Soil
Moisture from Atmospheric Low-Level Parameters. Part II: Implementation
in a Mesoscale Model. *Journal of Applied Meteorology*, Vol. 32, 1352-1364.

Calvet, J-C., Noilhan, J., Bessemoulin, P., 1998: Retrieving The Root-Zone Soil
Moisture From Surface Soil Moisture Or Temperature Estimates: A
Feasibility Study Based On Field Measurements. Journal Of Applied
Meteorology, Vol. 37, 371-386, April 1998.

Campbell, G. S., A simple method for determining unsaturated conductivity from
moisture retention data, *Soil Sci*., 117, 311-314, 1974.

Cosgrove, B. A., et al. (2003), Real-time and retrospective forcing in the North
American Land Data Assimilation System (NLDAS) project, J. Geophys.
Res., 108(D22), 8842, doi:10.1029/2002JD003118.

Chen, F., and K. Mitchell, 1998: Using the GEWEX/ISLSCP Forcing Data to
Simulate Global Soil Moisture Fields and Hydrological Cycle for 1987-1988.
Submitted to the Journal Of The Meteorological Society Of Japan, June 30,
1998 (Accepted).

Chen, F., K. Mitchell, J. Schaake, Y. Xue, H.-L. Pan, V. Koren, Q.-Y. Duan, M. Ek
and A. Betts, 1996: Modeling Of Land-Surface Evaporation by Four Schemes
and Comparison with Fife Observations. *Journal of Geophysical Research*,
Vol. 101, No. D3, 7251-7268.

Chen, F., Z. Janjic and K. Mitchell, 1997: Impact of Atmospheric Surface-Layer
Parameterization in the New Land-Surface Scheme of the NCEP Mesoscale
Eta Model. *Boundary-Layer Meteorology*, v 85, no. 3, 391-422.

Cohn, S. E., 1997: An Introduction To Estimation Theory. Journal Of The
Meteorological Society Of Japan.

Cohn, S. E., Todling, R., 1995: Approximate Data Assimilation Schemes For Stable And Unstable Dynamics. Journal Of The Meteorological Society Of Japan. (Accepted)

Cosby, B.J., Et Al., 1984: A Statistical Exploration Of The Relationships Of Soil Moisture Characteristics To The Physical Properties Of Soils. Water Resources Research, Vol. 20, No. 6, 682-690, June 1984.

Courtier, P. Et Al., 1993: Important Literature On The Use Of Adjoint, Variational Methods And The Kalman Filter In Meteorology. Tellus, 45a (1993) 5, 342-357.

Courtier, P., 1997: Variational Methods. Journal Of The Meteorological Society Of Japan, Vol. 75, No. 1b. 211-218, 1997.

Deardorff, J. W. 1972: Parameterization of the planetary boundary layer for use in general circulation models. *Mon. Wea. Rev*., 100, 93-106.

Deardorff, J. W. 1978: Efficient prediction of ground surface temperature and moisture with inclusion of a layer of vegetation. *J. Geophys. Res*., 83, 1889-1903.

Derber, J. C., 1987: Variational Four-Dimensional Analysis Using Quasi-Geostrophic Constraints. Monthly Weather Review, Vol. 115 No. 5. 998-1008.

Dirmeyer, P.A., 1997: Assessing GCM Sensitivity to Soil Wetness Using GSWP Data. Cola Report No. 47. Center For Ocean-Land-Atmosphere Studies. September 1997.

Dirmeyer, P.A., Zeng, F., 1997: A Two Dimensional Implementation of the Simple Biosphere (Sib) Model. Cola Report. Center For Ocean-Land-Atmosphere Studies. September 1997.

Dirmeyer, P.A.. et al., 2002: see International GEWEX Project Office, 2002 GSWP-2.

Duan, Q., Sorooshian, S., Gupta, V., 1992: Effective And Efficient Global Optimization For Conceptual Rainfall- Runoff Models. Water Resources Research, Vol. 28. No. 4. 1015-1031, April 1992.

Ek, M. And L. Mahrt, 1991: *A One-Dimensional Planetary Boundary Layer Model with Interactive Soil Layers and Plant Canopy. Users Guide Version 1.0.4.* College of Oceanic and Atmospheric Sciences, Strand Agriculture Hall, Rm. 326, Oregon State University Corvallis, Oregon 97331-2209 USA.

Ek, M. B., K. E. Mitchell, Y. Lin, E. Rogers, P. Grunmann, V. Koren, G. Gayno, and J. D. Tarpley (2003), Implementation of Noah land surface model advances in the National Centers for Environmental Prediction operational mesoscale Eta model, J. Geophys. Res., 108(D22), 8851, doi:10.1029/2002JD003296.

Entekhabi, D., Nakamura, H., Njoku, E.G., 1994: Solving The Inverse Problem For Soil Moisture And Temperature Profiles By Sequential Assimilation Of Multifrequency Remotely Sensed Observations. IEEE Transactions On Geoscience And Remote Sensing, Vol. 32, No. 2, 438-447. March 1994.

Farouki, O.T.,1986: Thermal Properties Of Soils. Series On Rock And Soil Mechanics, Vol. 11, Trans Tech, 136 Pp.

Garratt, J. R., 1993: Sensitivity of Climate simulations to Land-Surface and Atmospheric Boundary-Layer Treatments-A Review. *Journal Of Climate*, Vol. 6, 419-449.

Giering, R. And T. Kaminski, 1996: *Recipes for Adjoint Code Construction.* Tech. Report 212, Max-Planck-Institut Fur Meteorologie.

Giering, R., 1997: *Tangent Linear and Adjoint Model Compiler, Users Manual.* Max -Planck - Institut Fur Meteorologie.

Gill, P. E., W. Murray and M. H. Wright, 1981: *Practical Optimization.* Academic Press, New York.

Gutman, G., 1994: Global Data on Land Surface Parameters From NOAA AVHRR For Use In Numerical Climate Models. *Journal Of Climate*, Vol. 7, 669-680. May 1994.

Hicks, B.B., Deluisi, J.J., Matt, D. R., 1996: The NOAA Integrated Surface Irradiance Study (Isis)-A New Surface Radiation Monitoring Program. Bulletin Of The American Meteorological Society, Vol. 77, No. 12, December 1996. 2857-2864.

Hirlam 3 Workshop On Analysis, Initialization And Data Assimilation. Norrkoping 23-24 February 1994.

Hunt, B.R. , E. Kalnay, E.J. Kostelich, E. Ott, D.J. Patil, T. Sauer, I. Szunyogh, J.A. Yorke, and A.V. Zimin, 2004: Four-Dimensional Ensemble Kalman Filtering. Tellus 56A, 273-277.

International GEWEX Project Office, 2002: GSWP-2: The Second Global Soil Wetness Project Science and Implementation Plan. *IGPO Publication Series No. 37*, 65 pp.

Jacquemin, B. and J. Noilhan, 1990: Sensitivity study and validation of a land surface parameterization using the Hapex-Mobilhy data set. *Boundary Layer Meteorology*, 52: 93-134.

Jarviz, P. G., 1976: The interpretation of the variation in leaf water potential and stomatal conductance found in canopies in the field. Philosophical Transactions of the Royal Society of London B, 273, 593-610.

Jaervinen, Heikki, 1993: A direct conversion of model algorithms to their adjoints exemplified with a barotropic atmospheric model. Helsinki, Finland, University of Helsinki, Department of Meteorology, 1993. 41 pp. 1993.

Johansen, O., 1975: Thermal Conductivity Of Soils. Ph.D. Thesis, University Of Trondheim.w130)h

Jones, A. S., I. C. Guch, and T. H. Vonder Haar, 1998: Data Assimilation Of Satellite-Derived Heating Rates As Proxy Surface Wetness Data Into A Regional Atmospheric Mesoscale Model. Part I: Methodology. *Monthly Weather Review*, Vol. 126, 634-645.

Kalnay, Eugenia, 2003: Atmospheric Modeling, Data Assimilation and Predictability. Cambridge University Press, 341 pages.

Kapitza, H., 1991: Numerical Experiments With The Adjoint Of A Nonhydrostatic Mesoscale Model. Monthly Weather Review, Vol. 119, December 1991, 2993-3011.

Koren, V., J. Schaake, K. Mitchell, Q.-Y. Duan, F. Chen and JM Baker, 1999-A: A parameterization of snowpack and frozen ground intended for NCEP weather and climate models. *Journal Of Geophysical Research.* Vol. 104, no. D16, pp. 19569-19585.

Koren, V., Q.-Y. Duan and J. Schaake, 1999-B: Validation of a snow-frozen ground parameterization of the Eta model. Preprint *AMS 14 Hydrology Conference,* 10-15 January 1999, Dallas TX, Paper J1.3 .

Koster, R. D., and M. J. Suarez, 2003: Impact of Land Surface Initialization on Seasonal Precipitation and Temperature Prediction. J. Hydrometeorlogy, 4, 408-423.

LeDimet, F. X., and O. Talagrand, 1986: Variational algorithms for analysis and assimilation of meteorological observations. *Tellus* 38a , 97-110.

Lewis, J. M., J. C. Derber, 1985: The Use Of Adjoint Equations To Solve A Variational Adjustment Problem With Advective Constraints. *Tellus* 37a, 309-322.

Liang, X., E.F. Wood, D.P. Lettenmaier et al., The project for intercomparison of land-surface parameterization schemes (PILPS) phase-2c Red-Arkansas river basin experiment: 2. Spatial and temporal analysis of energy fluxes, *Global and Planetary Change*, 19(1-4), 137-159, 1998.

Lohmann, D., et al. (2004), Streamflow and water balance intercomparisons of four land surface models in the North American Land Data Assimilation System project, J. Geophys. Res., 109, D07S91, doi:10.1029/2003JD003517.

Luo, L. et al., 2003-A: Effects of Frozen Soil on Soil Temperature, Spring Infiltration, and Runoff: Results from the PILPS 2(d) Experiment at Valdai, Russia. *Journal of Hydrometeorology*: Vol. 4, No. 2, pp. 334–351.

Luo, L., et al., 2003-B: Validation of the North American Land Data Assimilation System (NLDAS) retrospective forcing over the southern Great Plains, J. Geophys. Res., 108(D22), 8843, doi:10.1029/2002JD003246.

Manabe, S., 1969: Climate and the circulation, I. The atmospheric circulation and the hydrology of the earth's surface. *Mon. Wea. Rev.*, 97, 739-774.

Mahfouf, J.-F., 1990a: A Numerical Simulation Of The Surface Water Budget During Hapex-Mobilhy. Boundary Layer Meteorology, 53: 201-222, 1990.

Mahfouf, J.-F., 1990b: A Variational Assimilation Of Soil Moisture In Meteorological Models. WMO International Symposium On Assimilation Of Observations In Meteorology And Oceanography. Clermont-Ferrand, France, July 1990.

Mahfouf, J.-F., 1991: Analysis Of Soil Moisture From Near-Surface Parameters: A Feasibility Study. *Journal Of Applied Meteorology*, Vol. 30 1534-1547.

Mahfouf, J-F. and P. Viterbo, 1996: Land Surface Assimilation. Proceedings Of Seminar On Data Assimilation. ECMWF. 2-6 September 1996. 319-347.

Mahrt, L. and M. Ek., 1984: The influence of atmospheric stability on potential evaporation. *Journal Of Climate and Applied Meteorology*, Vol. 23, no. 2, 222-234.

Mahrt, L., Pan, H. L., 1984: A Two-Layer Model Of Soil Hydrology. *Boundary-Layer Meteorology*, 29, 1-20

Marshall, C.H., 1998: *Evaluation Of The New Land-Surface And Planetary Boundary Layer Parameterization Schemes In The NCEP Mesoscale Eta Model Using Oklahoma Mesonet Observations*. M.Sc. Thesis. University of Oklahoma.

Marshall, C. H., K. C. Crawford, K. E. Mitchell and D. J. Stensrud. 2003: The Impact of the Land Surface Physics in the Operational NCEP Eta Model on Simulating the Diurnal Cycle: Evaluation and Testing Using Oklahoma Mesonet Data. *Weather and Forecasting*, 18, 748–768.

Mitchell, K. E., 1994: GCIP Initiatives In Operational Mesoscale Modeling And Data Assimilation At NMC. Preprint In The AMS Fifth Symposium On Global Change Studies, 23- 28 January 1994, Nashville TN, Paper 6.8, Pp.192-198.

Mitchell, K. E., J. Schaake, D. Tarpley, F. Chen, Y. Lin, M. Baldwin, E. Rogers, G. Manikin, A. Betts, Z. Janjic, Q.-Y. Duan, V. Koren, 1999-A: Recent GCIP Advancements in Coupled Land-Surface Modeling and Data Assimilation in the NCEP Mesoscale Eta Model. Preprint *AMS 14 Hydrology Conference,* 10-15 January 1999, Dallas TX, Paper 4B.1 .

Mitchell, K., P. Houser, E. Wood, J. Schaake, D. Tarpley, D. Lettenmaier, W. Higgins, C. Marshall, D. Lohmann, M. Ek, B. Cosgrove, J. Entin, Q. Duan, R. Pinker, A. Robock, F. Habets and K. Vinnikov, 1999-B: GCIP Land Data Assimilation System (LDAS) Project Now Underway. GEWEX News*,* Vol. 9, No. 4, November 1999, pp. 3-6, IGPO, Silver Spring, MD.

Mitchell, K. E., et al. (2004), The multi-institution North American Land Data Assimilation System (NLDAS): Utilizing multiple GCIP products and partners in a continental distributed hydrological modeling system, J. Geophys. Res., 109, D07S90, doi:10.1029/2003JD003823.

Namias, J., 1958: Persistence of mid-tropospheric circulations between adjacent months and seasons. The atmosphere and sea in motion (Rossby memorial volume). B. Bolin, Ed., New York: Rockefeller Inst.; Oxford University Press, 240-248

Nash, S. and A. Sofer, 1996: Linear and Nonlinear Programming. McGraw-Hill Co. Inc., 692 pp.

Navon, I. M., X. Zou, J. Derber and J. Sela, 1992: Variational Data Assimilation with an Adiabatic version of the NMC Spectral Model. *Monthly Weather Review*, Vol. 120, No. 7 1433-1446.

Noilhan J. and Planton, S.: 1989, 'A Simple Parameterization of Land Surface Processes for Meteorological Models', Mon. Wea. Rev. 117, 536–549.

Ottle, C., Vidal-Madjar, D., 1994: Assimilation Of Soil Moisture Inferred From Infrared Remote Sensing In A Hydrological Model Over The Hapex-Mobilhy Region. Journal Of Hydrology 158 (1994) 241-264.

Pan, H-L, 1990: A Simple Parameterization Scheme Of Evapotranspiration Over Land For The NMC Medium-Range Forecast Model. *Monthly Weather Review*, Vol. 118 No. 12, 2500-2512.

Pan, H-L, L. Mahrt, 1987: Interaction Between Soil Hydrology And Boundary-Layer Development. *Boundary-Layer Meteorology*, 38, 185-202.

Peters-Lidard, C. D., E. Blackburn, X. Liang, E. F. Wood, 1998: The Effect Of Soil Thermal Conductivity Parameterization On Surface Energy Fluxes And Temperatures. *Journal of the Atmospheric Sciences*, Vol. 55, 1209-1224.

Peters-Lidard, C.D., Zion, M.S., Wood, E.F., 1997: A Soil-Vegetation-Atmosphere Transfer Scheme For Modeling Spatially Variable Water And Energy Balance Processes. Journal Of Geophysical Research, Vol. 102, No. D4, 4303-4324, February 27, 1997.

Pinker, R., I. Laszlo, Y. Wang And J. D. Tarpley, 1996: GCIP Goes-8 Shortwave Radiation Budgets: Validation Activity. *Second International Scientific Conference On Global Energy And Water Cycle*, 245-249.

Pinker, R. T., et al. (2003), Surface radiation budgets in support of the GEWEX Continental-Scale International Project (GCIP) and the GEWEX Americas Prediction Project (GAPP), including the North American Land Data Assimilation System (NLDAS) project, J. Geophys. Res., 108(D22), 8844, doi:10.1029/2002JD003301.

Robock, A. Et Al., 1996: Soil Moisture Parameterization In GCMS And Evaluation of AMIP Simulations. Submitted To Earth Interactions. April 1996.

Schaake, J.C., Et Al., 1996: Simple Water Balance Model For Estimating Runoff At Different Spatial And Temporal Scales. *Journal Of Geophysical Research*, Vol. 101, No. D3, 7461-7475.

Shanno, D. F., 1978: Conjugate gradient methods with inexact linesearch. Math. Operations Res., 3, 244-256.

Shao, Y., Henderson-Sellers, A., 1996: Validation Of Soil Moisture Simulation In Land-Surface Parameterization Schemes With Hapex Data. Global And Planetary Change, 13 (1996) 11-46.

Smith, B., Et Al. 1994: Initialization Of Soil-Water Content In Regional-Scale Atmospheric Prediction Models. Hirlam 3 Workshop On Analysis, Initialization And Data Assimilation. Norrkoping 23-24 February 1994.

Sorooshian, S., Duan, Q., Gupta, V., 1993: Calibration Of Rainfall- Runoff Models: Application Of Global Optimization To The Sacramento Soil Moisture Accounting Model. Water Resources Research, Vol. 29. No. 4. 1185-1194, April 1993.

Stull, R., 1988: An Introduction To Boundary- Layer Meteorology. Kluwer, Massachusetts, 666 Pp.

Tarpley, J. D., I. Laszlo And R. T. Pinker, 1996: Experimental Goes Short-Wave Radiation Budget For GCIP. *Second International Scientific Conference On Global Energy And Water Cycle*, 284-285.

Todling, R., Cohn, S. E., Sivakumaran, N.S., 1997: Suboptimal Schemes For Retrospective Data Assimilation Based On The Fixed-Lag Kalman Smoother. Dao Office Note 97-Nn. Nasa. February 1997.

Van Den Hurk, B. J. J. M., Et Al., 1997: A New Methodology For Assimilation Of Initial Soil Moisture Fields In Weather Prediction Models Using Meteostat And NOAA Data. *Journal Of Applied Meteorology* V. 36 N. 9, 1271- 1283.

Viterbo, P. And C.M. Beljaars, 1995: An Improved Land Surface Parameterization Scheme In The ECMWF Model And Its Validation. *Journal Of Climate*. Vol. 8, 2716-2748.

Viterbo, P. And Illari, L. 1994: The Impact Of Changes In The Runoff Formulation Of A General Circulation Model On Surface And Near-Surface Parameters. *Journal Of Hydrology*. Vol. 155, no. 3 / 4 , 325-336.

Viterbo, P., 1996: *The Representation Of Surface Processes In General Circulation Models*. Ph.D. Thesis, University Of Lisbon, 201 Pp.

Viterbo, P., Courtier, P., 1995: The Importance Of Soil Water For Medium-Range Weather Forecasting. Implications For Data Assimilation. Proceedings Of WMO Workshop On Imbalances Of Slowly Varying Components Of Predictable Atmospheric Motions. Beijing, 1995.

Vukicevic, T. and R. Errico, 1993: Linearization and adjoint of parameterized moist adiabatic processes. *Tellus*, 45a, 493-510.

Wu, X., W. P. Menzel, and G. S. Wade (1999), Estimation of sea surface temperatures using GOES-8/9 radiance measurements, Bull. Am. Meteorol. Soc., 80, 1127– 1138.

Zou, X., I. M. Navon and J. Sela, 1993: Variational data assimilation with moist threshold processes using the NMC Spectral Model. *Tellus*, 45a, 370-387.

Zupanski, D., 1993: The effects of discontinuities in the Betts-Miller cumulus convection scheme on four-dimensional variational data assimilation. *Tellus*, 45a, 511-524.

Zupanski, D., 1996: A general weak constraint applicable to operational 4DVAR data assimilation systems. *Monthly Weather Review*, Vol. 125, 2274-2292.

Zupanski, D., Mesinger, F., 1995: Four-Dimensional Variational Assimilation Of Precipitation Data. Monthly Weather Review, Vol. 123, No. 4, 1112-1127. April 1995.Zupanski, M., 1993a: Regional Four-Dimensional Variational Data Assimilation In A Quasi-Operational Forecasting Environment. Monthly Weather Review, Vol. 121, No. 8, Pp.2396-2408. August 1993.

Zupanski, M., 1993b: A Preconditioning Algorithm For Large-Scale Minimization Problems. Tellus , 45a, 478-492.

Zupanski, M., 1996: A Preconditioning Algorithm for Four-Dimensional Variational Data Assimilation. Monthly Weather Review, Vol. 124, 2562-2573. November 1996.